The Impacts of Solvents, Heat Treatments and Hole Injection Layers on the Electroluminescent Lifetime of Organic Light-Emitting Devices

by

Elizabeth Salsberg

A thesis

presented to the University of Waterloo

in fulfillment of the

thesis requirement for the degree of

Master of Applied Science

in

Electrical and Computer Engineering

Waterloo, Ontario, Canada, 2019

Author's Declaration

I hereby declare that I am the sole author of this thesis. This is a true copy of the thesis, including any required final revisions, as accepted by my examiners.

I understand that my thesis may be made electronically available to the public.

Abstract

Since their invention over three decades ago, organic light-emitting devices (OLEDs) have attracted tremendous interest for display and solid-state lighting applications and have already been commercialized in smartphones, tablets and television screens. However, the most coveted potential of OLED technology is to enable ultra-low cost, roll-to-roll manufacturing of large-area panels on flexible substrates. To date, commercial OLED products rely on high-cost vacuum deposition techniques and thus fail to realize this potential. In particular, the lifetime, of solution-based (and thus printable) devices remains well below commercially acceptable standards.

The significant lifetime limitations of solution-based devices demand a more thorough understanding of the impact of the unique factors involved in the fabrication of these devices. Solution-processable hole injection layers (HILs), solvents, and heat or drying treatments are three such factors that play a crucial role in solution-processed devices. The principle aim of this work is to understand the influence of these factors on OLED lifetime in vacuum-deposited devices, independent of the multitude and variability of other parameters (e.g.: drying conditions, solubility, solution concertation) involved in most solution-processing methods; and to demonstrate proof-of-concept strategies to mitigate potentially adverse effects for application in solution-processed OLEDs.

Results show that solution-processed poly(3,4-ethylenedioxythiophene) polystyrene sulfonate (PEDOT:PSS) HILs are susceptible to electron-induced degradation, a mechanism that can lead to relatively short OLED electroluminescent (EL) lifetimes. This degradation can be minimized by selecting hole transporting materials and device structures that minimize electron leakage to the HIL, resulting in a lifetime improvement of up to 20x.

The effects of solvent and heat treatments on device efficiency and EL lifetime across a variety of hole injection and hole transport materials were found to vary considerably depending on the specific material combination. The extent of the morphological changes induced by the two treatments is highly material-dependent and does not necessarily correlate with device efficiency and EL lifetime. This suggests that additional, material-specific factors should be likely be considered in future correlations of device characteristics to the morphology of corresponding organic films for solution-processed devices.

Finally, solvent treatment of carbazole hole transport layers was found to induce substantial aggregation and lead to shorter EL lifetimes and lower device efficiency. The origin of this effect was found to be a decrease in photoluminescence quantum yield resulting from this aggregation. Material intermixing was shown to suppress this aggregation and resulted in improved device efficiency and a 2.5x increase in EL lifetime.

Acknowledgements

I would like to begin by acknowledging my supervisor, Prof. Hany Aziz, for his invaluable guidance, support and encouragement over the course of this research work and the past four years. My time in your research group has helped me evolve not only as an engineer, but also as a person; and has enabled me to develop essential critical thinking skills that will undoubtedly serve me throughout my career.

I would like to acknowledge Mr. Richard Barber, the G2N lab manager, for his unprecedented ability to keep the cleanroom running smoothly even amongst the most dire of circumstances. The hands-on, practical skills I gained from working with you will unquestionably prove themselves valuable in many situations.

I would like to acknowledge my fellow group members, past and present; Tyler Davidson-Hall, Christina Yu, Mozhgan Sadeghianlemraski, Viviane Nogueira Hamanaka, Sibi Sutty, Dr. Mike Zhang and Dr. Yong Joo Cho, for their day-to-day insight and many productive (and occasionally less productive, but fun) discussions.

I would like to acknowledge my funding sources that made this work possible: The University of Waterloo Provost Scholarship, the Queen Elizabeth II Graduate Scholarship in Science and Technology and the Waterloo Institute for Nanotechnology Nanofellowship.

I would like to acknowledge Prof. Dayan Ban and Prof. Irene Goldthorpe for graciously agreeing to read and evaluate my thesis.

Finally, I would like to thank my friends, hockey teammates and parents for their unwavering moral support (and then some) throughout this degree. None of this would have been possible without you.

Dedication

To those who inspired me to follow my dreams, wherever they take me.

Table of Contents

List of Figures

Chapter 4

Chapter 5

Chapter 6

List of Tables

List of Abbreviations

Alq$_3$	Tris-(8-hydroxyquinoline)aluminum
CBP	4,4′-Bis(N-carbazolyl)-1,1′-biphenyl
EIL	Electron Injection Layer
EL	Electroluminescence
EML	Emissive Layer
EQE	External Quantum Efficiency
ETL	Electron Transport Layer
HIL	Hole Injection Layer
HOMO	Highest Occupied Molecular Orbital
HTL	Hole Transport Layer
IQE	Internal Quantum Efficiency
Ir(ppy)$_3$	tris(2-phenylpyridine)iridium
ITO	Indium Tin Oxide
JVL	Current-Voltage-Luminance
LT50	Luminescence Half-Life
LUMO	Lowest Unoccupied Molecular Orbital
MoO$_3$	Molybdenum Oxide
NPB	*N,N*′-Di(1-naphthyl)-*N,N*′-diphenyl-(1,1′-biphenyl)-4,4′-diamine
OLED	Organic Light-Emitting Device
OSC	Organic Solar Cell
OTFT	Organic Thin-Film Transistor
PEDOT:PSS	poly(3,4-ethylenedioxythiophene) polystyrene sulfonate
PhOLED	Phosphorescent Organic Light-Emitting Device
PL	Photoluminescence
PLQY	Photoluminescence Quantum Yield
Spiro-CBP	2,2',7,7'-Tetrakis(carbazol-9-yl)-9,9'-spiro-bifluorene
TCTA	Tris(4-carbazoyl-9-ylphenyl)amine
TPBi	2,2',2"-(1,3,5-Benzinetriyl)-tris(1-phenyl-1-H-benzimidazole)
TRPL	Transient Photoluminescence
UV	Ultraviolet

Chapter 1: Introduction

Organic light-emitting devices (OLEDs) are thin-film electroluminescent devices based on organic semiconductors. Light emission from organic semiconductors was first discovered in the 1960s, when electroluminescence was observed in large (3 mm thick) anthracene single crystals with liquid electrodes, however these devices had driving voltages in excess of 100 V [1], [2]. Electroluminescence from anthracene films (500-3000 nm thick) deposited by vacuum deposition and solid-state electrodes later followed with a more reasonable driving voltage of 30 V [3]. The most significant breakthrough however, occurred with the advent of the bilayer OLED in 1987 by Tang and Van Slyke, which exhibited a high brightness of 1000 cd/m^2 at driving voltages < 10 V [4]. Since this breakthrough, OLED technology has attracted significant research interest and has emerged as a multi-billion dollar industry. OLEDs have been commercialized in smartphones, tablets and television screens [5]–[7] and also hold tremendous promise for solid-state lighting applications [8].

OLEDs offer several advantages over their inorganic counterparts, including the potential for printable, large-area panels utilizing ultra-low cost roll-to-roll manufacturing on flexible substrates [5]–[9]. However, most commercially available OLED products rely on high-cost vacuum deposition and thus fail to deliver the full potential of the technology. Indeed, the performance and in particular, the lifetime of solution-based, potentially printable devices remains well below commercially acceptable standards [10]–[15]. The significant lifetime limitations of solution-based devices demand a more thorough understanding of the impact of the unique factors involved in the fabrication of these devices. Three of these factors are the use of solution-processable hole injection layers, solvents, and heating or drying treatments. It is the principle aim of this work is to investigate the influence of these factors on OLED lifetime. However, first an understanding of the fundamentals of OLED technology is required and is provided in this chapter as follows: Section 1.1 outlines the OLED operation mechanism, Section 1.2 provides background on OLED device architectures, Section 1.3 addresses OLED performance and lifetime characterization and evaluation, Section 1.4 addresses OLED fabrication technologies and Section 1.5 provides an overview of the progress and limitations of solution-based OLEDs.

1.1 Operation Mechanism of Organic Light Emitting Devices

Figure 1.1 illustrates the operation mechanisms of OLEDs with four distinct steps: (1) Charge injection, (2) charge transport, (3) exciton formation and (4) radiative recombination and light emission. When an external bias voltage is applied between the cathode and anode contacts, electrons and holes are injected from the metal or conducting cathode and anode contacts into the organic stack, herein consisting of a hole transport layer (HTL) and electron transport layer (ETL). Electrons are injected (1) into the lowest unoccupied molecular orbital (LUMO) of the ETL from the Fermi level of the cathode metal contact, while holes are injected into the highest occupied molecular orbital (HOMO) of the hole transport material from the Fermi level of the anode contact. For charge injection to happen, electrons and holes must overcome the metal/organic interface energy barriers at the cathode and anode contacts respectively. The external applied bias voltage results in band tilting of the organic energy levels, which helps facilitate charge injection. The charges proceed to "hop" along the HOMO and LUMO levels of the molecules in their respective layers (2) (i.e.: HTL/holes, ETL/electrons) and form a bound electron-hole pair known as an exciton at the HTL/ETL interface (3). Finally, the electron and hole in the exciton recombine and emit a photon with energy roughly equal to the energy band gap of the material on which recombination is taking place, in this case the ETL (4). To maximize device performance and lifetime, device structures with a greater degree of complexity than that shown in **Figure 1.1** are used to optimize each step. More detail on these device structures and those relevant to this work is given in Section 1.2.
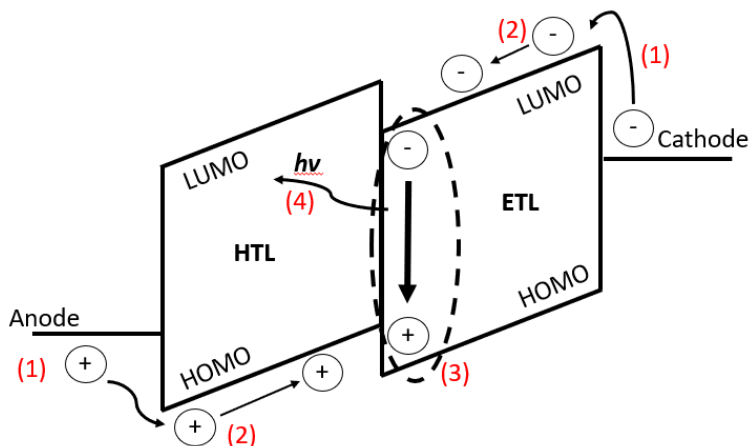
Figure 1.1: OLED operation mechanism: (1) Charge injection, (2) charge transport, (3) exciton formation, (4) radiative recombination and light emission.

1.2 Device Architectures & Materials Selection

The two device architectures utilized in this work consist of a well-studied fluorescent device and a phosphorescent device with a structure known as the simplified phosphorescent OLED (PhOLED). These structures are illustrated in **Figure 1.2** and **Figure 1.3** respectively. In contrast to the bilayer OLED in **Figure 1.1**, both device structures here feature a light emission layer (EML) as well as hole injection (HIL) and electron injection (EIL) layers to facilitate charge injection to the HTL and ETL respectively. The anode and cathode of each device consist of indium-tin-oxide (ITO) and Al respectively. One electrode is typically transparent (almost always ITO, as it is the most reliable transparent and conducting material available) and the other reflective (usually Al, Au or Ag) to maximize the light obtained from the OLED. LiF is used as the EIL and facilitates electron injection by lowering the injection barrier height from the cathode to the ETL [16], [17]. MoO_3 [18], [19] and poly(3,4-ethylenedioxythiophene) polystyrene sulfonate (PEDOT:PSS) [20]–[22] are used as HILs because of their ability to lower the hole injection barrier from ITO into the HTL, leading to improved device efficiency and stability. While the same contacts and charge injection layers (HILs/EILs) are used in both device structures, the other materials are significantly different, as outlined in the sections below.
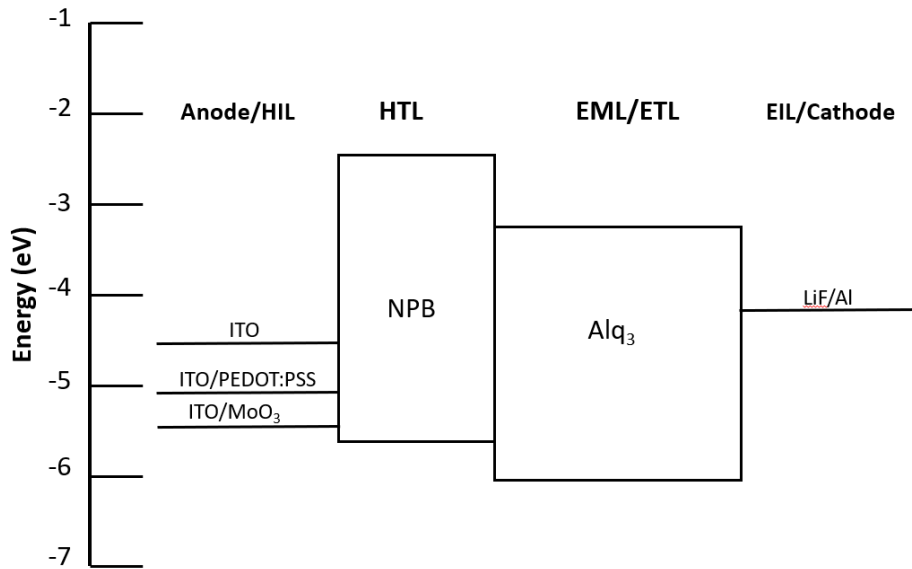
Figure 1.2: Fluorescent device structures and energy band diagrams.
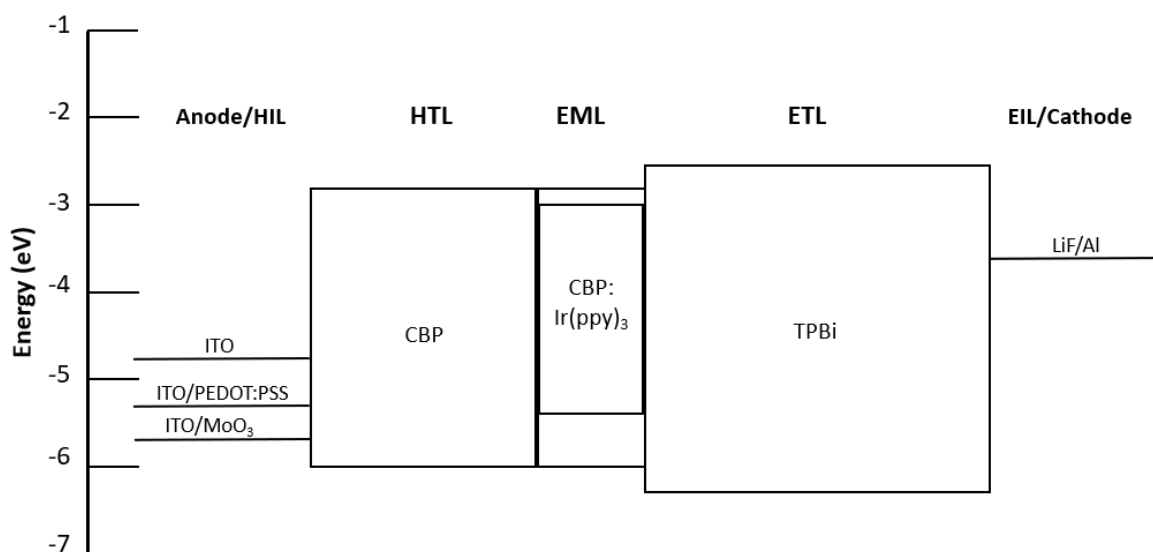
Figure 1.3: Phosphorescent device structure and energy band diagram.

1.2.1 Fluorescent Device

Fluorescent OLEDs function on light emission from singlet excitons, that is, excitons whose hole and electron's total spin angular momentum quantum number, $\vec{S}$, is equal to zero, i.e.: $\vec{S} = (\frac{1}{\sqrt{2}})(|\uparrow\downarrow> -|\uparrow\downarrow>)$ [23]–[25]. According to quantum mechanical theory, the probability of singlet exciton formation is 25%; with triplet excitons $(\vec{S} = 1,$ possible spins: $|\uparrow\uparrow>, |\downarrow\downarrow>, (\frac{1}{\sqrt{2}})(|\uparrow\downarrow> +|\uparrow\downarrow>))$ accounting for the other 75% [26]. Therefore, in fluorescent devices, only 25% of excitons contribute to light emission, severely limiting the efficiency of these devices. When the electron in the first singlet excited state decays to the ground state radiatively, light with energy corresponding to the S_1-S_0 transition is emitted, as illustrated in the Jablonski diagram in **Figure 1.4.** Note that it is also possible for excitons to decay via non-radiative processes, such as internal conversion and vibrational relaxation, as shown in **Figure 1.4.** Since triplet excitons are lower in energy than singlets, intersystem crossing (ISC) is also energetically favourable, whereby singlets are converted to lower-energy triplets. These alternative pathways can further take away from the ideal 25% of excitons that may contribute to light emission in these devices. Nevertheless, fluorescent devices formed the first generation of OLED technology and are still widely studied today.

4

The organic layers of the fluorescent device consist of an organic fluorescent HTL and ETL, which also serves as the emissive layer (EML). The most well-studied fluorescent device in the literature employs N,N′-Di(1-naphthyl)-N,N′-diphenyl-(1,1′-biphenyl)-4,4′-diamine (NPB) and 8-Hydroxyquinoline aluminum salt (Alq$_3$) as the HTL and ETL/EML respectively [27]–[31]. The chemical structures of these materials and others utilized in this work are given in **Table 1.1.** With the advent of HILs, the stability of fluorescent devices improved significantly [19], [28], [31]; it is for this reason, the fluorescent devices in this work make use of these materials.
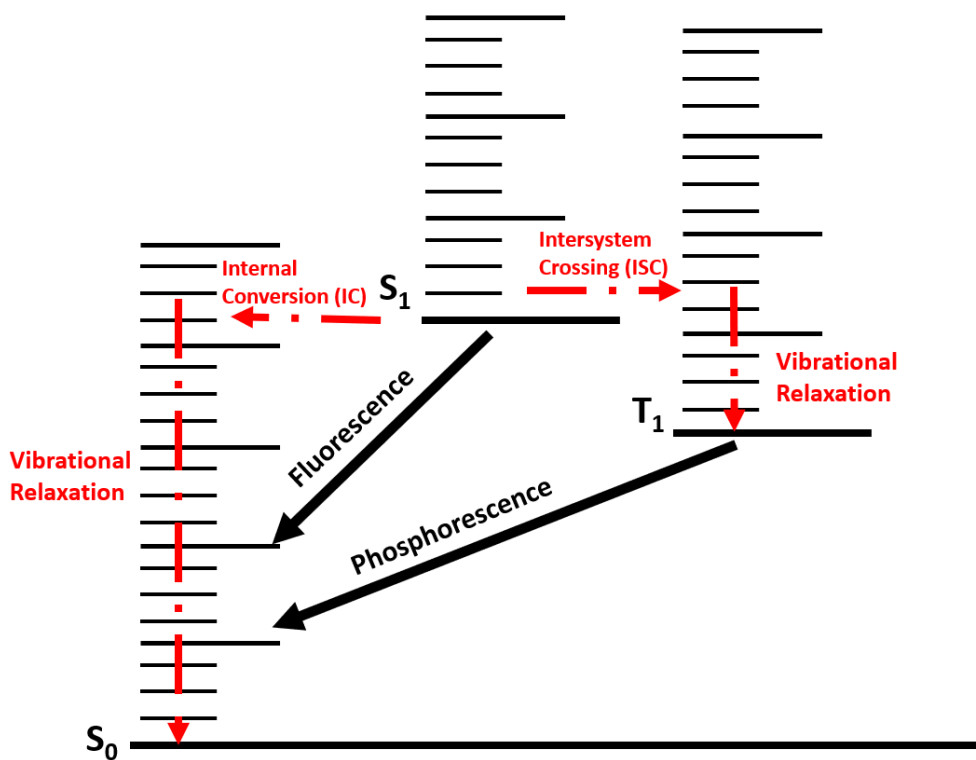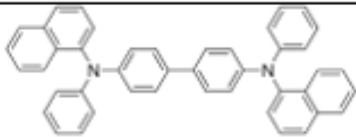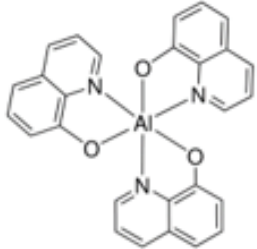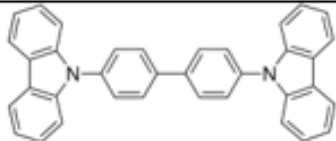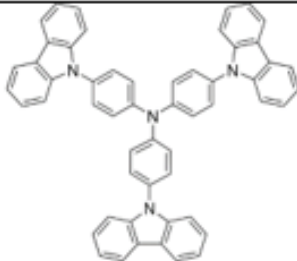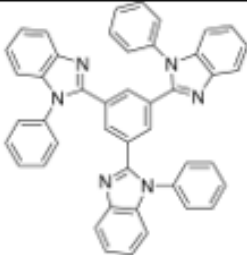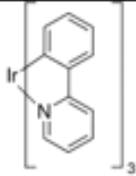
Figure 1.4: Jablonski diagram depicting relevant exciton decay pathways in OLEDs.
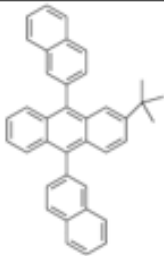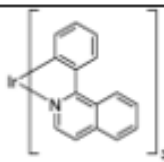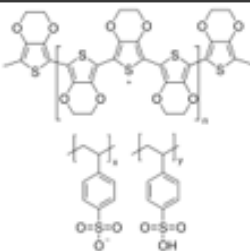
1.2.2 *Phosphorescent Device & The Simplified PhOLED*

Unlike fluorescent devices, phosphorescent OLEDs or PhOLEDs, are able to take advantage of the 75% share of triplet excitons, leading to substantially improved device efficiencies [32]–[34]. These devices utilize platinum and iridium-based metal complexes because they facilitate the otherwise forbidden T_1 - S_0 transition to form triplets via spin-orbit coupling [23], [32], [34]–[36]. In these materials, singlets are converted to triplets through intersystem crossing, forming nearly 100% triplets, which subsequently emit light via phosphorescence as shown in **Figure 1.4.** Early red phosphorescent devices used platinum octaethylporphyrin (PtOEP) as a dopant or "guest" in an Alq_3 "host" to form a dedicated EML and reported 4% peak external quantum efficiency (EQE) [33] (i.e.: the ratio of photons emitted from the device externally to electrons fed into the device). At the time this was considered quite high and is substantially better than fluorescent device efficiencies. For green devices, iridium-based dopants/guests with very high quantum yields, namely bis(2-phenylpyridine)iridium acetylacetonate [Ir(ppy)$_2$(acac)] (quantum yield ~ 94%) and tris(2-phenylpyridine)iridium [Ir(ppy)$_3$] (quantum yield ~ 90%) were developed [35]. Shortly thereafter, devices using these dopants/guests soon followed with a variety of host materials, leading to very impressive EQEs [34], [36], [37]. Unlike the first-generation fluorescent devices, these devices typically relied on four or more organic layers to achieve these high EQEs, spurring an abrupt increase in device structure complexity and ultimately higher manufacturing cost.

To solve this problem, Lu and coworkers developed a highly efficient "simplified PhOLED," consisting of only three organic layers, as shown in **Figure 1.3** [38]. This device utilized a 4,4′-Bis(9-carbazolyl)-1,1′-biphenyl 4,4-N,N′-Dicarbazole-1,1′-biphenyl (CBP) HTL, a 2,2',2"-(1,3,5-Benzinetriyl)-tris(1-phenyl-1-H-benzimidazole) (TPBi) and an Ir(ppy)$_2$(acac) green phosphorescent dopant and exhibited an exceptionally high EQE of 21.9% at a very high brightness of 10,000 cd/m^2 [38]. The wide bandgap of TPBi helps confine excitons on the CBP:Ir(ppy)$_2$(acac) EML, facilitating the high efficiency of the device. Due to its remarkable simplicity and high efficiency, the simplified PhOLED device structure is used to for the phosphorescent devices in this work. It should also be pointed out that Ir(ppy)$_3$ is selected as the guest dopant in place of Ir(ppy)$_2$(acac). Although its quantum yield (and hence device EQEs) are lower than that of Ir(ppy)$_2$(acac), device lifetimes with Ir(ppy)$_3$ dopants much longer [39], making it more suitable for the lifetime focus of this work.

Table 1.1: Chemical structures and classification of organic materials used in this work.

Material	Chemical Structure	Classification
N,N'-Di(1-naphthyl)-N,N'-diphenyl-(1,1'-biphenyl)-4,4'-diamine (NPB)		HTL
8-Hydroxyquinoline aluminum salt (Alq₃)		ETL and EML
4,4'-Bis(9-carbazolyl)-1,1'-biphenyl 4,4-N,N'-Dicarbazole-1,1'-biphenyl (CBP)		HTL and Host
Tris(4-carbazoyl-9-ylphenyl)amine (TCTA)		HTL
2,2',2"-(1,3,5-Benzinetriyl)-tris(1-phenyl-1-H-benzimidazole (TPBi)		ETL
tris(2-phenylpyridine)iridium [Ir(ppy)₃]		Green Phosphorescent Dopant

2-tert-Butyl-9,10-di(naphth-2-yl)anthracene (**TBADN**)		Green Fluorescent Dopant
Tris[1-phenylisoquinoline-C^2,N]iridium(III) [**Ir(piq)$_3$**]		Red Phosphorescent Dopant
Poly(3,4-ethylenedioxythiophene) polystyrene sulfonate (**PEDOT:PSS**)		HIL

1.3 Performance Characterization

The optoelectronic performance of an OLED is characterized by its current-voltage-luminance characteristics, electroluminescent (EL) lifetime, EL spectrum and external quantum efficiency (EQE). The following section provides an overview of these performance characteristics and highlights the key differences between the performance of fluorescent and phosphorescent devices. Finally, a brief outline of the factors affecting device EQE is given.

1.3.1   Current-Voltage-Luminance (JVL) & EL Lifetime

The current-voltage-luminance characteristics of an OLED are fundamentally important and ultimately influence device efficiency and lifetime. OLEDs are forward-biased devices in which current flows in only one direction, as shown in the sample JVL characteristics given in **Figure 1.5.** The voltage at which there is a sudden increase in current is called the "turn-on" voltage. Beyond this point, there steadily becomes enough current through the device to generate light. As the voltage (and current) increase, the luminance also increases, as shown in **Figure 1.5.** Typically, a "driving voltage" is measured for a specific current density (for devices in this work, this is 20 mA/cm^2).

The driving voltage is important for EL lifetime measurements which are run at this constant current value—during an EL lifetime measurement, the luminance decreases from its initial value (at the initial driving voltage measured at 20 mA/cm^2) and the driving voltage increases over time, as shown in **Figure 1.6**. For the EL lifetime measurements in this work, luminance is normalized to the initial, time-zero value at 20 mA/cm^2; the change in driving voltage is also measured relative to the initial, time-zero value at 20 mA/cm^2. The luminescence half-lifetime (LT50), shown in red in **Figure 1.6,** and is defined as the time taken for the luminance to reach half of its initial value. It may be used to compare the EL lifetimes of OLEDs provided they have similar initial luminance values.
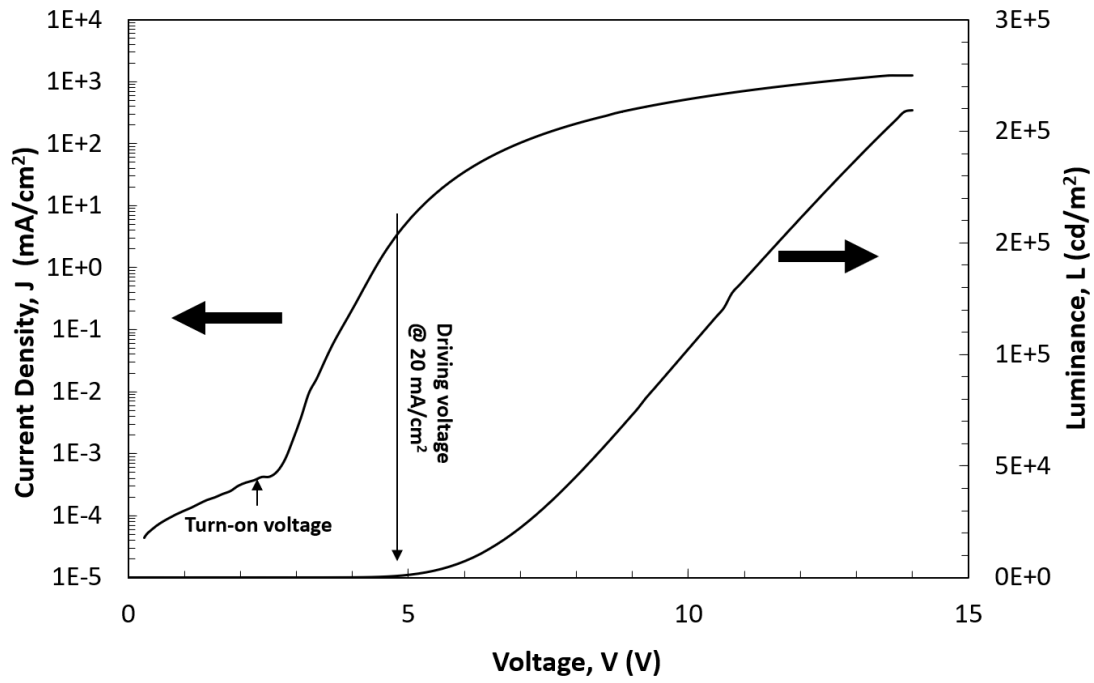
Figure 1.5: Sample JVL characteristics of a typical OLED in this work
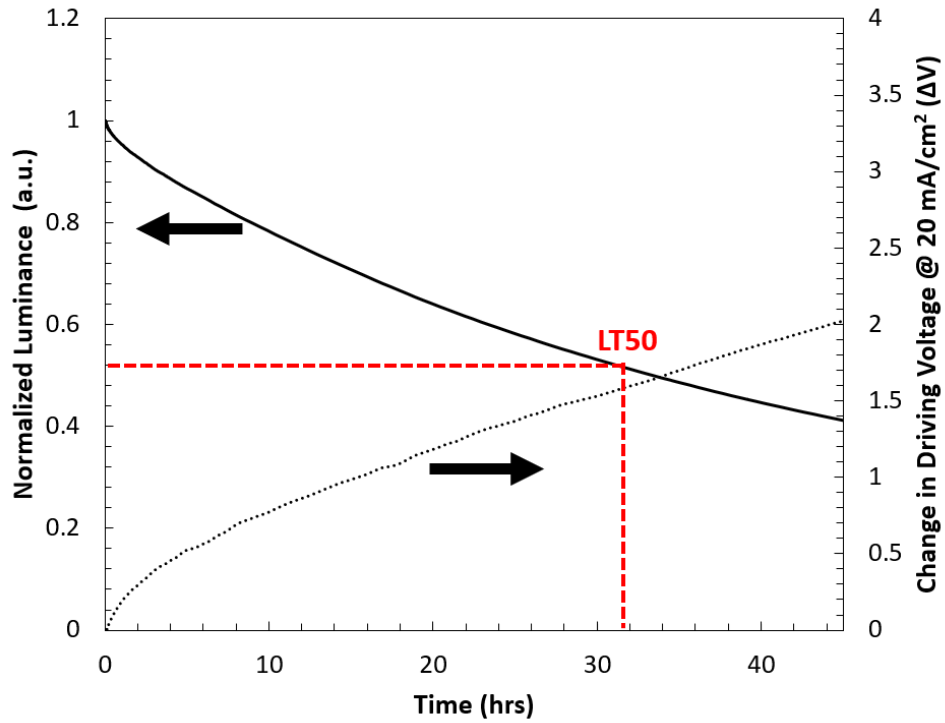
Figure 1.6: Sample EL lifetime characteristics of a typical OLED in this work.

1.3.2   Current Efficiency and EQE

Current efficiency is the ratio of luminance to current density, i.e.: L/J, and is thus directly proportional to the EQE, i.e.: the ratio of photons emitted from the device to electrons injected into it. Current efficiency is easily derived from the slope of the luminance versus current density (LJ) characteristics, which typically follow a linear trend, as shown in **Figure 1.7**. A plot of EQE (or CE) versus J is thus usually constant, also shown in **Figure 1.7.** However, phosphorescent devices do not follow this rule because they are subject to a phenomenon called "efficiency roll-off," where the EQE (and current efficiency) decrease substantially at high current density and high luminance [40], as illustrated in **Figure 1.8**. Among the phosphorescent dopants in the literature, Ir(ppy)$_3$ is one of the least prone to efficiency roll-off due to its very short exciton lifetime ($\tau = 0.5$ μs) [40], [41] and is thus considered state-of-the art in the field, another reason for its use in this work.
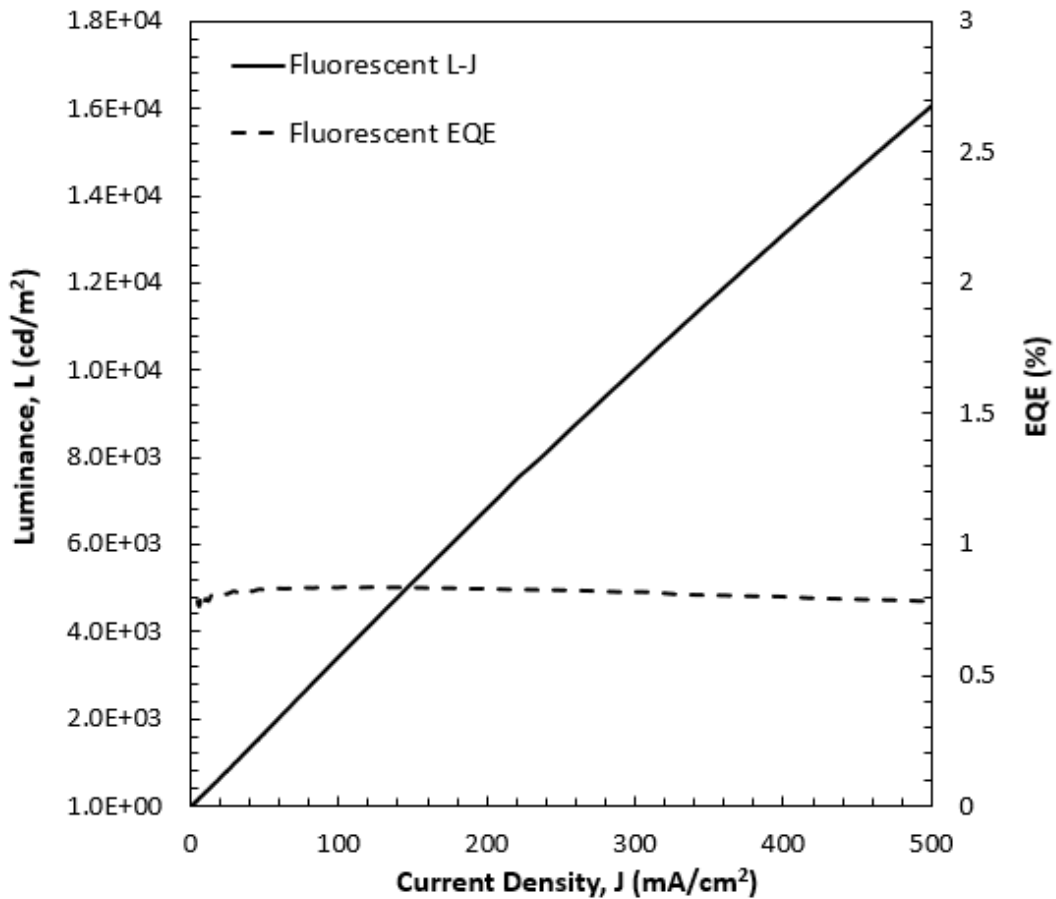
Figure 1.7: Sample LJ and EQE versus J characteristics of a typical fluorescent OLED.
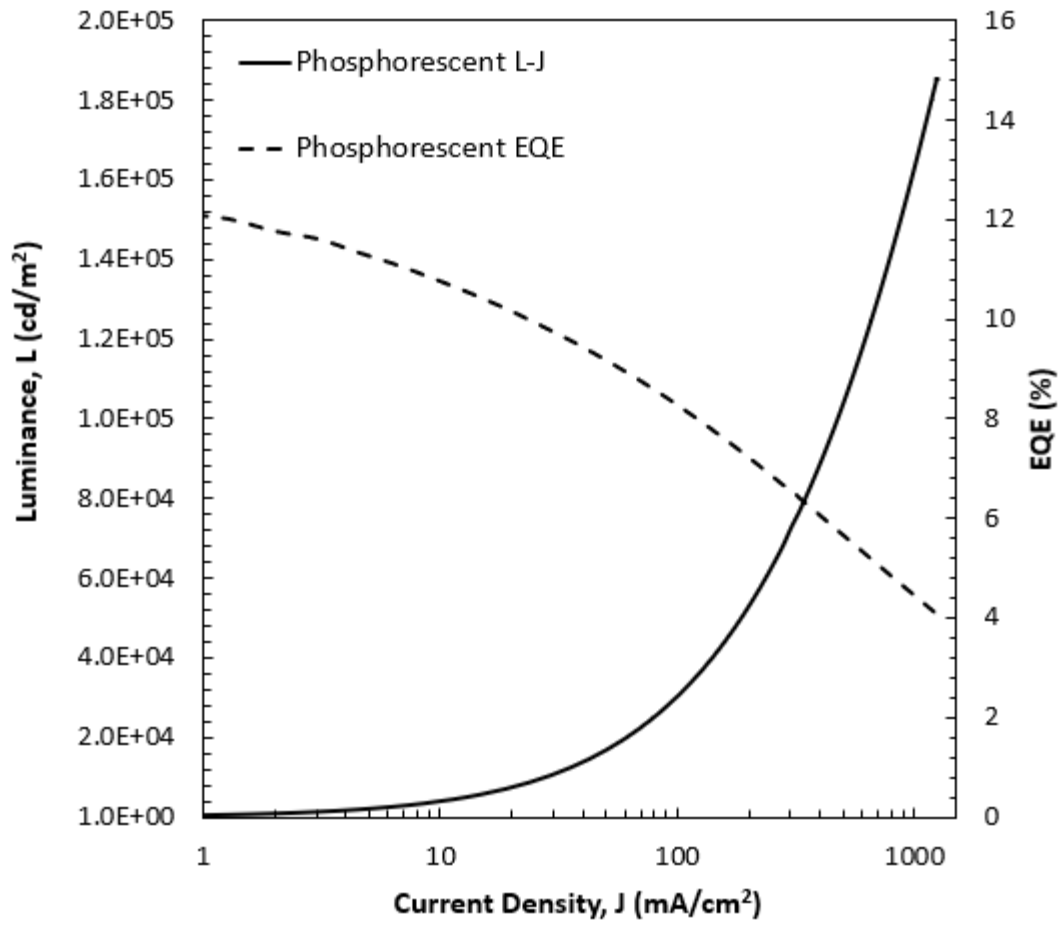
Figure 1.8: Sample LJ and EQE versus J characteristics of a typical phosphorescent OLED.

1.3.3   Factors Governing EQE

The EQE (η_{EQE}) of an OLED is governed by four factors as shown in **Equation (1)** where η_{OC} is the fraction of photons that escape from the device, η_{exci} is the fraction of excitons that recombine radiatively, η_{PL} is the photoluminescence quantum yield (PLQY) and η_{eh} is the charge balance factor [32]. The latter three factors make up the internal quantum efficiency (IQE) as shown in **Equation (2)**, which describes the efficiency of internal device-related processes. Each of these factors has been carefully optimized to reach values close to unity. In fluorescent devices, $\eta_{exci} < 25\%$ since only singlets contribute light emission. In phosphorescent devices $\eta_{exci} \rightarrow 100\%$ since most triplets contribute to light emission, and singlets are converted to triplets via intersystem crossing. η_{PL} or PLQY is determined by the competition between radiative and non-radiative transitions (e.g..: internal conversion, vibrational relaxation): The more radiative transitions, the closer to unity this value becomes. While the PLQY of phosphorescent dopants has been shown to be >90%, optimizing the host:guest ratio in the EML of phosphorescent devices has been critical to maximizing PLQY.

As guest dopant concentrations increase, exciton transfer from one dopant molecule to another becomes more probable, thus facilitating migration of excitons away from where they were created (i.e.: the recombination zone) and increasing their probability of being quenched [42]. Indeed, optimal guest concentrations in phosphorescent devices utilizing guests based on Ir(III) are typically well below 20% [43]. With the optimal host:guest ratio (dependent on the materials involved), η_{PL} values very close to unity have been achieved [43]. The charge balance factor, η_{eh}, describes the ratio of electrons to holes in the device; ideally the two carriers are present in relatively equal concentrations. Charge balance is primarily controlled by optimizing the thickness [44] of the electron and hole transport layers and by introducing electron and hole blocking layers to confine charges and excitons on the EML [45]. It is worth noting that simplified PhOLEDs tend to suffer from limited charge balance as they are inherently hole-rich and are subject to electron leakage—however, these limitations can be overcome by careful selection of HTLs with effective electron-blocking characteristics, which has been shown to increase EQE by up to 25% [46].   Collectively, all three device-related efficiency parameters have been optimized to achieve IQEs approaching 100% ins phosphorescent OLEDs [34], [47], hence the choice to base this study primarily on these devices.

$$\eta_{EQE} = \eta_{OC}\eta_{exci}\eta_{PL}\eta_{eh} \quad \textbf{(1)}$$

$$\eta_{IQE} = \eta_{exci}\eta_{PL}\eta_{eh} \quad \textbf{(2)}$$

EQE, on the other hand remains limited due to the poor light-outcoupling efficiency η_{OC} of planar OLEDs, with only 20%-30% of light able to escape the device [48], [49]. The light outcoupling limitation arises from total internal reflection (TIR) at the ITO/substrate and ITO/organic interfaces, resulting in two trapped waveguided modes that do not contribute to light emission. Several approaches for to improve η_{OC} have been undertaken in the literature. These approaches can be classified into two groups, those targeting the ITO/substrate modes and those targeting the ITO/organic modes. Strategies for light extraction from the ITO/substrate modes typically texture the substrate to improve light extraction; the most effective strategies include microlens arrays [50], [51], silica microsphere layers [52], [53] and volumetric light scattering films [54], [55]. Approaches for improving light extraction from the ITO/organic modes include high refractive-index substrates [56], [57], internal nanoparticle-based scattering layers [58], grid electrodes [59]–[61], and introducing Bragg gratings into the organic stack [62]–[64]. These strategies have enabled η_{OC} and EQE enhancements of up to 3x, though cost and manufacturing practicalities remain significant issues.

1.4 OLED Fabrication: Vacuum Thermal Deposition versus Solution Coating

OLEDs may be fabricated by vacuum deposition or by solution-based methods. Indeed, the prospect of ultra low cost, roll-to-roll manufacturing and compatibility with flexible substrates are widely considered among the most attractive advantages of OLED technology; made possible because organic materials can be integrated into liquid, solution-based inks and can be processed at relatively low temperatures compared to their inorganic counterparts. However, most commercial OLED products to date are fabricated by vacuum deposition techniques due to limitations in performance and device stability associated with solution-based devices. This section will give an overview of vacuum thermal deposition, solution coating and printing techniques, and review the progress and limitations of solution-based OLEDs in the field to date.

1.4.1   *Vacuum Thermal Deposition*

During vacuum deposition, organic materials are sublimed into the vapour phase via resistive heating in a high-vacuum environment (pressure $< 10^{-5}$ Torr). The organic material is placed in a small container known as a Knudson cell, which is connected to the resistive heating source [65], [66]. The vapour passes through a metal "shadow mask" and then condenses on to form the organic film in the desired locations/pattern on the substrate as determined by the mask [67], [68]. This process is illustrated in **Figure 1.9**. It is worth noting that vacuum thermal deposition is only suitable for organic small molecules and not polymers due to their high molecular weight [9]. This is however not considered a significant issue because to date, small molecule-based OLEDs have generally outperformed their polymer counterparts [15]. High vacuum is required to minimize the mean free path (i.e.: the distance traveled by a particle in a medium before colliding with another particle) of the sublimed organic molecules to ensure that they do not collide with impurity species as they make their way to the substrate. The higher the vacuum, the greater the mean free path, hence the stringent requirement for high vacuum in this process. Additionally, organic materials are extremely sensitive to contamination from impurities; minor impurities can result in extremely poor performance [9], [66]. Industrial vacuum chambers are designed to ensure isotropic emission from the source material (i.e.: modeled as a point source), facilitating deposition on many substrates at a time [69]. Since organic materials are also highly contamination-sensitive, separate vacuum deposition chambers are required for each organic material to be deposited during fabrication [65]. This results in very high manufacturing costs and constitutes the main drawback of vacuum thermal deposition [69].

For OLED displays, patterning of the red green and blue (RGB) pixels is another important and challenging consideration for the OLED industry. Presently, this is achieved using fine metal mask (FMM) technology [68], [69]. There are however critical limitations to FMM, such as limited resolution, mask alignment and mask definition [70], [71], further contributing to the relatively high manufacturing costs for OLED displays.
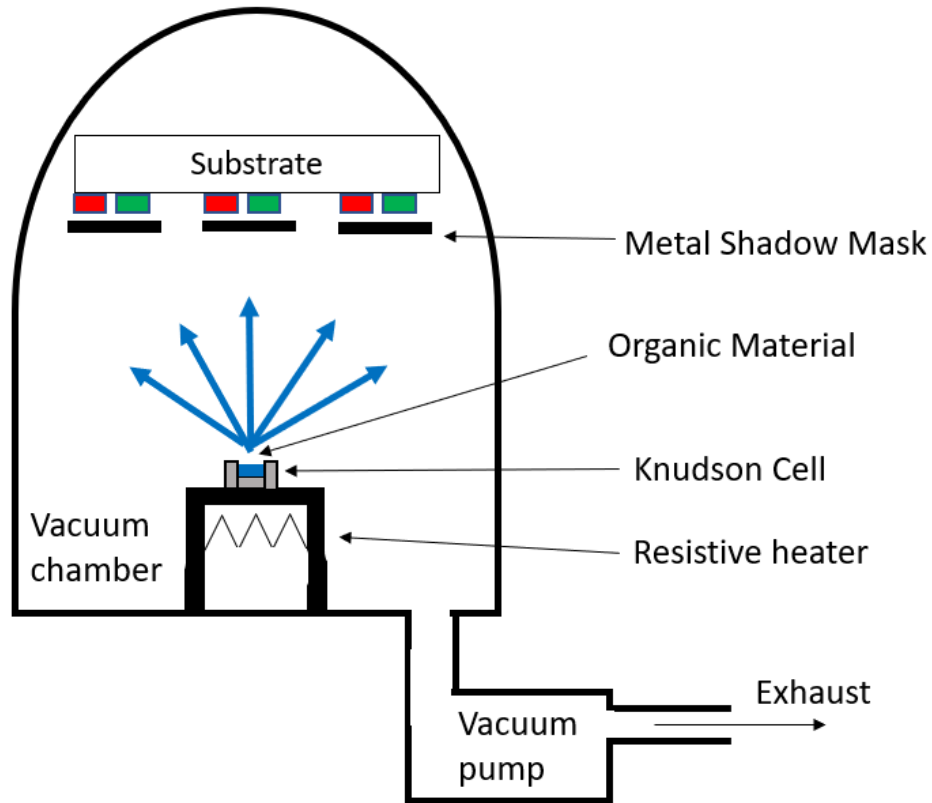
Figure 1.9: Schematic diagram of a vacuum thermal deposition chamber with shadow mask.

1.4.2   *Solution Coating and Printing Techniques*

Solution-based fabrication technologies can be broken down into two categories, coating techniques and printing techniques. The main distinction between these two types of techniques is that printing typically implicates some form of patterning capability, whereas coating may not [72]. Some examples of solution-coating techniques include spin-coating, blade-coating and dip-coating [17], among which spin-coating is the most well studied, with blade coating rapidly gaining importance in the field.

1.4.2.1 Spin-Coating

As shown in **Figure 1.10**, spin-coating involves placing the substrate on a rotating chuck typically with a vacuum to ensure the substrate does not move. The liquid solution is then dispensed onto the substrate and the angular velocity (i.e.: spin-speed) of the chuck is accelerated; causing a radial flow from which most of the dispensed solution is quickly ejected away [73]. This process, along with evaporation of some of the solution, leaves behind a thin, dry film on the substrate following spin coating. The thickness of the deposited films is controlled by the spin speed and the solution concentration; faster speeds and low concentrations lead to thinner films, while slower speeds and higher concentrations lead to thicker films [72], [73]. While spin-coating is recognized as a useful experimental technique, it is difficult to scale up since it not compatible with roll-to-roll processing; only one substrate can be processed at time. Another limitation that affects spin-coating is the poor solubility of many small-molecule organic materials; often very low concentrations are required, thus limiting the thickness of the film [74]. Finally, spin-coating is also challenging for multi-layer devices since deposition of a subsequent layer may re-dissolve the previous layer underneath if both materials are deposited from chemically similar solvents; that is, spin-coating often demands the use of orthogonal solvents [75].
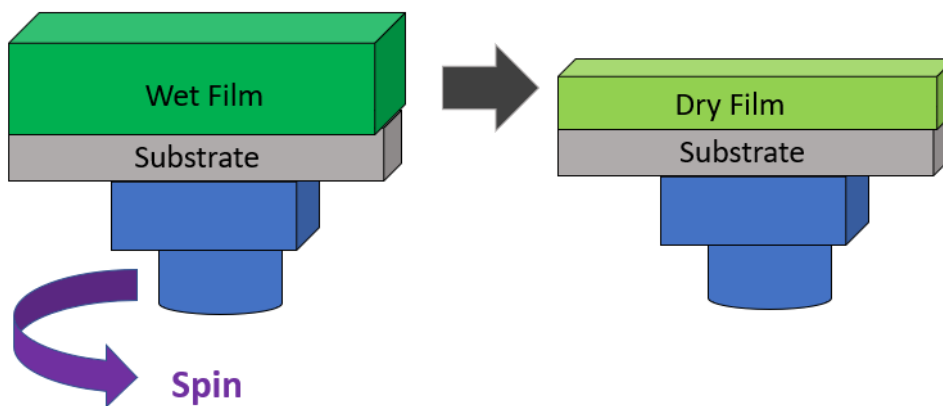
Figure 1.10: Schematic of the spin-coating process.

1.4.2.2 Blade Coating

On the other hand, blade coating is easily integrable into a roll-to-roll process [72], [76]–[78] and provides greater flexibility with respect to film thickness, since high solubility is not stringently required [77]. Solvent orthogonality is also not regarded as critical for blade-coating because the substrate is heated from the bottom during deposition and hot air is applied from above to dry the films [79], as shown in **Figure 1.11**. To deposit the film, a small amount of solution, typically a few µl, is dispensed between the blade and the substrate. As the blade moves, the droplet spreads along the blade by capillary force and leaves a wet film behind. The entire process takes place on a hotplate; the simultaneous top (hot air) and bottom (hotplate) heating ensures that dissolution of underlying dry films is prevented [79]. Despite its roll-to-roll compatibility, a disadvantage with blade-coating is that patterning is still very difficult [72]. For this reason, the printing techniques discussed in the following section are gaining importance in the manufacturing of solution-processed OLEDs and organic electronics in general.
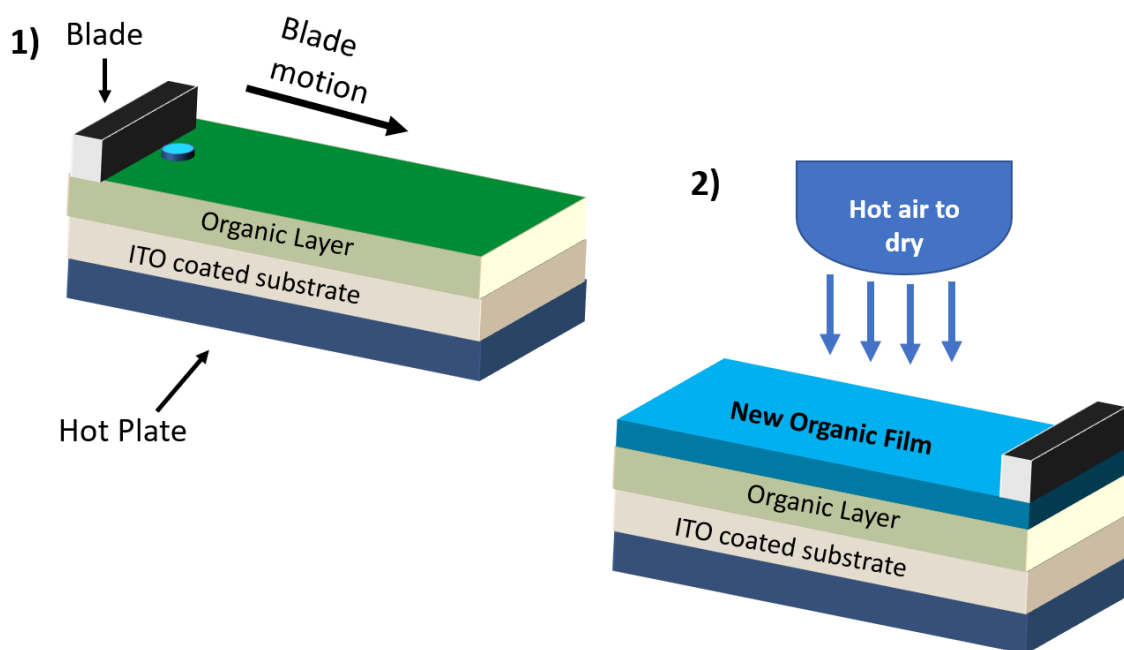
Figure 1.11: Schematic of the blade coating process.

1.4.2.3 Printing Methods

Among the myriad of printing technologies explored for organic electronics, screen-printing, gravure printing and inkjet printing are some of the most well-studied. Screen-printing is the simplest among these techniques and is very low-cost and roll-to-roll compatible. In this process, ink is transferred using a screen through a mask or stencil to the substrate. A squeegee is used to press the ink through the mask and onto the substrate [80], as shown in **Figure 1.12**. While this technique is very low-cost, it is limited with respect to film thickness and resolution and is thus often not suitable for deposition of the active layers of many organic optoelectronic devices [81]. However, it can still be used to deposit metallic layers for electrodes and conducting polymers such as PEDOT:PSS [81]–[83]. Gravure printing and a closely related technique, flexographic printing, use respectively metal or rubber cylindrical patterned rollers to deliver the solution to the substrate [72], [83], as shown in **Figure 1.13 a)**. The main advantages of gravure printing are that it facilitates high resolution and very high throughput (up to 10 m^2/s) [84], [85]. However, new master cylinders must be produced for each new pattern, making this technique very expensive [72], particularly if many patterns are required. For this reason, flexographic printing, which utilizes a rubber cylinder, is considered more promising for minimizing cost [83]. Unlike the previous two methods, which require a physical master pattern (i.e.: engraved cylinder or stencil/screen), inkjet printing uses electronic data in a digital form to create the desired pattern on the substrate [86]. The ink or solution is ejected in a fixed quantity from a printhead nozzle controlled by a piezoelectric actuator [87], as shown in **Figure 1.13 b)**. There have been multiple demonstrations of OLEDs [88], [89] and other organic optoelectronic devices such as organic photovoltaics [90] and organic thin film transistors [91] with reasonable performance, but poor wetting of ink on the substrate, nozzle clogging and the "coffee-ring" effect continue to be significant issues that need to be overcome [92], [93].
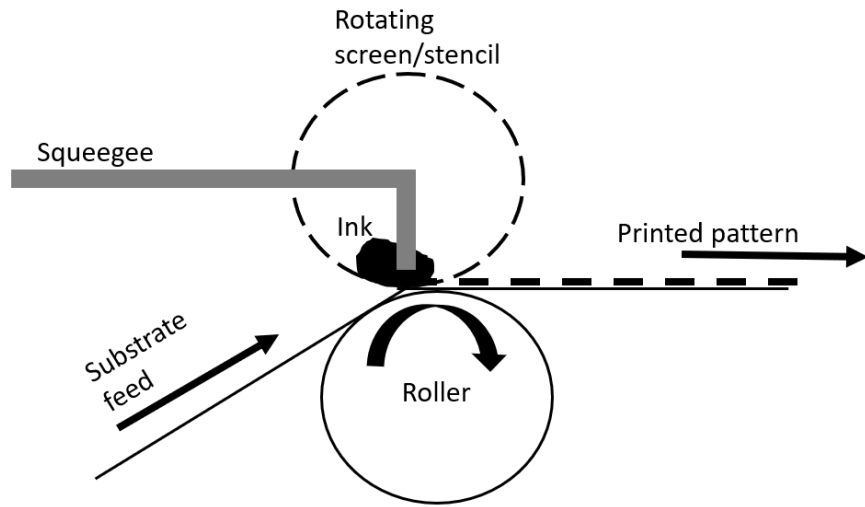
Figure 1.12: Schematic of the screen-printing process. Adapted from ref. [72].
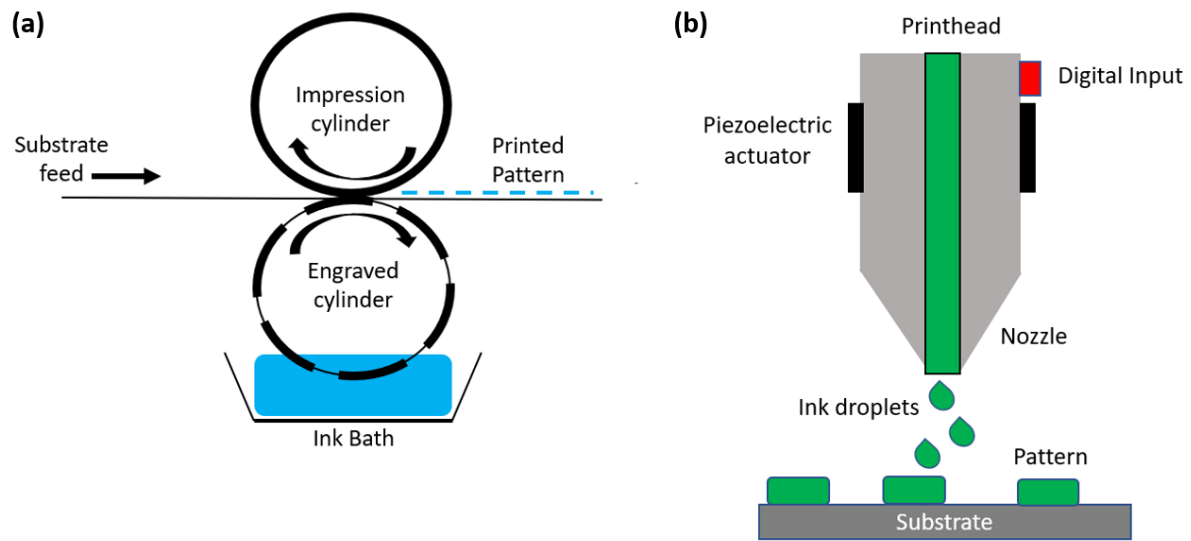
Figure 1.13: Schematics of a) gravure printing and b) inkjet printing processes.

1.5 Progress and Limitations of Solution-Based OLEDs

Solution coating has gradually evolved through the various layers (i.e.: HIL, HTL, EML, etc.) in OLEDs since its rise in the field. For example, PEDOT:PSS has been used as a ubiquitous solution-processable HIL material since the first developments of OLEDs with charge injection layers [94], [95] and its properties have been extensively investigated. This is because PEDOT:PSS is readily soluble in water and simple alcohols, and is also highly transparent and very conductive [17], [94]–[97]. Excess water is removed by simply heating the substrate around 120-130°C for at least 20-30 min, facilitating subsequent deposition of the typically hydrophobic organic layers. Traditionally, solution-coating has been considered more conducive to polymer-based OLEDs, since polymers readily dissolve in many organic solvents, such as toluene, tetrahydrofuran, dichloromethane and chlorobenzene [9]. However, small molecules generally lead to significantly better device performance [98], [99], thus making them the preferred choice.

Small molecule solution-based OLEDs have witnessed remarkable progress over the past decade, with device EQEs approaching their vacuum-deposited counterparts across the colour spectrum [100]–[106]. This progress has been realized despite the fact that many of these small molecular materials, especially heavy atom-based phosphorescent dopants such as Ir(III) complexes, are nearly insoluble in most common organic solvents [15]. To overcome this issue, Ir(III) complexes with specific ligands designed to increase their steric hinderance and hence their overall solubility have been developed and been shown to lead to impressive EQEs [101], [107], [108].

Parallel advances in small molecular host and hole transport materials have also played a critical role in the progress of solution-based OLEDs [15], [98], [99], [109]. Carbazole-based materials such as CBP have attracted significant interest because of their high triplet energy, wide bandgap, and reasonable solvent solubility, making them suitable and versatile hosts for a variety of guest dopants for red [110], green [98], blue [111], and white [109] solution-based OLEDs. Other carbazole derivatives have also shown tremendous promise as host/hole transport materials for solution-based OLEDs, including Tris(4-(9H-carbazol-9-yl)phenyl)amine (TCTA) [99], 1-Methylcyclopropene (mCP) [106], and 2-6-bis[3-(9H-Carbazol-9-yl)phenyl]pyridine (26DczPPy), a pyridine-modified carbazole [77].

Several solution-processable electron transporting materials have also been developed, though many of them are not yet commercially available and are synthesized by research groups in-house [112], [113]. Exceptions to this however are 2,2′,2"-(1,3,5-Benzinetriyl)-tris(1-phenyl-1-H-benzimidazole) (TPBi) and 4,7-diphenyl-1,10- phenanthroline (BPhen) known for their solubility in alcohols, and have demonstrated impressive device EQEs in all-solution-processed OLEDs [114]–[116].

It is however important to note that in most studies of solution-processed OLEDs, solution coating is limited to the HIL, HTL and EML at most, with the ETLs deposited by vacuum thermal deposition to avoid dissolution of the underlying layers [15]. While the use of orthogonal solvents (i.e. alternating hydrophobic solvents such as benzene with hydrophilic solvents such as alcohols) has been regarded as a promising approach, it is limited by the fact that many organic small molecular materials are inherently hydrophobic. This presents a unique challenge for deposition of ETL layers following solution-coated HTLs/EMLs from hydrophobic solvents.

Although studies of all solution-processed (i.e.: HIL/HTL/EML/ETL), small molecule OLEDs have been conducted [76], [112], [114], [117], [118], there are much fewer compared to those with only the HIL, HTL or EML being solution coated. In these studies, TPBi and BPhen were typically employed as the ETL layers and were solubilized in methanol or other short-chain alcohols [114]–[116]. Blade-coating has also been shown to be a promising method for getting around the poor solubility of small molecular organic materials and the need for orthogonal solvents [76], [77], [114], [117].

Despite these demonstrations, all-solution, all-small-molecule OLEDs remain in the early stages of development. Furthermore, solution devices, regardless of the number of layers coated from solution, tend to have significantly shorter electroluminescent lifetimes than their vacuum-deposited counterparts despite their EQE's being relatively similar [100]–[106]. This lifetime limitation remains a significant barrier to the commercial development of products based on solution-coated OLEDs [10]–[15]. The root causes of the degradation mechanisms behind the lifetime gap between solution and vacuum-deposited OLEDs remain unclear [14], [15]. For these reasons, investigating the factors behind the limited EL lifetime of these OLEDs is the principal focus of this work.

Chapter 2: Background and Literature Review

In this chapter, a literature review of the known degradation mechanisms of solution-coated OLEDs is given. First, the known impact of solution-coated PEDOT:PSS HILs on device lifetime will be discussed. Second, the differences between solution-coated and vacuum deposited organic films and their potential impact on device lifetime will be outlined.

2.1 PEDOT:PSS HILs and their Impact on OLED Stability

PEDOT:PSS has been at the forefront of hole injection materials for OLEDs and other organic optoelectronic devices such as organic solar cells (OSCs) and organic thin film transistors (OTFTs) for more than two decades [94], [119]–[122]. This is because PEDOT:PSS is both optically transparent and highly conductive, with metal-like properties [121]. It is easily synthesized via oxidative polymerization of the 3,4-ethylene-dioxythiophene (EDT) monomer in the presence of polystyrene sulfonic acid (PSS) in water; with the final product forming a remarkably stable micro-dispersion [121], [122]. PEDOT:PSS dispersions are readily commercially available and may be deposited by spin-coating, blade-coating and all printing methods covered in Section 1.4 and are thus easily integrable into any solution process. Additionally, PEDOT:PSS films are thermally stable up to 200°C [121], are mechanically flexible [123], [124], and can be formed with sufficiently smooth surface morphology (i.e.: root mean square roughness < 2 nm) for OLED applications [125]. PEDOT:PSS however, is not immune to degradation. Exposure to air [126], humidity [127] and ultraviolet light [128], [129] have been shown to decrease the conductivity of PEDOT:PSS over time. Encapsulation is thus an essential requirement to prevent ambient-induced degradation, particularly since PEDOT:PSS is hygroscopic (i.e.: absorbs water) [121], [127]. Electron bombardment has also been shown to lead to a decrease in the conjugation of PEDOT:PSS, thereby decreasing its conductivity [127], [129]–[131], suggesting that electrons in OLEDs and other organic optoelectronic devices with PEDOT:PSS could potentially lead to accelerated device degradation. Nevertheless, the favourable optical, electronic, mechanical and chemical properties of PEDOT:PSS have made it among the most well-studied hole injection materials for applications in solution-processed OLEDs.

In the early stages of its use in OLEDs, PEDOT:PSS was considered among the limiting factors for because of its slight acidity and thus tendency to erode the underlying ITO transparent electrode, resulting in the diffusion of indium atoms into the organic stack [132]. The most widely cited strategies to overcome this issue include the use of a self-assembled monolayer sandwiched between ITO and PEDOT:PSS [133] and additives to chemically stabilize PEDOT:PSS [134]. However, neither of these became common practise in most research groups because OLED materials and devices structures evolved tremendously and greatly improved device stability was realized over the years, making it progressively more challenging to identify the contribution of this issue to device lifetime. Most significantly, transition metal oxides such as MoO_3 began to rival PEDOT:PSS as the go-to HIL in OLEDs and other organic optoelectronic devices [18], [19]. MoO_3 in particular led to significantly improved EL lifetimes in simplified PhOLEDs [135]. The issue however with transition metal oxides is that their solubility is extremely limited and are thus typically deposited by vacuum thermal evaporation [17]. Though work has begun to overcome solubility limitations, [136]–[138], most solution-processed OLEDs still rely on PEDOT:PSS HILs.

2.1.1 *Outstanding Questions: Role of PEDOT:PSS in Limiting EL Lifetime*

For the above reason, understanding the contribution of PEDOT:PSS to device degradation in the context of more advanced, modern device structures has become an issue of significant importance. Lee and coworkers have repeatedly demonstrated that combining tetrafluoroethylene-perfluoro-3,6-dioxa-4-methyl-7- octene-sulfonic acid copolymer (PFI) with PEDOT:PSS greatly enhances the efficiency and lifetime of polymer [139] and small-molecule [140], [141] OLEDs. This lifetime improvement is attributed to reduction of the hole injection barrier at the PEDOT:PSS/organic interface, thereby streamlining hole injection into the organic layers and preventing hole accumulation at this interface that otherwise leads to accelerated device degradation [139]–[141]. While hole accumulation at the PEDOT:PSS/organic interface may be a contributing factor, it is difficult to generalize this mechanism to HTL materials with a wide range of HOMO levels and thus different injection barriers. For example, devices with NPB HTLs (HOMO ~5.2 eV [142]) have a very small injection barrier at the PEDOT:PSS/NPB interface, since the work function of ITO/PEDOT:PSS is ~5.1 eV [143]. Therefore, hole accumulation at this interface would be negligible compared to PEDOT:PSS/carbazole interfaces typically found in phosphorescent devices, which may have injection barriers up to 1 eV [40], [144]. Indeed, the hole accumulation mechanism seems to be highly dependant on the choice of HTL and not specifically the use of PEDOT:PSS.

Double-stacked PEDOT:PSS/MoO$_3$ hole injection layers led to improved lifetime in ultraviolet OLEDs [145]. This was once again related to hole injection barrier reduction without further analysis of alternative possible degradation mechanisms. This is likely due to the extremely poor stability of ultraviolet OLED materials; thus making them unsuitable for understanding the role of PEDOT:PSS in the degradation of OLEDs in a broader context. Moreover, the proposed hole accumulation mechanism cannot explain the relatively long lifetimes realized with poly[(9,9-dioctylfluorenyl-2,7-diyl)-co-(4,4′-(N-(4-sec-butylphenyl)diphenylamine)] (TFB) interlayers coated on PEDOT:PSS, which have a larger hole injection barrier than NPB [146]. Finally, in all these cases, the ITO/PEDOT:PSS interface remains unmodified, making it difficult to discern its possible role in PEDOT:PSS-related device degradation in more recent OLED device structures. It is therefore evident that the existing understanding the role of PEDOT:PSS in device degradation has many gaps and thus demands a more detailed and systematic approach directed specifically to PEDOT:PSS. This constitutes the first objective of this research work, as outlined in Chapter 3.

2.2 Solution versus Vacuum Processing of non-HIL OLED Layers

To examine the influence of solution-based processing on EL lifetime, the key differences between vacuum and solution processed organic films must first be understood. These differences are reviewed in the first sub-section. Soluble small molecule HTL and EML materials are now making it possible to identify these differences since the same materials may be used to compare vacuum deposition and solution processing. With such an understanding, correlations to device efficiency and lifetime and degradation mechanisms (as outlined in the second sub-section) can become possible.

2.2.1   *Film Properties of Solution versus Vacuum-Processed Small Molecule Organic Films*

Film density, molecular orientation and thermal stability (glass transition temperature) are widely considered the three essential parameters in evaluating the suitability of organic films for devices. In general, vacuum deposited, small-molecule organic films exhibit high densities, a high degree of horizontal molecular orientation and high thermal stability [147]. These properties are those that initially made vacuum deposition the preferred technique for OLED fabrication [148]. It is therefore critical to examine these parameters in solution-processed films. Studies of the film density of solution-based films suggest that their density is consistently lower than that of their vacuum deposited counterparts, as demonstrated by Shibata and coworkers for Alq$_3$, CBP and a several other organic small molecular materials [147]. The decrease in film density for solution coated films has been attributed to increased aggregation and thus free-space voids within the films; which have been shown to lead to poor device lifetimes in OLEDs with solution-based EMLs [14].

With respect to molecular orientation (**Figure 2.1**), vacuum-deposited films were shown by Yokoyama and coworkers to have a high degree of horizontal molecular orientation [149], which has been correlated to improved charge transport and optical outcoupling in OLEDs [150]. Horizontal molecular orientation, also known as face-on orientation, facilities π-π stacking, thereby improving charge transport across the organic layer, leading to higher efficiencies and longer device lifetimes [151]. Solution-coated films on the other hand tend to have a more random molecular orientation [147], [151]. It is worth noting however that the extent to which this limits the efficiency and lifetime of solution-processed devices remains a question of considerable debate, with film density [152] and thermal stability [153] often considered the more important parameters.
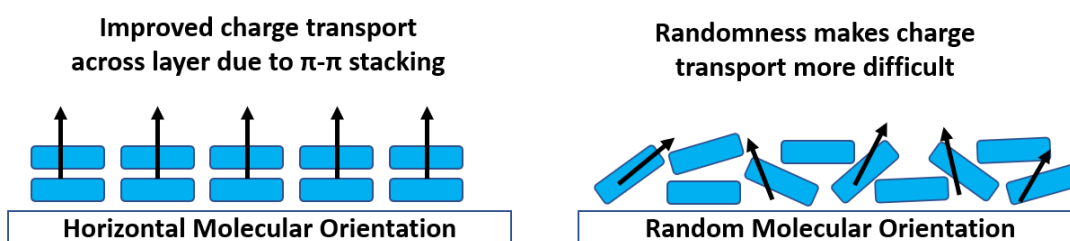
Figure 2.1: Concept of horizontal/face-on molecular orientation.

Finally, high thermal stability is an essential requirement for achieving long EL lifetimes [153]. This is characterized by the glass transition temperature (Tg), i.e.: the temperature at which molecules in amorphous materials gain sufficient energy to move out of their frozen, "glassy" state and re-arrange themselves into a more crystalline state [154]. Tokito and coworkers first demonstrated the correlation of Tg to thermal stability in triphenylamine (TPA)/Alq$_3$ OLEDs by examining various oligomeric (i.e.: dimer, trimer, tetramer, pentamer) forms of TPA as the hole transport layer and subjecting them to heating during device operation [155]. The "critical temperature" at which device EL output decreased dramatically was remarkably close to the Tg for each material. Later studies on various hole transporting small molecular materials confirmed this result [156], [157]. Though the Tg is an intrinsic material property, i.e.: does not change if the material is in the solid state versus dissolved in solution, studies of cyclic heating and cooling of vacuum processed versus solution-coated films show that the vacuum ones are more thermally stable when the same materials are used [147].

This observation has been attributed to the surface self-diffusion of vacuum-processed films: During vacuum deposition, molecules on the surface of the film have on the order of seconds to arrange themselves in a stable, ordered confirmation before the next layer of molecules arrives, resulting in films with high densities [147], [158]. Solution-processed films on the other hand, cannot benefit from this mechanism. The molecules in these films are rapidly solidified in place following deposition and annealing (to accelerate the removal of solvent), with equally "frozen" surrounding molecules limiting their ability to form a stable, ordered confirmation and leaving voids in the films.

While these two contrasting film formation mechanisms highlight the of higher thermal stability and film density of vacuum-deposited films, some materials will form better solution-processed films than others. This is once again dependant on the Tg: Solution-processable small molecules should have high Tg to avoid crystallization during the annealing step [15]. This can be achieved by utilizing molecules that are less planar or have more steric hinderance ("bulky" groups) that limit π-π stacking. For example, referring to **Table 1.1**, CBP is less bulky than TCTA, and also has a lower Tg (62℃ [159]) compared to 151℃ for TCTA [76]. Indeed solution-processed TCTA has been shown to form stable enough solution-processed films to obtain reasonable device efficiency, though lifetime data is still lacking [151], [160]. While limiting π-π stacking may appear counterintuitive from the established understanding of the best-performing vacuum-deposited small molecules, a highly crystallized organic layer leads to the formation of aggregates [14] which may be sufficiently large to short the device.

From the work outlined above, solution-coated films tend to have lower film density and thermal stability and lack horizontal molecular orientation compared to their vacuum counterparts. While an understanding of the origins of these differences has emerged, their consequences for device efficiency and EL lifetime of solution-processed OLEDs remain unclear. Very few correlations between film properties and device characteristics have been made thus far, particularly with respect to EL lifetime. This makes it very difficult to assess the impact of these key differences on device characteristics. As outlined later in Section 2.2.3, it is also not clear what aspects (i.e.: solvents, annealing treatments, atmosphere, etc.) of the solution-coating process are responsible for these poor film characteristics and potentially also EL lifetimes. It is therefore evident that further work is required to facilitate film/device correlations and ideally use them to improve the EL lifetime of solution-coated devices.

2.2.2   Known Degradation Mechanisms in Solution-Processed OLEDs

As mentioned previously, most studies on solution-processed OLEDs have tended to focus on device efficiency, with little attention paid to EL lifetime. However, two degradation mechanisms previously observed in vacuum processed devices have been found to limit the EL stability of solution processed devices more than their vacuum deposited counterparts, namely exciton-polaron interactions [10] and exciton-induced aggregation [11].

Exciton-polaron interactions (EPIA) have been found to induce aggregation in a variety of wide-bandgap host materials [161] and phosphorescent and fluorescent guest emitters [162]. Summarizing from ref. [161], the mechanism proceeds as follows: During electrical driving, both charges (i.e.: polarons) and excitons will exist in the OLED. In hole transport materials for example, positive polarons (i.e.: holes) may interact with excited host molecules (i.e.: excitons on host molecules or monomers) and form a host molecule that has *both* an exciton and polaron. This molecule is now at an unstable high-energy state since it has an electron in its LUMO and an unoccupied HOMO. This excess energy may then be transferred to a neighboring molecule to reach a more stable energy state, forming a dimer. Repeating this process many times results in aggregate formation in the host/hole-transport material. These aggregates/dimers have narrower bandgaps than that of the monomer and thus produce red-shifted EL emission relative to the monomer band and have also been shown to increase charge trapping and act as quenchers, thereby reducing the efficiency and increasing the driving voltage of the device over time [161].

Recently, EPIA was found to be more significant in solution-processed devices compared to vacuum deposited ones [10]. In this study, the EL degradation behaviour of vacuum and solution processed phosphorescent OLEDs utilizing three host materials, CBP, TCTA and 4,4′-Cyclohexylidenebis[*N,N*-bis(4-methylphenyl)benzenamine] (TAPC) with and without an $Ir(ppy)_3$ guest were compared. As per previous findings [161], host aggregation was found to lead red-shifted aggregate EL bands of increasing intensity over time in both doped and undoped cases; proceeding to a greater extent for the solution devices. The presence of EPIA in these devices was confirmed by studies of "hole-only" devices with the structure $ITO/MoO_3/host/TPBi/MoO_3/Al$, where the host was CBP or TAPC. Under forward bias (defined as the ITO being held at a more positive potential relative to the Al), the MoO_3 adjacent to the Al cathode blocks electron injection, making holes the predominant charge carriers in these devices.

These hole-only devices were subjected to three different stress scenarios, namely current driving only (I only), UV irradiation only (L only) or both combined (I + L). For the I-only scenario, only positive polarons are present in the stack. For the L-only scenario, singlet excitons are formed in the host material since the wavelength of UV irradiation is selected such that it is sufficiently high enough in energy (i.e.: greater than the bandgap) to induce the π-π* transition in the given host molecules. Finally, in the I + L scenario, both polarons and excitons are present at the same time, thereby facilitating EPIA. Since hole-only devices do not emit light, their degradation is characterized by changes in driving voltage at a constant current over time, as shown in **Figure 2.2**. The I + L scenario was found to lead to a much faster increase in driving voltage than either of the I only or L only scenarios for all host materials and vacuum/solution devices. Taking the algebraic sum of the I only and L only curves, i.e.: Σ (I + L), resulted in a substantially lesser increase in driving voltage compared to the I + L case, confirming that both excitons and polarons are needed to accelerate device degradation. Most interestingly, plots of (I + L) - Σ (I + L) for both host materials (**Figure 2.2 (c) and (d)**) demonstrated a much more dramatic increase in driving voltage for solution devices compared to their vacuum counterparts. These results demonstrated one of the root causes of the poor EL lifetime of solution-processed devices for the first time.
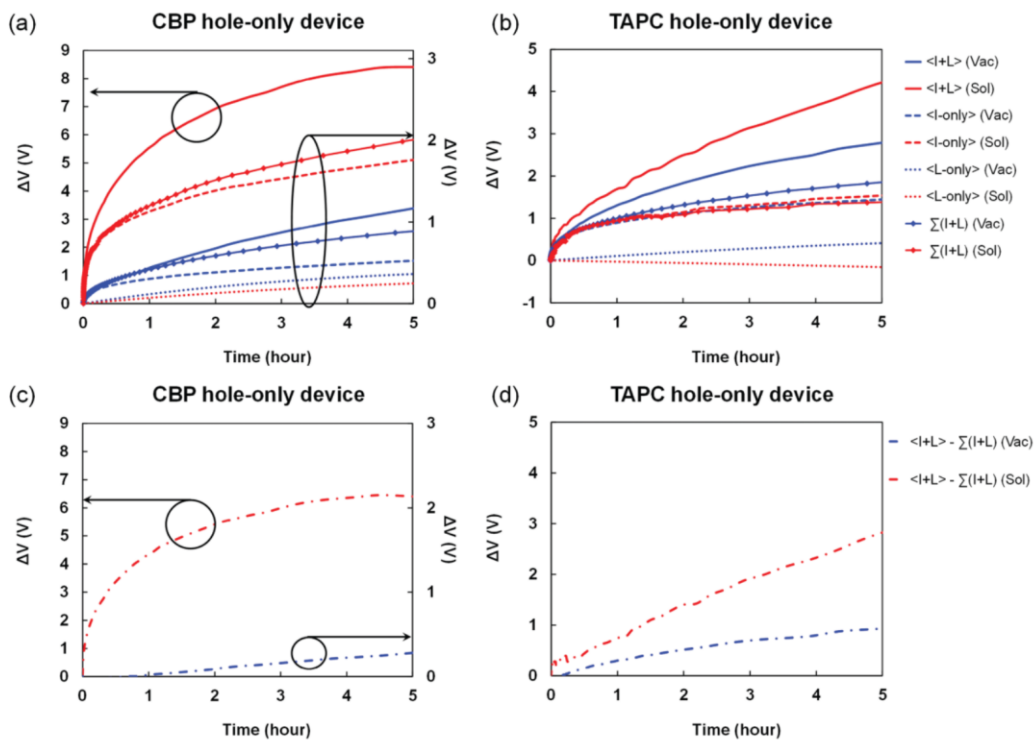
Figure 2.2: (a), (b) Changes in driving voltage under 5 mA/cm² constant current driving for (a) CBP and (b) TAPC for all test conditions; (c), (d) the corresponding values for the quantity {ΔV for <I + L> – ∑(ΔV for <I> +ΔV for <L>)} for the same traces. Reproduced from ref. [10] with permission.

Shortly thereafter, the same authors examined the effect of excitons on solution and vacuum-deposited carbazole films typically found in phosphorescent OLEDs by subjecting these materials to prolonged UV irradiation [11]. As mentioned previously, UV irradiation leads to the formation of singlet excitons and thus facilitates the examination of the effects of excitons without the confounding effects of current flow. Results from this study showed that UV-irradiated solution and vacuum-deposited films both had red-shifted PL spectra relative to un-irradiated controls, demonstrating that excitons alone lead to the formation of aggregate species. This red-shift however was significantly more pronounced in the solution-processed film. While these aggregates led to a decrease in PLQY and exciton lifetime (as demonstrated by transient PL data) of both films, the solution-processed film experienced these to a significantly greater extent. Similar effects were observed for CBP films doped with Ir(ppy)₃ as found in typical simplified PhOLEDs.

Interestingly, the extent of the exciton-induced aggregation (i.e.: changes in PL spectra) in the solution-coated films varied depending on the solvent used, as shown in **Figure 2.3**. This suggests that the solvent itself may influence initial film morphology, thereby making the solution-coated devices more susceptible to exciton-induced degradation. While one might initially speculate that residual solvent left over in the films may be behind these morphological changes, the decrease in exciton lifetime observed in each case did not correspond to the boiling points of the solvents used—as shown in **Figure 2.4,** the chloroform-based film exhibited the greatest decrease in exciton lifetime but did not have the highest boiling point. The authors also point out that care was taken during the experimental procedure to remove residual solvent by including an annealing step following deposition of the solution-coated films. To investigate the possibility that solvents induced morphological changes in solution-processed films, vacuum films were prepared and subjected to solvent vapours to see if similar morphological changes to those observed in the solution-processed films would occur. The exciton lifetime of these solvent-exposed films was remarkably similar to that of the solution-processed film, suggesting that aggregation had indeed occurred with solvent-exposure. These results convincingly demonstrate that solution-coated and vacuum-deposited films have different morphologies, and that film morphology influences susceptibility to exciton-induced aggregation.
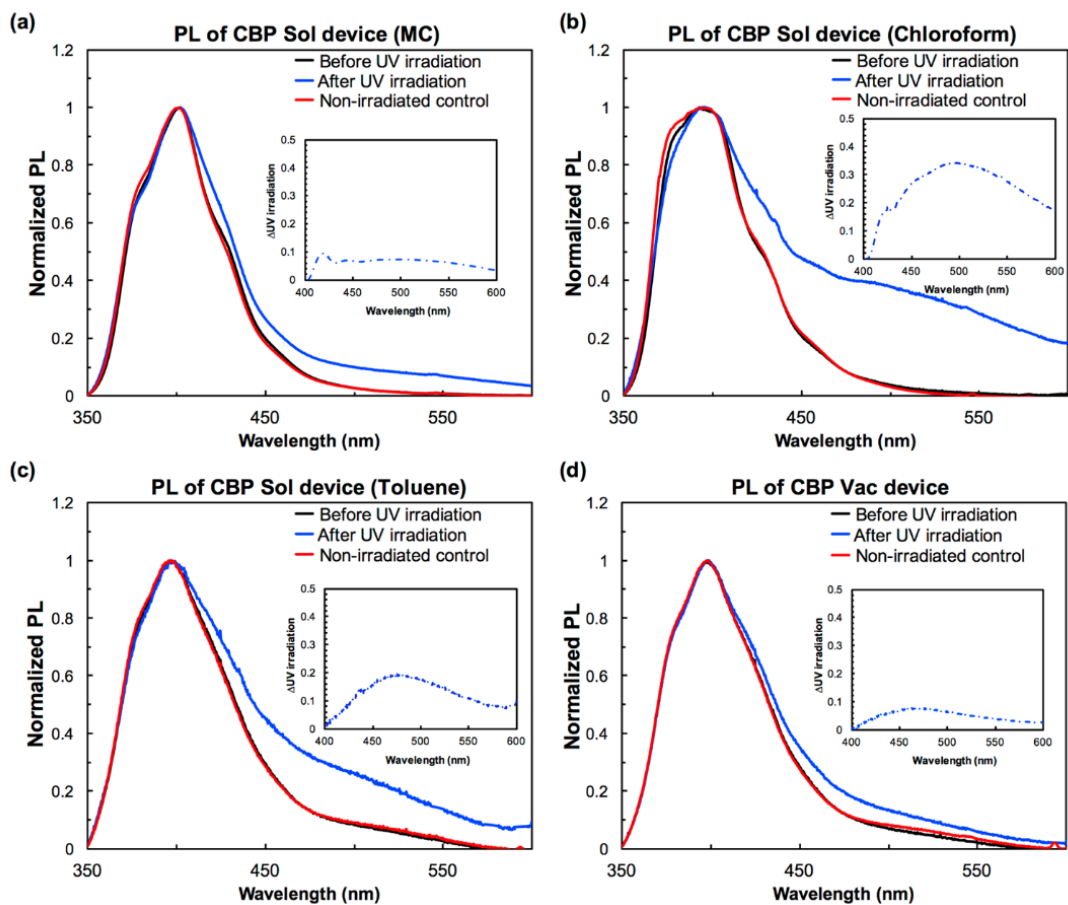
Figure 2.3: Normalized PL spectra collected from solution-coated CBP films with (a) dichloromethane (MC), (b) chloroform, and (c) toluene and (d) vacuum-deposited test samples before and after the UV irradiation. Insets: The net change in the spectra, obtained by subtracting the "before UV irradiation" spectrum from the "after UV irradiation" spectrum in each case. Reproduced from ref [11] with permission.
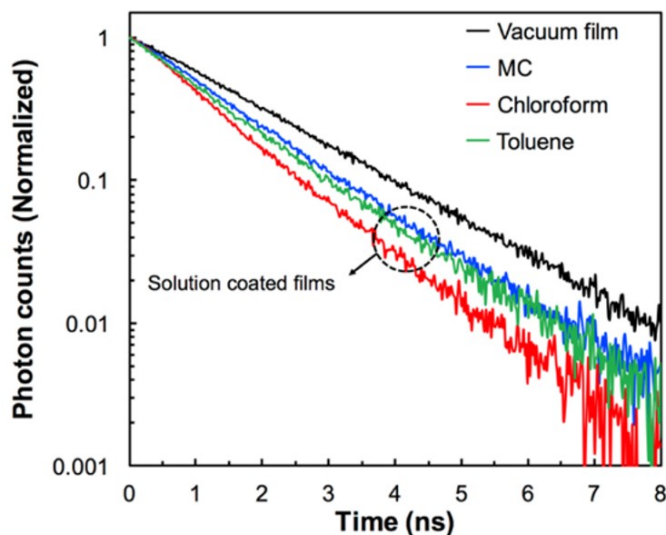
Figure 2.4: Exciton lifetime of vacuum-deposited and solution-coated CBP films using dichloromethane (MC), chloroform, or toluene solvents. Reproduced from ref [11] with permission.

2.2.3 *Outstanding Questions: Influence of Solvents and Solution-Coating Parameters on EL Lifetime*

In contrast to vacuum deposited films, where high density, favourable horizontal molecular orientation and high thermal stability have been definitively shown to correlate to high device efficiencies and long EL lifetimes, there appears to be a trade-off between charge transport properties (π-π stacking) and thermal stability and film density in solution-coated films. Moreover, the importance of molecular orientation in solution-coated films is unclear because solution-coated films overwhelmingly favour a random orientation; making this parameter extremely difficult to control. For these reasons, it has been very difficult to correlate film properties to device efficiency and EL lifetime in solution-processed OLEDs. Studies of solution-coated films and devices tend to focus on one or the other, with emphasis on device efficiency and not EL lifetime: Except for the work in the preceding section, very little is known about why solution-coated OLEDs have poor EL lifetimes compared to their vacuum counterparts. This work has also tended to focus on films and not full OLED devices, making it difficult to asses the potential impact of these degradation mechanisms on the device level. These works also do not consider the possible influence of the HIL on film morphology (and hence possible susceptibility to degradation mechanisms) since evaporated MoO_3 is used exclusively as the HIL

.

Further, evaporated MoO_3 is not a feasible HIL for solution-coated devices for two reasons: It may be eroded or chemically changed on exposure to solvents and atmospheric conditions, and more importantly, it is not compatible with a fully-integrated roll-to-roll process. Finally, the existing body of work on solution-processed OLEDs does not consider what specific aspects (e.g.: solvents, annealing treatments, atmosphere, drying conditions etc.) of the solution process may contribute to the morphology observed in solution-coated films and lead to poor efficiency and lifetime. Solvents are of special interest because they are one of the most fundamental factors behind solution-based processes (e.g.: spin-coating, blade-coating, printing), making it critical to understand their possible contribution to device degradation and EL lifetime. Since other parameters (e.g.: annealing) may vary among different solution processing methods, it is essential to isolate the effect of solvents from these other parameters. Investigating these issues is critical for understanding degradation mechanisms in these solution-processed devices and how they can potentially be mitigated, and thus constitutes the second objective of this work, as outlined in Chapter 3.

Chapter 3: Research Objectives

The overarching goal of this research is to understand the impact of solution-processable hole injection layers and solvent use with heating treatments on the EL lifetime of vacuum-deposited, small-molecule organic light-emitting devices. All OLEDs in this study are fabricated by vacuum deposition to investigate the effects of the specific process parameter independent of the multitude and variability of other parameters (e.g.: drying conditions, solubility, solution concertation) involved in most solution-processing methods.

The specific objectives of this work may be summarized as follows:

1) In consideration of solution-processed PEDOT:PSS hole injections layers:

   a) Elucidate the root causes of the lower stability of OLEDs with PEDOT:PSS HILs;

   b) Investigate possible strategies to mitigate them;

2) In consideration of the specific role of solvents and baking/high-temperature annealing treatments frequently utilized for solution-processing:

   a) Their effect on the morphology of vacuum-deposited small molecules in the context of device efficiency and EL lifetime for phosphorescent and fluorescent OLEDs with different HTLs;

   b) Examine the influence of the HIL on the treatment-induced morphological effects from a);

   c) For HIL/HTL combinations sensitive to treatment-induced effects as per a) and b), illustrate possible strategies to mitigate treatment-induced morphological effects.

Chapter 4 - The Root Cause of the Lower EL Lifetime with PEDOT:PSS HILs: Electron-Induced Degradation

Chapter Summary

This chapter addresses the first objective of this work, elucidating the root causes of the lower stability of OLEDs with PEDOT:PSS HILs and investigating possible strategies to prevent or mitigate them. Towards this end, the causes of degradation resulting from device operation (i.e.: under electrical bias) in OLEDs with common hole transporting materials and PEDOT:PSS hole injection layers (HILs) are systematically investigated. Results demonstrate that the acidity of PEDOT:PSS is not singularly responsible for device degradation and that species present during device operation have a very significant impact on the EL lifetime of these devices. We first demonstrate that a PEDOT:PSS/MoO$_3$ hole injection layer in place of PEDOT:PSS alone results in a ~20x improvement in the EL lifetime of phosphorescent OLEDs with a CBP hole transporting layer (HTL). In contrast, a less significant effect was observed in fluorescent OLEDs with NPB HTLs. Electrical aging of hole-only devices shows that hole accumulation at the HIL/HTL interface does not play a major role in device degradation. Results from UV irradiation tests show that excitons are also not primarily responsible for this degradation. However, when electrons are introduced into the hole-only stack, significant degradation parallel to that occurring in full (i.e. bipolar) devices is observed; and is subsequently prevented using electron-blocking layers. These results demonstrate that the degradation of PEDOT:PSS HILs by electrons plays an important role in limiting the EL lifetime of OLEDs, particularly those utilizing HTLs with weak electron-blocking characteristics, such as CBP; and further emphasizes the importance of such characteristics in the development of novel hole transporting and electron blocking materials. The findings provide new and critical insights into degradation mechanisms in OLEDs utilizing PEDOT:PSS HILs and considerations for future device design.

4.1 Introduction

PEDOT:PSS (poly(3,4-ethylenedioxythiophene)-poly(styrenesulfonate) has long been a mainstay in hole injection and extraction layers of organic optoelectronic devices such as organic light emitting devices (OLEDs) and organic solar cells (OSCs) because of its solution processability [17], [96], [134], [141], [165]. Despite its promise, PEDOT:PSS is known to be a significant source of instability in these devices [141], [166]–[168] as its acidic nature leads to reactions with underlying ITO electrode [132]. Replacing PEDOT:PSS hole injection layers (HILs) by transition metal oxides such as MoO_3 [19], [135], [169], [170] has been widely used as an alternative to get around the ITO etching issue. However, given the rise of solution-processed OLEDs, PEDOT:PSS HILs still have a crucial role to play.

While reactions at the PEDOT:PSS/ITO interface may account for the relatively lower stability of devices utilizing PEDOT:PSS HILs, this phenomenon does not readily explain the shorter electroluminescence (EL) lifetime (i.e. under electrical bias) of these devices. It is therefore worth exploring alternative sources of instability that may be present during device operation.

To that end, it has been demonstrated that gradient hole injection layers (so-called GraHILs), made using a Nafion-based polymer blend with PEDOT:PSS, greatly enhance the efficiency and lifetime of polymer [139] and small-molecule [140], [171] OLEDs. By reducing the hole injection barrier and streamlining hole injection into the organic layers, hole accumulation at the PEDOT:PSS/organic interface was eliminated, thereby leading to longer device lifetimes [139], [140], [171]. Another approach using a "double HIL" of PEDOT:PSS/MoO_3 was recently shown to improve the efficiency and durability of ultraviolet OLEDs [145]. Beyond this, there has been relatively little work on the degradation of PEDOT:PSS in the context of device operation. The effects of electron bombardment on PEDOT and PSS with high-energy electrons have been studied via x-ray photoelectron spectroscopy [127], [130]. Studies of ultraviolet-induced degradation of PEDOT and its derivatives have also been carried out [172]. Though these studies investigate the effect of species similar to those present during device operation, the role of PEDOT:PSS in limiting the EL lifetime of OLEDs remains poorly understood.

In this work, we systematically investigate the causes of degradation resulting from device operation in OLEDs with common hole transporting materials and PEDOT:PSS HILs. The results demonstrate that electron-induced degradation of PEDOT:PSS HILs plays an important role in limiting the EL lifetime of OLEDs. Findings also show that this degradation can be overcome via electron-blocking layers or by employing hole transport materials with low electron mobility as HTLs.

37

4.2 Experimental Methods

In this work, two device structures are examined, a phosphorescent device with the structure ITO/HIL/CBP (30 nm)/CBP:Ir(ppy)$_3$ (5%, 15 nm)/TPBi (40 nm)/LiF (1 nm)/Al (80 nm) and a fluorescent device with the structure ITO/HIL/NPB (60 nm)/Alq$_3$ (40 nm)/LiF (1 nm)/Al (80 nm). TPBi (2,2,2"-(1,3,5-benzinetriyl)-tris(1-phenyl-1-H-benzimidazole) and Alq$_3$ (Tris-(8-hydroxyquinoline)aluminum) are used as the electron transport layers in the phosphorescent and fluorescent devices respectively. Tris(2-phenylpyridine)iridium(III) (Ir(ppy)$_3$) is used as the guest emitter in the phosphorescent device; Alq$_3$ functions as the emitting material in the fluorescent device. PEDOT:PSS and MoO$_3$ are used as hole injection materials and LiF is used as an electron injection layer for both types of devices. Indium tin oxide (ITO) and Al are used as the anode and cathode contacts respectively. CBP, NPB, Alq$_3$ and TPBi were obtained from Shanghai Hang Feng Chemical Co., Ir(ppy)$_3$ was obtained from Luminescence Technology Corp. 2-tert-Butyl-9,10-di(naphth-2-yl)anthracene (TBADN, Shanghai Hang Feng Chemical Co.), Tris(1-phenylisoquinoline)iridium(III) (Ir(piq)$_3$, Luminescence Technology Corp) and Tris(4-carbazoyl-9-ylphenyl)amine (TCTA, Shanghai Hang Feng Chemical Co.) were also used. All materials were used as obtained. PEDOT:PSS (Sigma Aldrich, 2.8 wt. % dispersion in H$_2$O, low conductivity grade) was prepared by diluting with 2-propanol in a 1:5 volume ratio and filtering with a 0.22 μm PTFE filter. Devices were fabricated on ITO patterned glass substrates (15 Ω/sq, Kintec); these were sonicated in deionized water/Micro-90 solution for 10 min and treated with O$_2$ plasma for 5 min prior to use. PEDOT:PSS was spin coated at 5000 rpm for 60s and annealed at 130°C for 30 min under ambient conditions. All other materials were deposited via thermal evaporation at a base pressure < 5x10^{-6} Torr using an Angstrom Engineering EvoVac system at a deposition rate of 0.1-2 Å/s.

Current-voltage-luminance measurements were carried out using an Agilent 4155C Semiconductor Parameter Analyzer connected to a silicon photodiode. An Ocean Optics QE65000 spectrometer was used to measure the electroluminescence spectra of the OLEDs. All EL lifetime tests were carried out at a current density of 20 mA/cm^2 using a custom lifetime test setup. The devices were kept in N$_2$ atmosphere at all times.

4.3 Effect of PEDOT:PSS HIL on Lifetime of CBP Phosphorescent OLEDs

We first investigate and compare the EL lifetime and device characteristics of phosphorescent OLEDs with PEDOT:PSS (30 nm thick) and MoO_3 (5 nm thick) HILs, the latter a common alternative HIL to PEDOT:PSS. We also include a device with a PEDOT:PSS/MoO_3 HIL which was recently shown to improve the efficiency and EL lifetime of ultraviolet OLEDs [145]. With the exception of the HIL, the rest of the organic stack remained the same, forming OLEDs with the device structure ITO/HIL/CBP (30 nm)/ CBP:Ir(ppy)$_3$/TPBi (40 nm)/LiF (1 nm)/Al (80 nm). For EL lifetime measurements, all devices were driven at a constant current density of 20 mA/cm^2. **Figure 4.1** gives the current density versus voltage **(a)**, external quantum efficiency (EQE) versus current density **(b)**, and EL lifetime characteristics representing relative changes in luminance and driving voltage over time under constant current driving **(c)** of the devices. For the stability traces, normalized luminance is plotted on the primary y-axis and the change in driving voltage (ΔV) with respect to the initial (time zero) driving voltage is plotted on the secondary y-axis. From **Figure 4.1 (c),** the PEDOT:PSS device clearly has much lower stability compared to the MoO_3 device, despite the two devices being otherwise identical in terms of materials and device fabrication process. The PEDOT:PSS device has a luminescence half-life (LT50, defined as the time elapsed until the luminance decreases to half its initial value under constant current driving), of 53 min, compared to ~40 hours for the MoO_3 device. This observation suggests that PEDOT:PSS may be responsible for a substantial component of device degradation. However, the device with the PEDOT:PSS/MoO_3 HIL has a remarkably longer EL lifetime; with an LT50 of 17.5 hrs, ~20x longer than the PEDOT:PSS device (LT50 = 53 min).

Initially, one might speculate that the faster degradation is simply due to the acidity of PEDOT:PSS, which is known to lead to poor device stability due to erosion of the underlying ITO electrode. However, observations from the PEDOT:PSS/MoO_3 EL lifetime characteristics suggest that this is not the case. Since the ITO/PEDOT:PSS interface is present in both cases, any adverse effects resulting from PEDOT:PSS on the ITO electrode would be the same. The significant difference in EL lifetime of the two devices therefore precludes the possibility that erosion of the underlying ITO electrode by PEDOT:PSS is behind the lower stability of the PEDOT:PSS HIL device and indicates that additional degradation mechanisms must be at play, consistent with recent reports [139], [140], [171].

A close examination of the current density versus voltage (**Figure 4.1 (a)**), EQE versus current density (**Figure 4.1 (b)**) and change in driving voltage versus time traces **Figure 4.1 (c)**) reveals some additional interesting trends. **Figure 4.1 (a)** shows that the PEDOT:PSS/MoO$_3$ device has significantly lower leakage current than with the PEDOT:PSS HIL. Further, the ΔV-t trace for the PEDOT:PSS device is significantly steeper than that of the PEDOT:PSS/MoO$_3$. A steep ΔV-t trend indicates that progressively higher bias voltages are required to drive the device at the given current (i.e: 20 mA/cm^2). This signifies deterioration of charge injection and transport in the device, an effect that may be associated with the shorter LT50 of the PEDOT:PSS device. When MoO$_3$ is placed in between PEDOT:PSS and CBP, the ΔV-t rise becomes much slower, resembling that of the MoO$_3$ only case, and a substantially longer LT50 is realized. This slower ΔV-t rise means that charge injection and transport do not significantly degrade in these devices over time. Together, these findings suggest that the PEDOT:PSS/HTL interface, which exists only in the case of the PEDOT:PSS device, may play a crucial role in the limited EL lifetime of these devices.
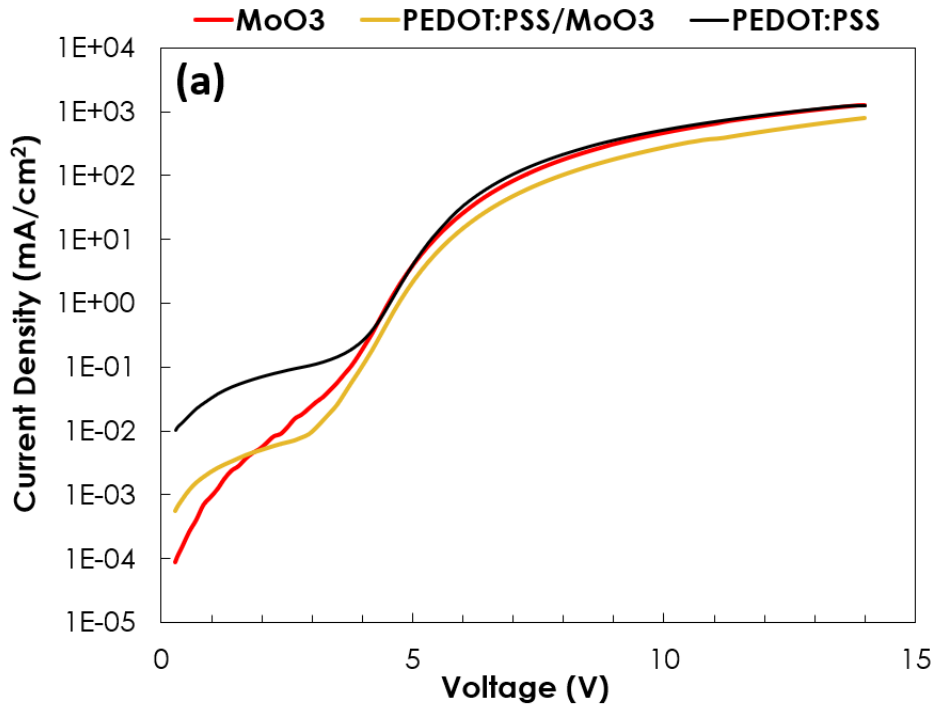
Figure 4.1: (a) Current versus voltage, (b) EQE vs. current, (c) EL lifetime characteristics (relative changes in luminance and change in driving voltage versus time traces under 20 mA/cm^2 constant current driving) of OLEDs with PEDOT:PSS (black), MoO$_3$ (red) and PEDOT:PSS/MoO$_3$ (yellow) hole injection layers.

4.4 Effect of PEDOT:PSS HIL on Lifetime of NPB Fluorescent OLEDs

To investigate if the PEDOT:PSS/HTL interface has a similar effect on the EL lifetime in fluorescent OLEDs with non-CBP HTLs, the EL lifetime and device characteristics of OLEDs with a PEDOT:PSS, MoO_3, or a PEDOT:PSS/MoO_3 HIL were compared in a fluorescent device with the structure: ITO/HIL/NPB (40 nm)/Alq_3 (60 nm)/LiF (1 nm)/Al (80 nm). The current density versus voltage **(a)**, EQE versus current density **(b)**, and EL lifetime characteristics **(c)** of the devices are given in **Figure 4.2**. At voltages below the turn-on voltage (V < 3 V), the current density versus voltage curves of the PEDOT:PSS and PEDOT:PSS/MoO_3 devices are very similar. Unlike the previous case, there is negligible difference in leakage current between the two devices. The EQE versus current density plots in **Figure 4.2** are also remarkably similar for the PEDOT:PSS and PEDOT:PSS/MoO_3 devices. Their EQE remains relatively constant over all current densities, consistent with the similar leakage current for both devices. What is strikingly different from the previous case however is that the EL lifetime characteristics of the three devices (**Figure 4.2 (c)**) are very similar, and all exhibit more stable ΔV-t trends relative to the previous set of devices. The contrast in EL lifetime characteristics of the two sets of devices suggests that the HTL material influences the role of the PEDOT:PSS/HTL interface with respect to device degradation; indicating that certain degradation factors are present under electrical bias for devices with the PEDOT:PSS/CBP interface but are less prevalent in those with the PEDOT:PSS/NPB interface.

To understand the differences between the two interfaces, we first consider the energy level mismatch between the HOMO (highest occupied molecular orbital) of the HTLs and the work function of the various HILs. It is widely known that depositing MoO_3 on ITO results in a substantial increase in work function [19], [135], [169], [170]. Since CBP has a relatively deep HOMO (~6 eV [144], [173]), the increase in work function leads to a reduced hole injection barrier at the MoO_3/CBP interface that facilitates hole injection into the device, an effect that would lead to improved stability according to previous reports [169]. A separate investigation of ITO/PEDOT:PSS/MoO_3 contacts demonstrated a work function of 6.1 eV [174], which also aligns closely with the CBP HOMO. In contrast, the work function of the ITO/PEDOT:PSS contact is ~5.1-5.2 eV [143], leading to a hole injection barrier between PEDOT:PSS and CBP as large as 1 eV. This large injection barrier can lead to hole accumulation at the PEDOT:PSS/CBP interface, possibly leading to degradation of PEDOT:PSS by the accumulated holes [139], [140], [171]. On the other hand, the HOMO of NPB (~5.2 eV [142]) is close to the ITO/PEDOT:PSS work function, making the hole injection barrier at the PEDOT:PSS/NPB interface very small; which would streamline hole injection and prevent accumulation at this interface.

Therefore, considering all of the findings thus far and the energy level/work function alignment of the relevant materials, it is possible that the absence of hole accumulation in the NPB devices and in the CBP devices with PEDOT:PSS/MoO$_3$ HILs may be the source of the improved EL lifetime characteristics in these devices compared to those with PEDOT:PSS HILs.
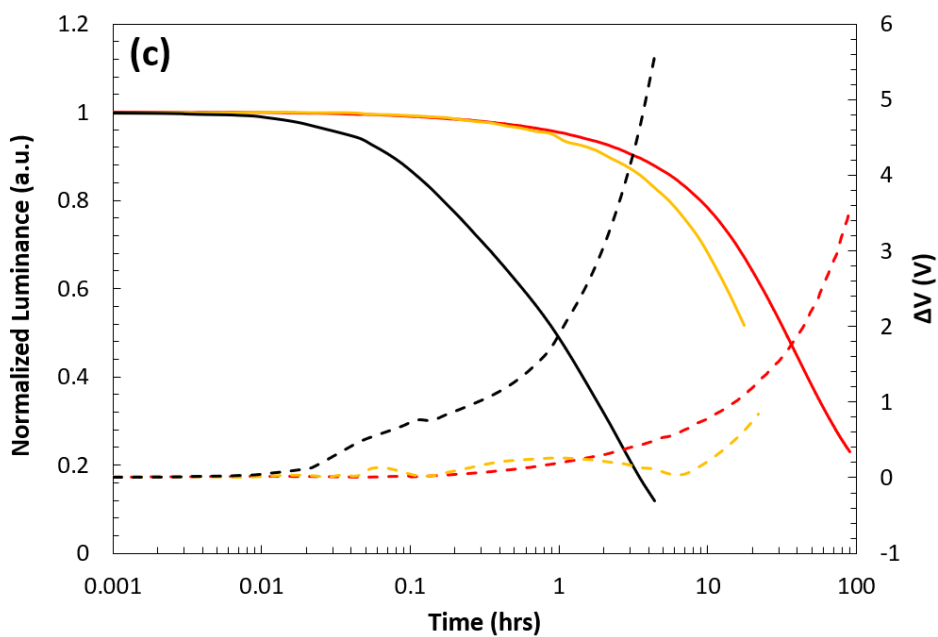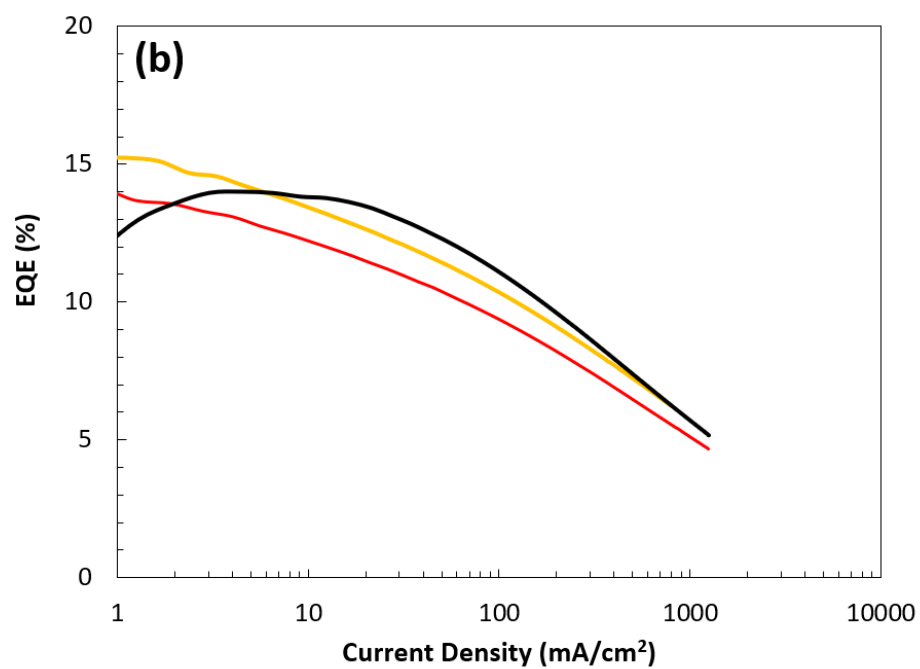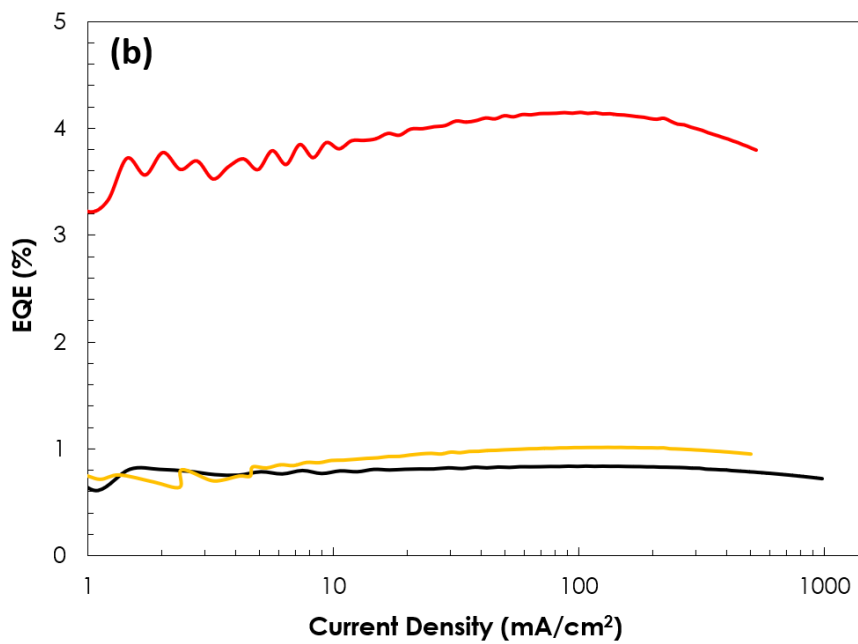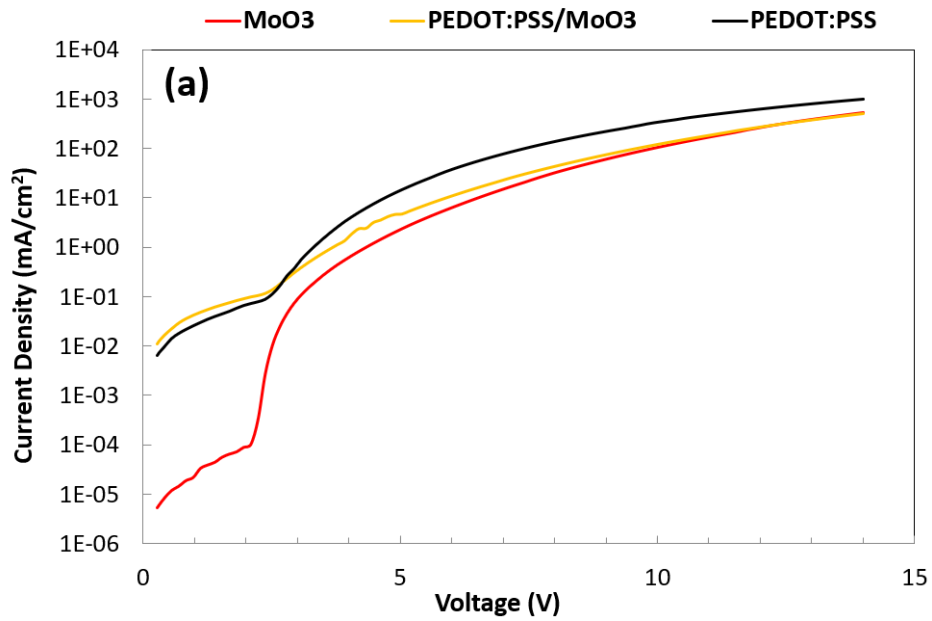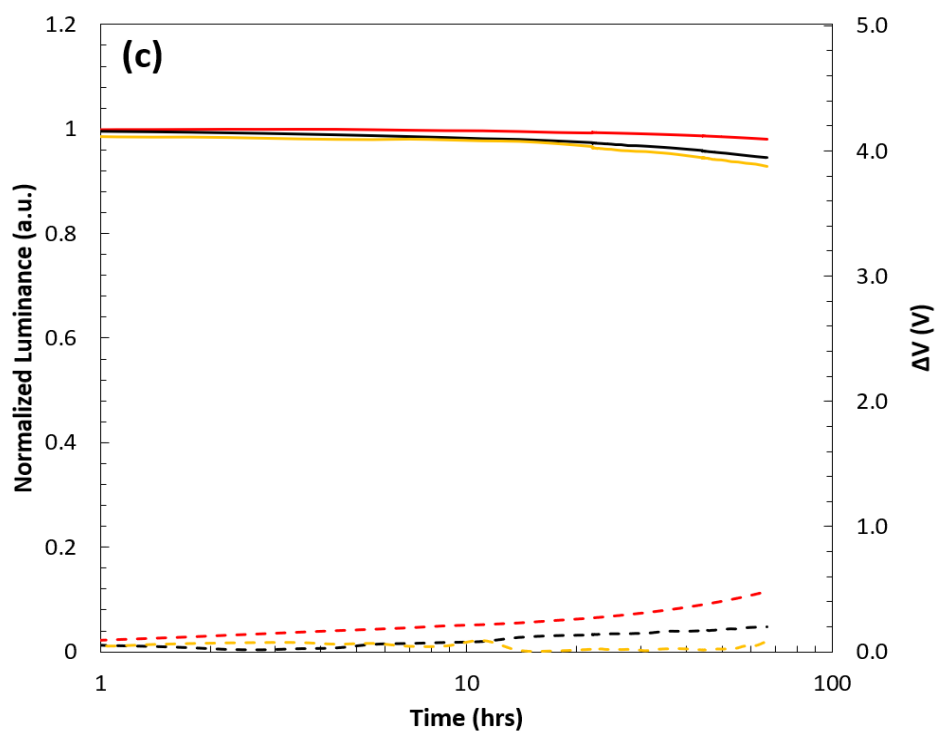
Figure 4.2: a) Current versus voltage, b) EQE vs. current, c) EL lifetime characteristics (relative changes in luminance and change in driving voltage versus time traces) of OLEDs with PEDOT:PSS (black), MoO_3 (red) and PEDOT:PSS/MoO_3 (yellow) hole injection layers.

4.5 Investigating the Role of Holes

To investigate the role of hole accumulation as a possible degradation mechanism, the change in voltage over time and device characteristics of hole-only devices with CBP or NPB hole HTLs and PEDOT:PSS or PEDOT:PSS/MoO$_3$ HILs are compared. The structure of the hole-only devices was ITO/HIL/HTL (40 nm)/MoO$_3$ (5 nm)/Al (80 nm). The MoO$_3$ layer adjacent to the Al contact acts as an electron blocking layer. Therefore, under forward bias, defined as holding the ITO contact at a more positive potential relative to Al contact, holes are injected from the ITO contact, transported across the stack then collected at the Al contact. On the other hand, the injection of electrons from the top contact is blocked by MoO$_3$, making holes the predominant charge carrier in these devices. In this way, we may interpret the following results as being primarily connected with hole injection and transport. **Figure 4.3 (a)** gives the current density versus voltage characteristics of these devices; the change in voltage over time (ΔV-t) at a constant drive current density of 20 mA/cm^2 is given in **Figure 4.3 (b)** and an energy band diagram of the relevant materials is given in **Figure 4.3 (c).**

From **Figure 4.3 (a)**, the current density at a given voltage is much lower for the CBP-PEDOT:PSS case as compared to the other three cases. This is likely attributable to the significantly larger injection barrier present for this case as previously discussed and as illustrated in the energy band diagram in **Figure 4.3 (c)**. However, examining the ΔV-t curves in **Figure 4.3 (b)**, there is very little (< 25 mV) change in voltage over time for all cases, indicating that changes in the charge injection and transport characteristics of the devices are negligible; especially when compared with those of the CBP OLEDs in **Figure 4.3 (c).** Since holes are the predominant charge carriers in these devices and do not appear to cause deterioration of charge injection and transport, they are most likely not responsible for the degradation observed in the CBP OLEDs with the PEDOT:PSS HIL. Consequently, the hole accumulation mechanism at the PEDOT:PSS/CBP interface cannot be the principal cause of degradation in that device.

(a)

Legend: CBP, PEDOT:PSS — NPB, PEDOT:PSS — CBP, PEDOT:PSS/MoO3 — NPB, PEDOT:PSS/MoO3

Axes: Hole Current Density (mA/cm²) vs Voltage (V)

(b)

Axes: ΔV (V) vs Time (hrs)

46
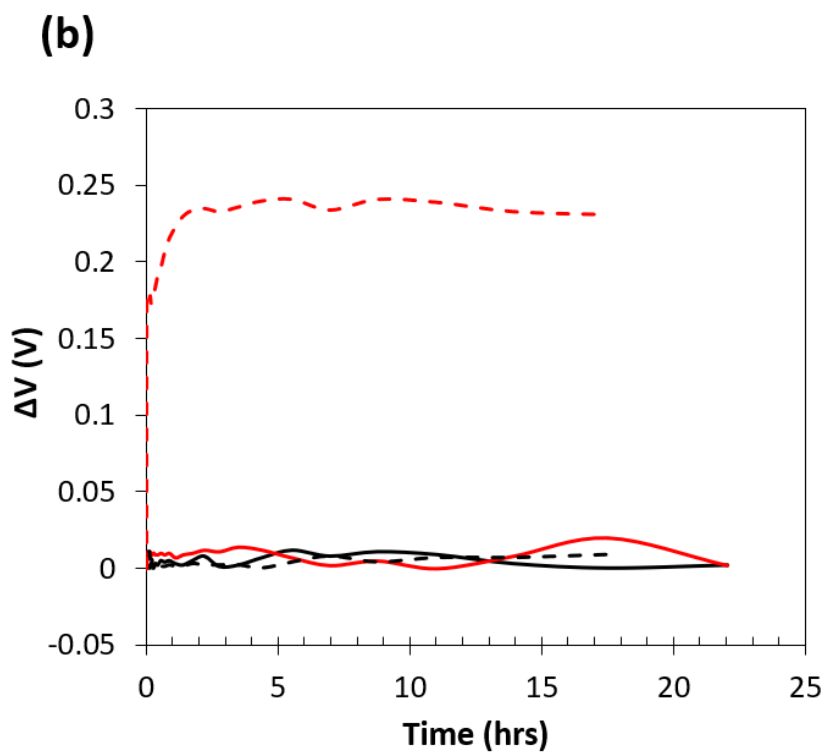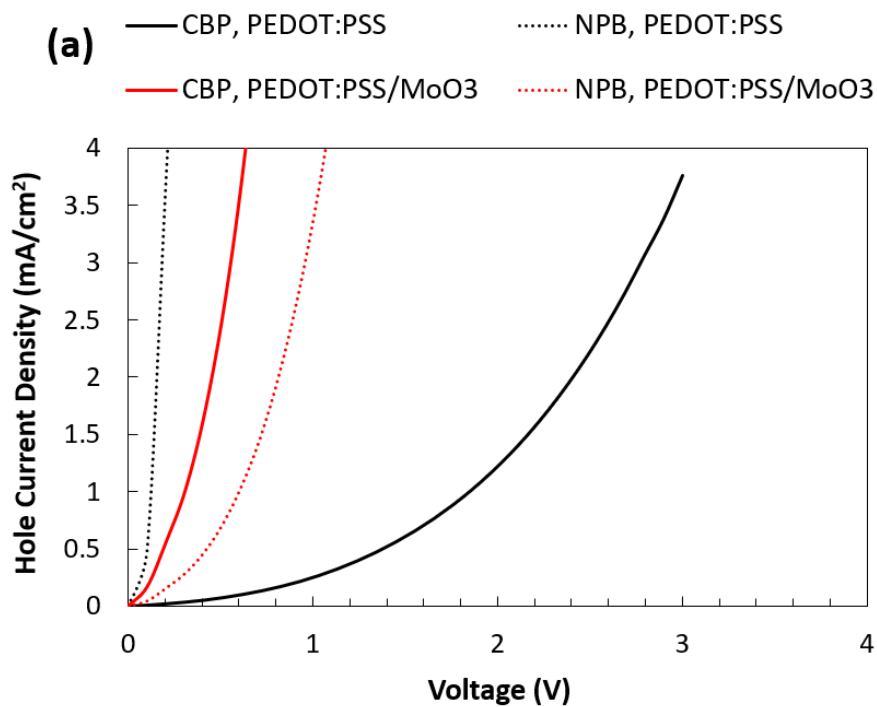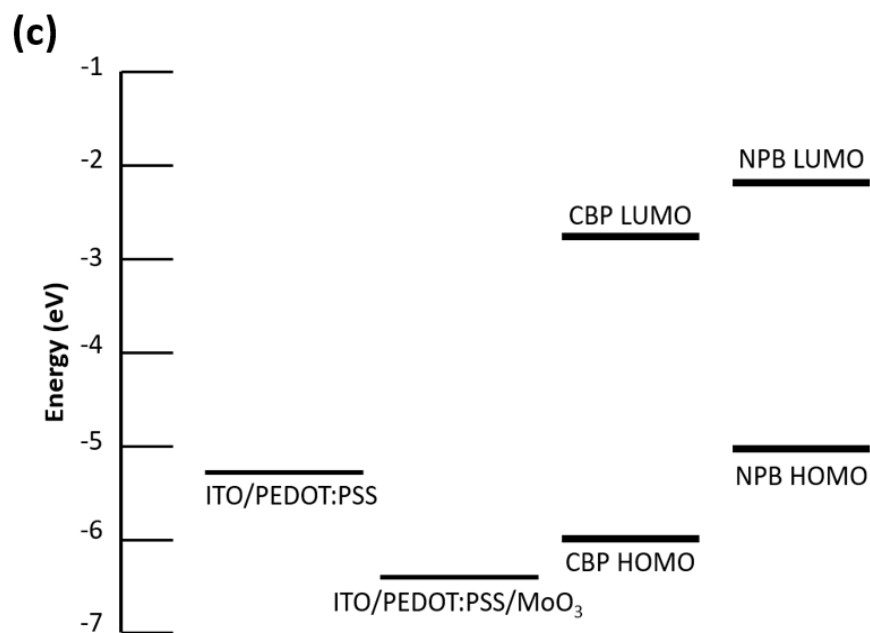
Figure 4.3: a) Current density versus voltage characteristics, and b) Change in voltage versus time under constant current driving of 20 mA/cm^2 of the hole-only devices discussed in the text; c) Energy band diagram of NPB and CBP with the two HIL contacts.

4.6 Investigating the Role of Excitons

Having established that holes are not the primary source of degradation in the CBP OLEDs with the PEDOT:PSS HIL, it becomes important to investigate the possible role of other species that are present during device operation. It is known that excitons and electrons can lead to degradation in some hole injection materials, and therefore their presence in significant concentrations in the vicinity of HILs can be detrimental to device stability [175], [176]. **Figure 4.4** gives the EL spectra of the CBP OLEDs with PEDOT:PSS and PEDOT:PSS/MoO$_3$ HILs. Clearly, the device with the PEDOT:PSS HIL has detectable EL emission in the 390-430 nm range, which corresponds to CBP emission [177]. In contrast, the device with the PEDOT:PSS/MoO$_3$ HIL has relatively less EL in the same wavelength range, which can be attributed to exciton quenching by MoO$_3$ [178]. These observations suggest that excitons are indeed present near the HIL in case of devices with a CBP HTL, in agreement with previous reports [175].

To further verify this notion, we fabricate and test a device with a fluorescent marking layer placed adjacent to the HIL. TBADN (2-tert-Butyl-9,10-di(naphth-2-yl)anthracene), a blue fluorescent material, is used as the marking layer. The device structure is: ITO/PEDOT:PSS (30 nm)/CBP:TBADN (5%, 15 nm)/CBP (30 nm)/CBP:Ir(piq)$_3$ (5%, 15 nm)/TPBi (40 nm)/LiF (1 nm)/Al (80 nm). In this device, tris(1-phenylisoquinoline)iridium(III) (Ir(piq)$_3$) is used as the guest emitter in place of Ir(ppy)$_3$ due its longer wavelength emission (λ_{peak} = 620 nm) which makes it easier to distinguish the TBADN emission (λ_{peak} = 470 nm). The EL spectrum of this device is included in **Figure 4.4**. TBADN emission (430-500 nm) is clearly observed in this case, corroborating the earlier conclusion. Given that excitons are clearly present near the HIL interface, it is quite possible that they play a role in the faster degradation of the CBP OLEDs with the PEDOT:PSS HILs.
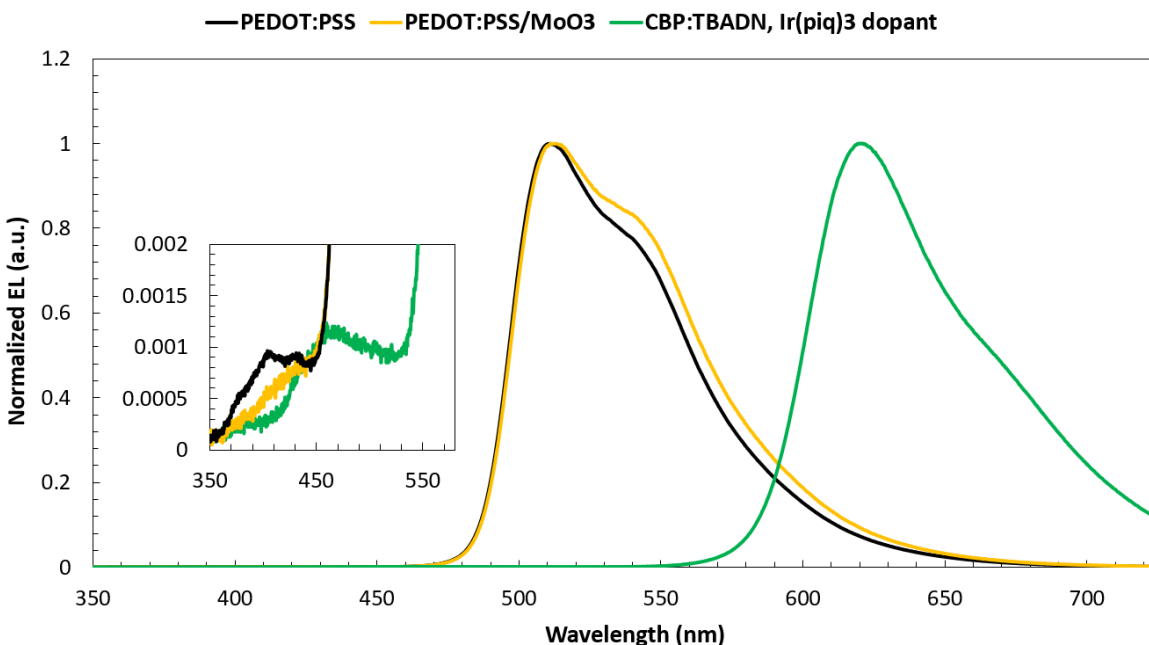
Figure 4.4: EL spectra of CBP OLEDs with PEDOT:PSS and PEDOT:PSS/MoO$_3$ HILs. EL spectrum of the OLED with the TBADN marking layer (with Irpiq$_3$ as the guest emitter) is also included. Inset: Enlarged view of the EL spectra in the 350-550 nm range.

In general, the presence of excitons in the vicinity of the HIL could result from either i) the diffusion of excitons from the electron-hole recombination zone of the device towards the HIL, or ii) the drift of un-recombined electrons towards the HIL and their recombination with holes in the HTL resulting in the formation of excitons near the HIL. In this context, the faster degradation of devices with the PEDOT:PSS/CBP interface could be a result of degradation of the interface by either excitons or electrons. Therefore, to first investigate the possible role of excitons, the previously described hole-only devices with PEDOT:PSS and PEDOT:PSS/MoO_3 HILs and CBP or NPB HTLs were exposed to UV irradiation (λ = 365 nm at 2.3 mW/cm^2) for a 24-hour period. 365 nm (~3.4 eV) was selected because it can induce the $\pi\rightarrow\pi^*$ transition in both CBP and NPB, and thus produce excitons with energy typical of those produced by electrical driving. The current density-voltage characteristics of these devices were measured before and after the UV irradiation and no significant changes were observed. This indicates that exciton damage has a negligible effect on the charge injection and transport characteristics of the device and likely does not play a major role in the lower EL lifetime observed in PEDOT:PSS/CBP OLEDs.

4.7 Investigating the Role of Electrons

Having ruled out holes and excitons as the main degradation agents in OLEDs with the PEDOT:PSS HIL and CBP HTLs, it follows that the effect of electrons should be examined. For this purpose, we compare between the ΔV-t trends under constant driving current conditions at 20 mA/cm^2 of the hole-only devices described above and another set of devices that are in all respects similar to the hole-only devices except that the MoO_3 electron blocking layer is replaced with LiF. Replacing the MoO_3 by LiF allows for electron injection from the Al contact to occur under forward bias. Thus, any differences between the two devices may be directly related to the presence or absence of electrons. The structure of these devices is therefore ITO/HIL/CBP (100 nm)/LiF (1 nm)/Al (80 nm) with the HIL as PEDOT:PSS or PEDOT:PSS/MoO_3.

The ΔV-t traces for these devices and the previously discussed CBP hole-only devices are compared in **Figure 4.5**. As shown previously, the voltage rise of the PEDOT:PSS hole-only device (MoO$_3$/Al top contact) is negligible (change in voltage < 12 mV) over the test period. On the other hand, its counterpart with an electron-injecting top contact demonstrates a much faster rise in voltage (> 1V, i.e. two orders of magnitude higher). Since the only difference between the two devices is the nature of the top contact, i.e.: electron-injecting LiF versus electron-blocking MoO$_3$, the observed voltage rise can be directly attributed to the presence of electrons. The faster voltage rise means that more bias is required to drive these devices at the same current over time, implying deterioration in charge injection and/or charge transport properties. Conversely, the ΔV-t behaviour of the LiF/Al and MoO$_3$/Al top contacts for devices with the PEDOT:PSS/MoO$_3$ HIL is nearly identical. This demonstrates that electron injection does not cause significant degradation in this case and proves that the voltage rise in the earlier case is indeed due to the effect of electrons on the PEDOT:PSS and not due to degradation phenomena at the CBP/LiF/Al contact. CBP is known to have bipolar charge transport properties with an electron and hole mobilities of 3×10^{-4} cm^2/Vs and 2×10^{-3} cm^2/Vs respectively [41]. It is therefore quite possible for unrecombined electrons to diffuse towards the PEDOT:PSS/CBP interface and cause degradation. Previous studies have shown that electrons can lead to a decrease in the conjugation of the PEDOT and thus a deterioration in charge transport properties [127], [129]–[131]. Further, bond-breaking effects induced by electrons to PEDOT:PSS results in the release of reactive, mobile oxygen atoms [130] as well as oxygen and sulphur-containing [129]–[131] moieties that can diffuse within the organic stack, chemically modifying the organic materials and influencing charge transport. This degradation is prevented when the MoO$_3$ layer is introduced in between the PEDOT:PSS and CBP (i.e., the case of devices with PEDOT:PSS/MoO$_3$ HIL) due to the electron-blocking nature of MoO$_3$ which prevents electrons from reaching the PEDOT:PSS, hence the increased ΔV-t stability.

This conclusion is further corroborated by the lower leakage current observed for the PEDOT:PSS/MoO$_3$ device compared to that with the PEDOT:PSS HIL in **Figure 4.1 (a).** It is worth noting that this leakage current results in lower EQE at current densities less than 10 mA/cm^2 in the device with the PEDOT:PSS HIL compared to that with PEDOT:PSS/MoO$_3$ HIL as shown in **Figure 4.1 (b)**. At low injection currents, the effect of leakage is more pronounced, resulting in lower EQE for the PEDOT:PSS HIL. As the ratio of injection current to leakage current increases, the EQEs of devices with the three HILs become similar.
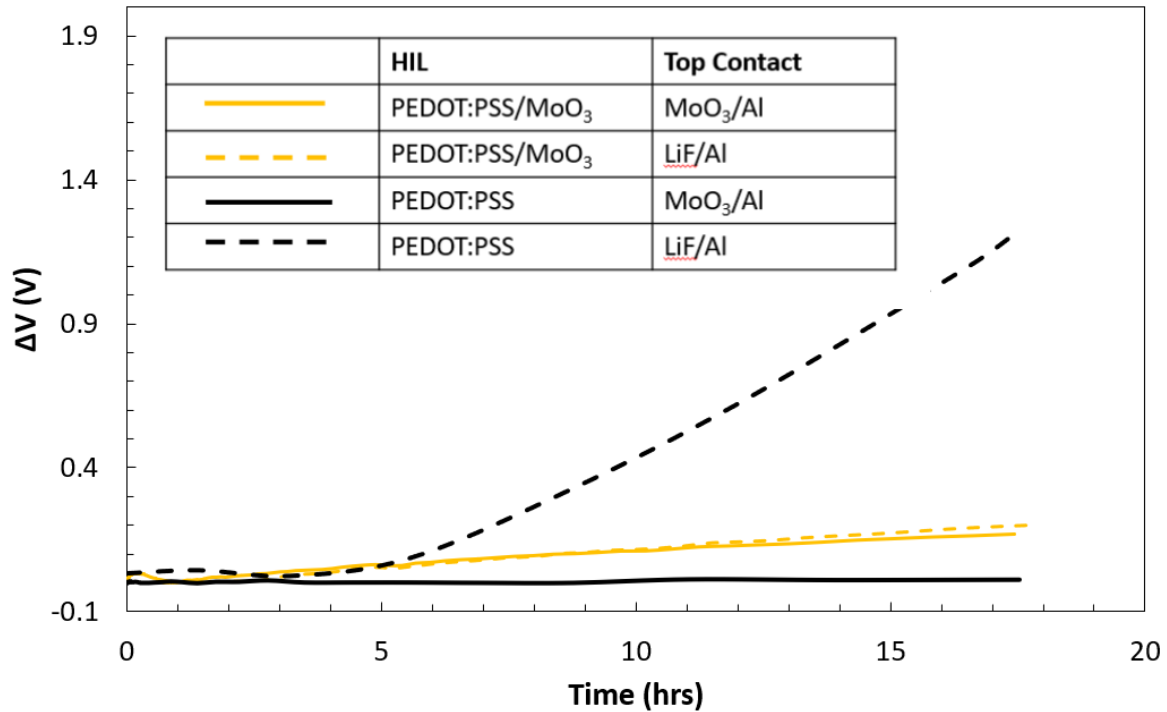
Figure 4.5: Change in driving voltage over time under 20 mA/cm^2 constant driving current for the hole-only devices described in the text and the corresponding devices with the electron-injecting top contact.

4.8 Effect of Using Electron-Blocking HTLs

To further verify that electron-induced degradation of PEDOT:PSS is the main cause of the lower EL stability of the devices with PEDOT:PSS HILs and CBP HTLs and that the increase in EL lifetime upon introducing MoO$_3$ in between PEDOT:PSS and HTL is due to the electron-blocking nature of MoO$_3$, we investigate the effect of replacing MoO$_3$ with NPB. Due to its limited electron mobility (μ_e) and highly unipolar charge transport characteristics (NPB hole mobility, $\mu_h \sim 10^{-3}$ cm^2/Vs [15]), NPB can be expected to efficiently block electrons. However, the bandgap of NPB is smaller than that of CBP ($E_g = 2.9$ eV [142] and 3.1 eV [179] for NPB and CBP, respectively), thus it should not block excitons. Therefore, if preventing electrons from reaching the PEDOT:PSS HIL is the main mechanism behind the observed EL lifetime improvement, we would expect to see similar results upon replacing MoO$_3$ with NPB in the phosphorescent device stack. We therefore fabricate and test the EL lifetime characteristics of devices with the structure ITO/PEDOT:PSS (30 nm)/NPB (x nm)/ CBP (30 nm)/ CBP:Ir(ppy)$_3$/TPBi (40 nm)/LiF (1 nm)/Al (80 nm) where x = 0, 10, 20 or 30 nm.

51

Figure 4.6 shows results from these tests, demonstrating that the device EL lifetime indeed increases significantly upon introducing the NPB layer. A 17x improvement in LT50 is immediately realized upon introducing a 10 nm NPB layer. For 30 nm NPB, LT50 improves by a factor of 25. These improvements are on the same order of those observed with the PEDOT:PSS/MoO$_3$ HIL as compared to PEDOT:PSS alone (~20x). The ΔV-t traces were much less steep for all devices with NPB. Due to the 0.8 eV hole injection barrier between NPB and CBP (**Figure 4.3 (c)**), voltage changes (ΔV) in these devices are greater than those observed in the device with the PEDOT:PSS/MoO$_3$ HIL since higher voltages are needed to reach a drive current of 20 mA/cm^2. It should be noted that this injection barrier also creates a hole-blocking interface adjacent to the NPB layer, making the NPB/CBP interface conducive to hole accumulation. Despite this, significant LT50 improvement and much reduced voltage rise is observed, proving that hole accumulation does not significantly contribute to device degradation. Together, the 11-fold decrease in voltage rise and improved LT50s observed with NPB demonstrate that blocking electrons from reaching PEDOT:PSS prevents degradation. These results explain the stark difference between the EL lifetime characteristics of devices with CBP vs NPB HTLs (i.e., the data in **Figure 4.1 (c)** and **Figure 4.2 (c)** respectively), and indicate that when PEDOT:PSS is used as HIL, approaches for minimizing electron leakage through the HTL must be taken. Finally, it is worth noting that this progressive improvement in LT50 with increasing NPB thickness also shows that the degradation observed in CBP OLEDs with PEDOT:PSS HILs is not due to morphological factors at the interface, such poor wetting of PEDOT:PSS by the CBP. If this were the case, the LT50s of these devices would be similar regardless of the NPB thickness.

We also conducted surface roughness measurements of the PEDOT:PSS, PEDOT:PSS/MoO$_3$ and MoO$_3$ films by atomic force microscopy. The images are shown in **Figure 4.7**. The results show RMS roughness's of 1.98, 2.22, 2.92 nm respectively, thus verifying very similar surface morphologies for all three HILs.
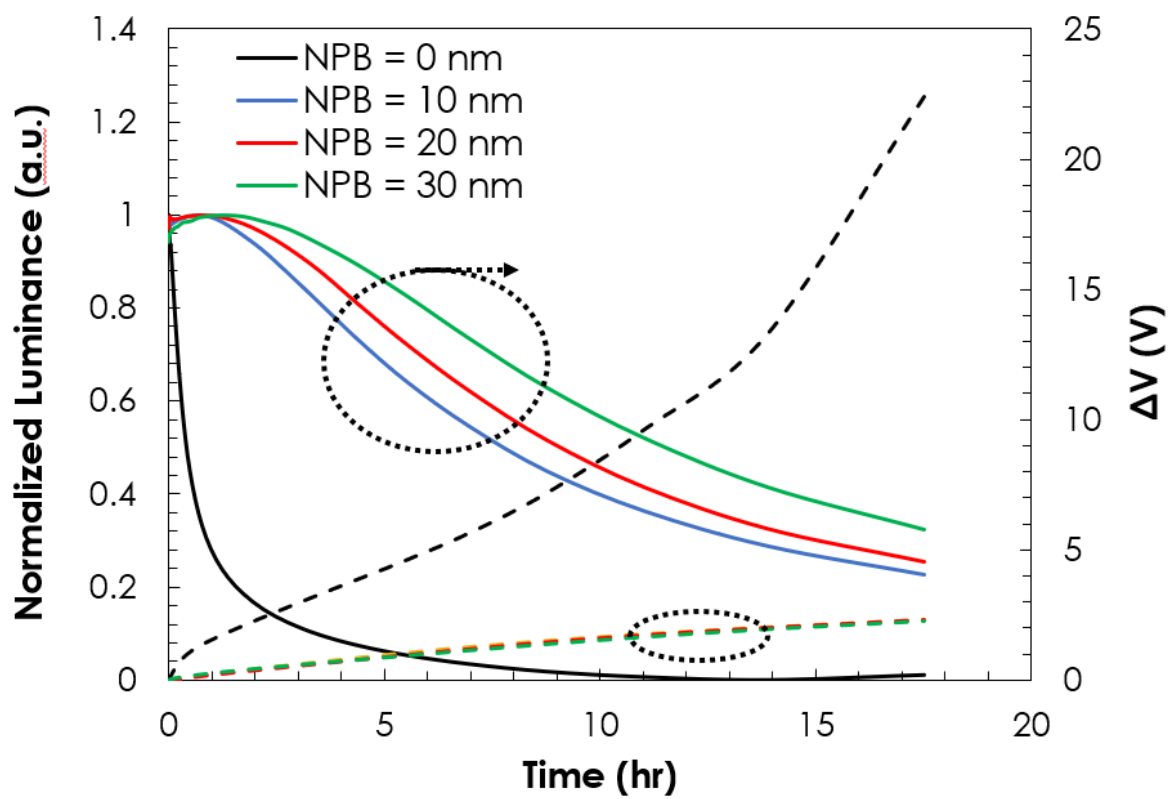
Figure 4.6: EL lifetime characteristics of OLEDs with NPB electron blocking layer of various thicknesses.
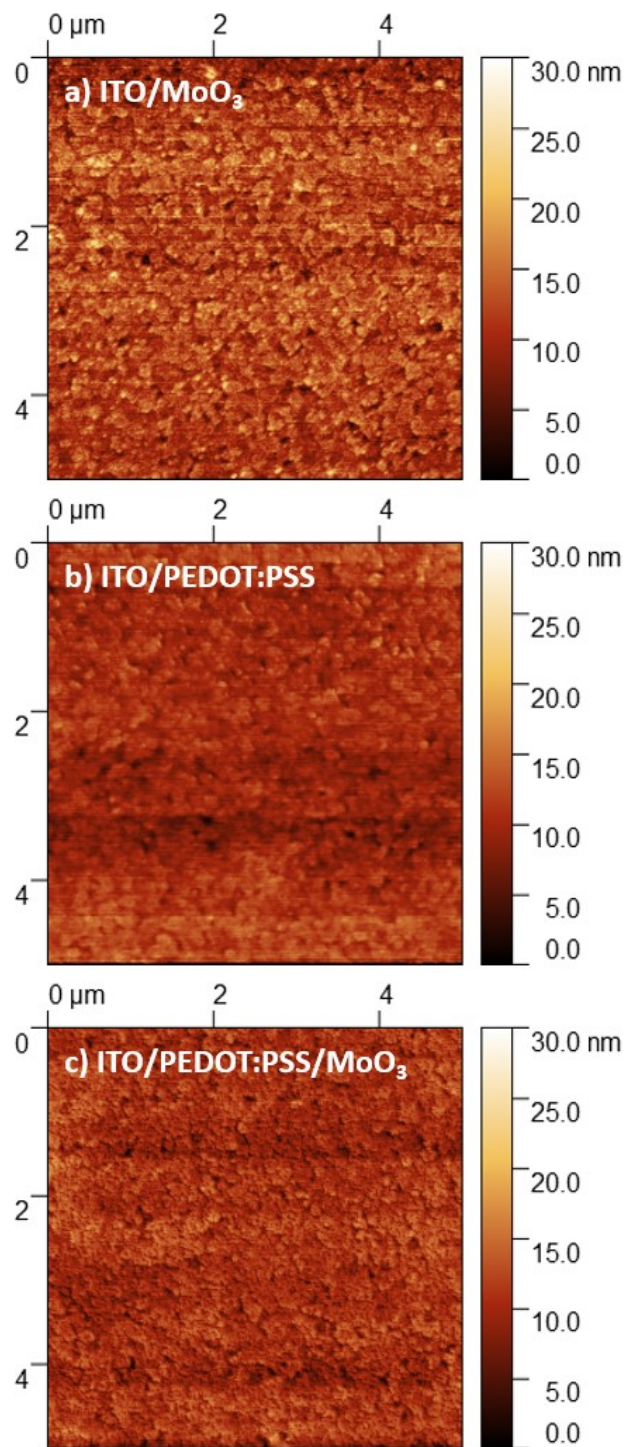
Figure 4.7: AFM images of (a) MoO$_3$ on ITO, (b) PEDOT:PSS on ITO and (c) PEDOT:PSS/MoO$_3$ on ITO.

To further verify that reducing electron leakage to PEDOT:PSS is the mechanism behind the improvement in EL lifetime observed in **Figure 4.6,** the lifetimes of PEDOT:PSS OLED devices with TCTA in place of CBP were investigated and compared in **Figure 4.8** (i.e.: ITO/PEDOT:PSS (30 nm)/CBP or TCTA (30 nm)/ CBP:Ir(ppy)$_3$/TPBi (40 nm)/LiF (1 nm)/Al (80 nm).

TCTA was selected because of its shallower LUMO (2.3 eV [47]) than CBP (~3 eV [179]) that reduces electron leakage from the emissive layer to the HTL. As shown in **Figure 4.8**, a nearly two-fold increase in LT50 is observed for OLEDs with the TCTA HTL along with a shallower voltage rise compared to the CBP case. These results conclusively show that, in addition to electron-blocking layers, the use of HTLs with good electron blocking characteristics (i.e.: shallower LUMOs and/or $\mu_e \ll \mu_h$) is beneficial for EL lifetime in devices with PEDOT:PSS HILs. Although these results were obtained from OLED stacks with CBP and NPB, given the detrimental effect of electrons on PEDOT:PSS, one can expect this phenomenon to affect OLEDs utilizing any HTL material that does not sufficiently block electron leakage to the HIL.
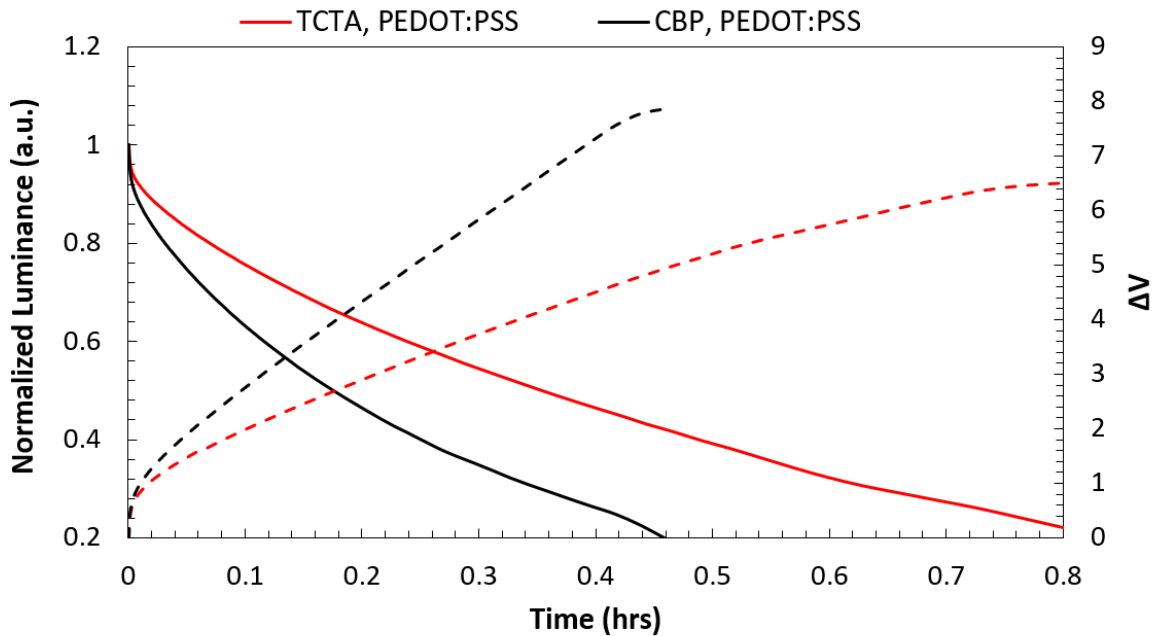
Figure 4.8: EL lifetime characteristics of OLEDs with PEDOT:PSS HILs and TCTA versus CBP HTLs.

4.9 Conclusion

In conclusion, these results show that PEDOT:PSS HILs are susceptible to degradation by electrons; a mechanism that can lead to relatively short EL lifetimes. The use of hole transporting materials and device structures that minimize electron leakage to the HIL leads to significant improvements in device EL lifetime. Furthermore, PEDOT:PSS HILs appear to be less susceptible to degradation by excitons and by hole accumulation at the PEDOT:PSS/HTL interface. These findings provide key insights for improved device design of OLEDs utilizing PEDOT:PSS HILs.

Chapter 5 - Impact of Solvents, Baking Treatments and Hole Injection Layers on the Electroluminescent Lifetime of Organic Light-Emitting Devices with Various Hole Transport Layers

Chapter Summary

This chapter addresses the second objective of this work: First, to explore the effects of solvent and baking treatments frequently utilized in solution processing on the morphology of vacuum-deposited, small molecule hole transport materials in the context of device operation (sub-objective 2a); and second, to investigate the possible influence of the HIL on the morphological changes induced by these treatments on the HTLs given that the HIL plays a key role in device efficiency and lifetime, as shown in the previous chapter (sub-objective 2b). For this purpose, a comprehensive investigation of the effects of solvent and baking treatments on common hole transport (HTL) and host materials in phosphorescent and fluorescent OLEDs utilizing ubiquitous PEDOT:PSS and MoO_3 HILs is conducted in this chapter. Results show that the effects of solvent and baking treatments on device efficiency and EL lifetime vary considerably by HTL/HIL combination. The findings demonstrate that solvent and baking treatments utilized in solution processing can significantly alter device efficiency and EL lifetime because they directly influence film morphology. However, the extent of the morphological changes observed varied by treatment and by the HTL/HIL combination. The most significant changes in device efficiency and EL lifetime were observed for CBP and TCTA with MoO_3 HILs, suggesting that carbazole-based materials are more sensitive to solvent and baking treatments when an MoO_3 HIL is used instead of PEDOT:PSS. Hole-only device analysis corroborates this conclusion, with CBP and TCTA showing a more significant increase hole current density with solvent treatment for both CBP and TCTA on MoO_3 compared to PEDOT:PSS. For the PEDOT:PSS HIL, TCTA appears to be the most resistant to solvent-induced morphological changes, as also reflected in the relatively smaller changes in device EQE and EL lifetime with the treatments. Fluorescent NPB/Alq_3 device EQE and EL lifetime appeared to be most sensitive to baking alone and less sensitive to solvent treatment for both HILs compared to the carbazole materials used for the phosphorescent OLEDs, despite the baking temperature being quite a bit lower than its glass transition temperature. Hole-only analysis demonstrated that hole injection and transport was relatively unaffected by the treatments in these devices. The findings emphasize the importance of the HIL and HTL materials and demonstrate that care must be taken to identify material combinations that are less prone to solvent and baking-induced morphological effects for solution-processed OLEDs.

5.1 Introduction

Organic Light-Emitting Devices (OLEDs) have long promised the possibility of low-cost, solution-based roll-to-roll manufacturing to realize flexible, large-area products for displays and solid-state lighting [9], [86], [180]. However, most commercially available OLED-based products are still fabricated by expensive vacuum-deposition techniques. Though impressive device efficiencies have been achieved for solution-based OLEDs [100], [101], [103]–[106], [181], their significantly lower EL lifetime compared to their vacuum-deposited counterparts remains a considerable obstacle to their commercialization [35], [48]–[52]. Comparisons of organic films fabricated by solution processing versus vacuum deposition have shown that solution films tend to have lower film density, are less thermally stable and are generally more amorphous (i.e.: have less ordered molecular structure) than vacuum-deposited films [15], [147], [182]. These characteristics have been found to significantly influence the morphology of the deposited organic films, which in turn has consequences for device efficiency and EL lifetime [10]–[12], [15], [183]. Despite their amorphous nature, solution-coated films have been shown to have isolated aggregate domains with strong intermolecular interactions, leading to faster deterioration in device EL output over time compared to vacuum deposited devices [12]. More recently, exciton-polaron interactions [10] and exciton-induced [11] degradation were found to play a fundamental role in the limited EL lifetime of solution devices. Beyond this, the body of work on understanding the degradation mechanisms that limit the EL lifetime of solution processed devices remains limited.

Among the key differences between solution and vacuum processing is the use of solvents and high temperature annealing or baking treatments. Given the much reduced EL lifetimes of solution devices, it becomes important to understand the contribution of these parameters to degradation in these devices independent of the specific solution-coating method (e.g.: spin-coating, blade-coating, dip-coating, etc.). To this end, we conduct a comprehensive investigation of the effects solvent on common hole transport (HTL) and host materials in phosphorescent and fluorescent OLEDs utilizing ubiquitous PEDOT:PSS and MoO_3 HILs. The extent of solvent-induced effects may differ for different organic materials, hence the need to survey multiple HTL materials. The findings demonstrate that the effects of the various treatments are highly dependent on the HTL/HIL material combination and have implications for the development of novel hole transporting materials.

5.2 Experimental Methods

Phosphorescent OLEDs with the structure ITO/HIL/HTL (30 nm)/CBP:Ir(ppy)$_3$ (5%, 15 nm)/TPBi (40 nm)/LiF (1 nm)/Al (80 nm) were fabricated, where MoO$_3$ or PEDOT:PSS, TPBi, Ir(ppy)$_3$ and LiF are used as the hole injection, electron transport, guest emitter and electron injection layers respectively. 4,4′-Bis(9-carbazolyl)-1,1′-biphenyl 4,4-N,N′-Dicarbazole-1,1′-biphenyl (CBP) and Tris(4-carbazoyl-9-ylphenyl)amine (TCTA) are used as hole transport materials in the HTLs. Fluorescent OLEDs utilized N,N′-Di(1-naphthyl)-N,N′-diphenyl-(1,1′-biphenyl)-4,4′-diamine (NPB) as the HTL material, while Tris(8-hydroxyquinoline)aluminum (Alq$_3$) served as both the emissive and electron transport layer, forming devices with the structure ITO/ MoO$_3$ (5 nm)/NPB (40 nm)/ Alq$_3$ (60 nm)/LiF (1 nm)/Al (80 nm). LiF and MoO$_3$ are once again used as the electron and hole injection layers respectively. Indium tin oxide (ITO) and Al are used as the anode and cathode contacts respectively. CBP, TCTA, NPB, Alq$_3$, and TPBi were obtained from Shanghai Hang Feng Chemical Co., Ir(ppy)$_3$ was obtained from Luminescence Technology Corp. MoO$_3$ was obtained from American Elements. PEDOT:PSS (Sigma Aldrich, 2.8 wt. % dispersion in H$_2$O, low conductivity grade) was prepared by diluting with 2-propanol in a 1:5 volume ratio and filtering with a 0.22 μm PTFE filter. Devices were fabricated on ITO patterned glass substrates (15 Ω/sq, Kintec); these were sonicated in deionized water/Micro-90 solution for 10 min and treated with O$_2$ plasma for 5 min prior to use. PEDOT:PSS was spin coated at 5000 rpm for 60s and annealed at 130°C for 30 min under ambient conditions. All other materials were deposited via thermal evaporation (base pressure < 5x10^{-6} Torr), using an Angstrom Engineering EvoVac system at a deposition rate of 0.1-2 Å/s.

To test the effect of solvent treatment, the vacuum was broken following deposition of the bottom two thirds of the HTL material. Samples were then exposed to toluene (Sigma-Aldrich) vapours in a sealed container, with the sample taped to the lid for 3 min. Samples were then baked at 60°C for 5 min and re-loaded in the vacuum chamber to complete deposition of the remaining HTL thickness and subsequent layers.

Current-voltage-luminance measurements were carried out using an Agilent 4155C Semiconductor Parameter Analyzer connected to a silicon photodiode. An Ocean Optics QE65000 spectrometer was used to measure the electroluminescence and photoluminescence spectra of the OLEDs, with photoluminescence induced by illumination with a 200 W Hg–Xe lamp controlled with an Oriel-77200 monochromator.

All EL lifetime tests were carried out at a current density of 20 mA/cm^2 using a custom lifetime test setup. Transient photoluminescence response (also known as exciton lifetime) was measured with an Edinburgh Instruments FL920 spectrometer equipped with a 375 nm peak emission EPL375 picosecond pulsed laser diode. Devices were kept in N$_2$ atmosphere throughout fabrication and characterization.

5.3 Effect of Treatments on Performance Characteristics

We begin by investigating and comparing the effects of solvent exposure (3 minutes of exposure to toluene vapour and 5 minutes of baking at 60°C, denoted "Solvent + Bake") and high-temperature annealing only (5 minutes of baking at 60°C, denoted "Bake Only") on the bottom two thirds of the HTL on OLED performance characteristics and EL lifetime to untreated, "Vacuum" controls, labeled "VAC." The sample preparation procedure is illustrated in **Figure 5.1.** PEDOT:PSS and MoO$_3$ HILs are compared for all HTLs and treatments. Performing the treatment two thirds of the way through the HTL facilitates evaluation of the effects of the treatment on the HTL material independent of interface-induced effects at the HTL/EML interface. 60°C is chosen as the baking temperature because it is close to the glass transition temperature (Tg) of CBP, 62°C [177] In solution-processing, the annealing temperature is often close to or greater than the Tg of the organic material. The purpose of the annealing step is to remove residual solvent molecules left behind in the film. For this study, toluene is chosen as the solvent because of it easily dissolves a variety of organic small molecules and is commonly used in solution processing [14], [15], [81]. For consistency, the annealing (baking) temperature is kept the same for all three HTLs (CBP, TCTA and NPB), though they have different Tg's (62°C [177], 151°C [76] and 96°C [15] respectively).
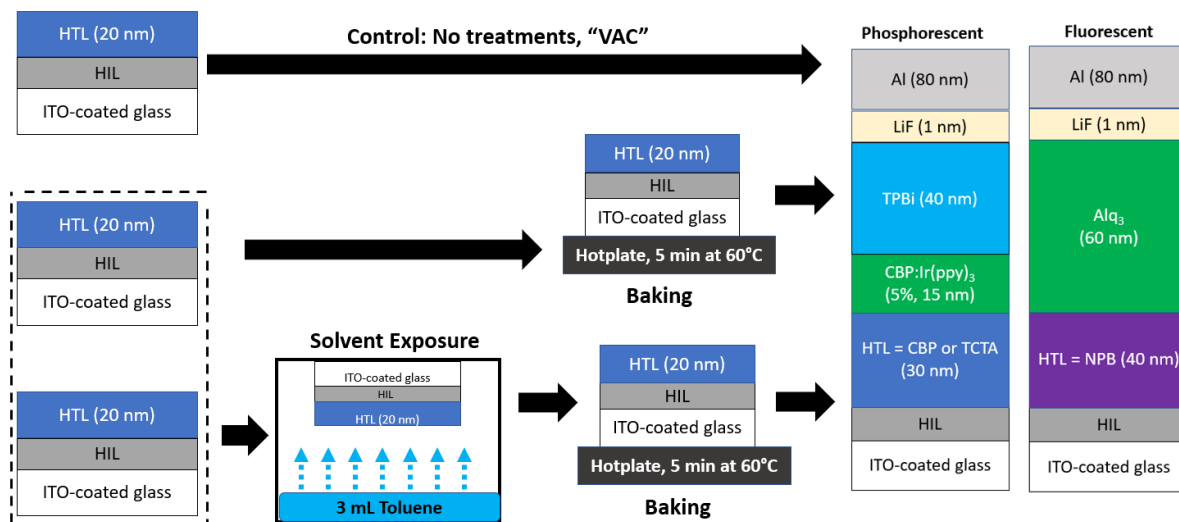
Figure 5.1: Sample preparation procedure used in this work.

Figure 5.2 gives the current-density versus voltage (J-V) characteristics for all treatment/HIL/HTL combinations, with the NPB case denoted NPB/Alq$_3$. For the MoO$_3$ HIL, there are minimal changes to the J-V characteristics resulting from the treatments for all three HTLs. This means that charge injection and transport properties of these OLEDs remain relatively unaffected for the MoO$_3$ HIL. For the CBP and NPB OLEDs with the PEDOT:PSS HIL, the treatments lead to a decrease in current through device across all voltages. This is especially prominent for the leakage current (current over the 0-3 V range). In contrast, TCTA has relatively little negligible change in its J-V characteristics with treatments when using a PEDOT:PSS HIL, including no changes to leakage current. Interestingly, the decrease in current observed for the CBP/PEDOT:PSS and NPB/PEDOT:PSS cases do not negatively impact device efficiency, as shown in the external quantum efficiency (EQE) data in **Figure 5.3**, where device EQE improves with treatments for CBP and remains roughly similar for NPB. For TCTA, baking only remains similar to the vacuum case, while solvent treatment leads to a slight decrease in EQE for both HILs. Unlike CBP/PEDOT:PSS, CBP/MoO$_3$ has a substantial decrease in EQE with solvent treatment (albeit not with baking alone), despite having remarkably similar J-V characteristics. Finally, NPB/MoO$_3$ devices show a slight decrease in EQE with treatments, where baking alone appears to have a more significant effect than solvent treatment.

Figure 5.4 gives the EL emission spectra for all treatment/HIL/HTL combinations, with the insets giving an enlarged view of the expected emission from the hole transport materials over the 350-500 nm range. From this data, the EL spectra remain unaffected with either treatment. This means that the same colour light is emitted from the device regardless of treatment. There is a small exception to this for the CBP/PEDOT:PSS case, where the treatments lead to a wider shoulder at ~550 nm and correspondingly, less emission from 400-450 nm. However, this difference is very small and thus likely due to minor thickness differences between the treated and untreated samples. Given that solution processing has been shown to produce different film morphologies than vacuum deposition leading to differences in device performance, these results may suggest that solvent and baking treatments alone (i.e.: independent of the specific solution process) may influence film morphology. However, these morphological changes do not affect the EL emission spectra of the devices, and more importantly, the extent of these effects appears to vary considerably depending on the HTL material and HIL.

Figure 5.2: Current density versus voltage characteristics of OLEDs with various treated and untreated HTLs on PEDOT:PSS and MoO₃ HILs.
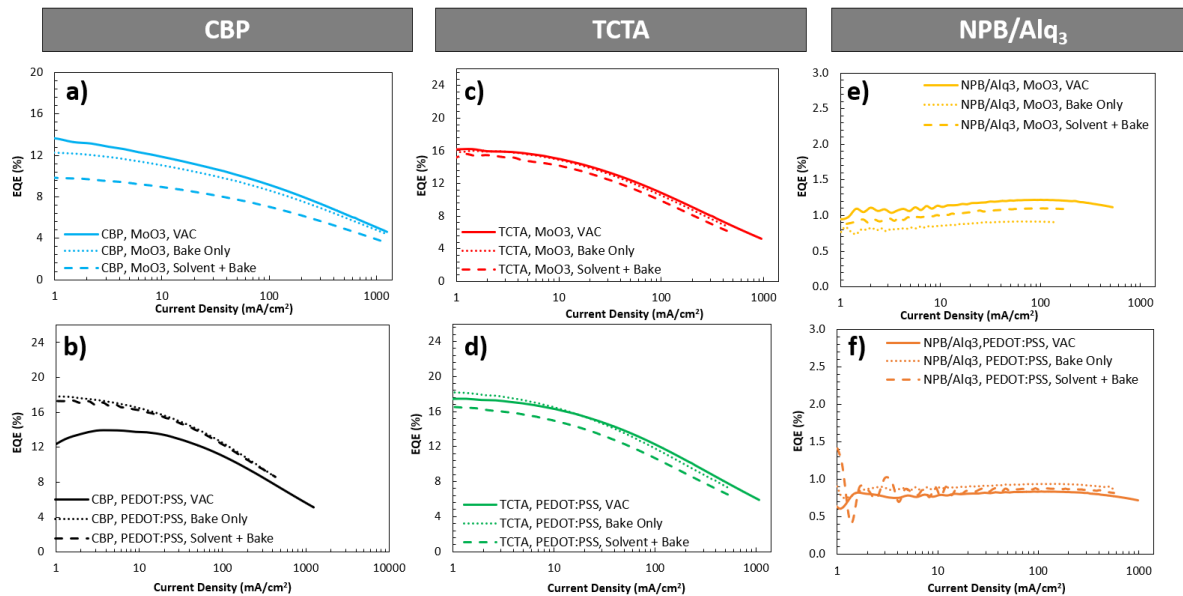
Figure 5.3: EQE versus current density of OLEDs with various treated and untreated HTLs on PEDOT:PSS and MoO₃ HILs.
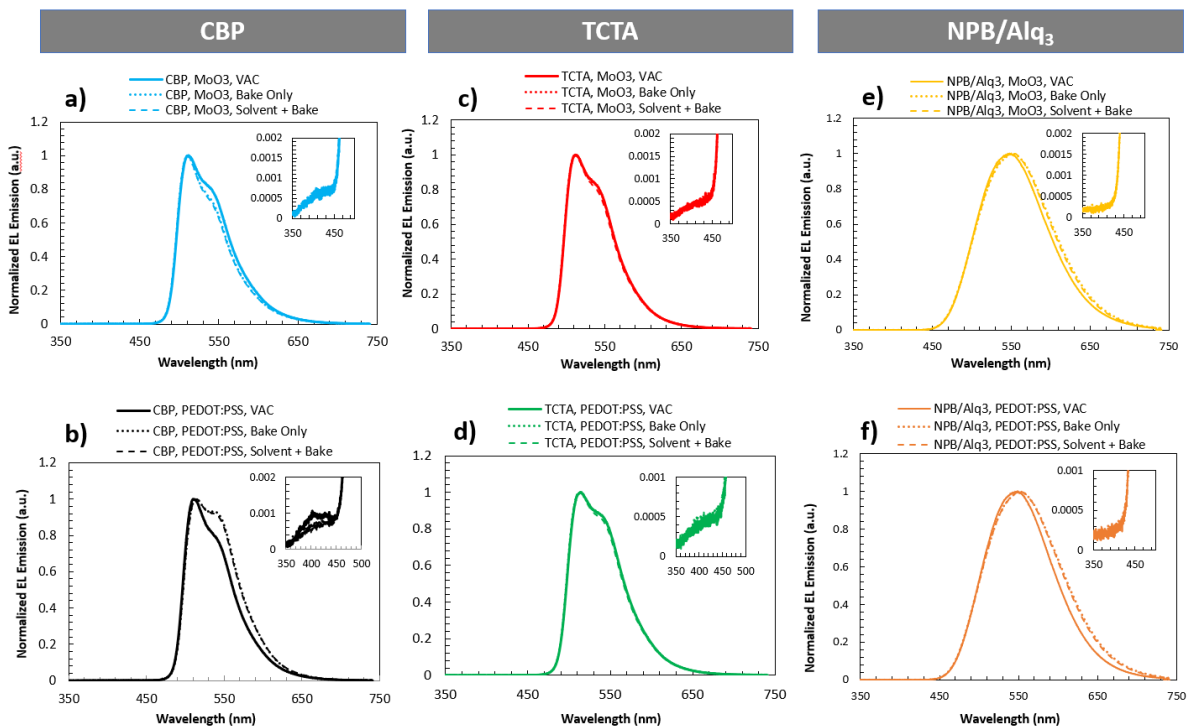
Figure 5.4: EL spectra of various treated and untreated HTLs on PEDOT:PSS and MoO$_3$ HILs. Insets: Enlarged view of emission from hole transport materials (350-500 nm).

5.4 Effect of Treatments on EL Lifetime

The EL lifetime characteristics for all cases are given in **Figure 5.5**. For these measurements, devices are driven at a constant current density of 20 mA/cm^2; normalized luminance is plotted as a function of time on the primary y-axis, while the change in voltage with respect to the time-zero initial driving voltage (ΔV) is plotted on the secondary y-axis. For all cases, the ΔV versus time trends closely mirror the decrease in luminance over time, demonstrating that the decline in EL output over time is directly related to deterioration in charge injection and transport properties for all material systems studied here. For CBP, the EL lifetime decreases dramatically with solvent treatment but remains unaffected with baking only on MoO$_3$. This is in contrast to PEDOT:PSS, where baking alone appears to have a much more substantial effect. On the other hand, baking only has a very significant effect for TCTA on both HILs, with solvent treatment leading to lower EL lifetimes only for the MoO$_3$ HIL. These results suggest that carbazole-based materials may be more sensitive to solvent and baking treatments when an MoO$_3$ HIL is used. For NPB, baking only results in the lowest EL lifetimes, particularly with the MoO$_3$ HIL; solvent-treated devices also show a decrease in EL lifetime, albeit not to the same extent as baking alone.

63

These results corroborate the earlier observation that solvent and baking treatments likely influence film morphology despite the baking temperature being lower than Tg for several of the materials. This in turn affects EL lifetime, however, the extent of these effects varies considerably depending on the HTL material and HIL.
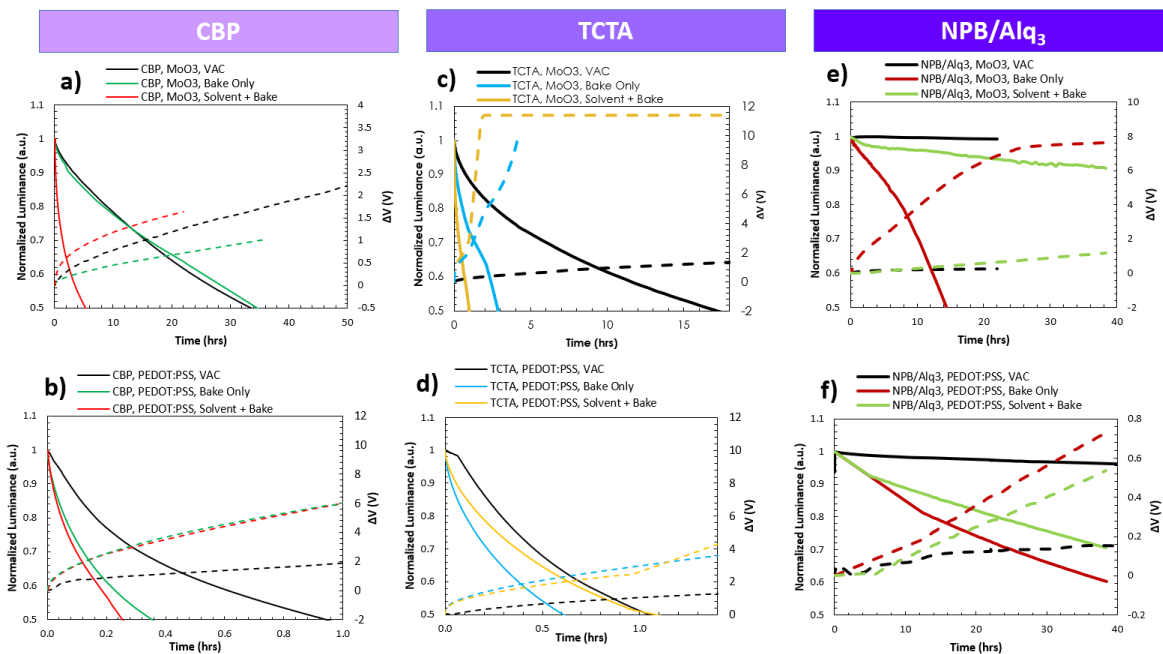
Figure 5.5: EL lifetime characteristics (initial luminance - solid, change in voltage - dashed) of OLEDs with various treated and untreated HTLs on PEDOT:PSS and MoO$_3$ HILs.

5.5 Effect of Treatments on Hole Injection and Transport Properties

Given the variability in EL lifetime changes observed with solvent and baking treatments across the HTL/HIL combinations and the fact that these treatments are performed within the HTL, it is worth investigating the possible relationship between the treatments and hole transport properties. For this purpose, treated and untreated "hole-only" devices with the three HTLs on both HILs are compared. The device structure of these devices is as follows: ITO/HIL/HTL (100 nm)/MoO$_3$ (5 nm)/Al (80 nm), where the HIL is MoO$_3$ or PEDOT:PSS and the HTL is CBP, TCTA or NPB, as for the OLEDs. The MoO$_3$ layer adjacent to the Al contact acts as an electron blocking layer. Therefore, under forward bias, defined as holding the ITO contact at a more positive potential relative to Al contact, holes are injected from the ITO contact, transported across the stack then collected at the Al contact. On the other hand, the injection of electrons from the top contact is blocked by MoO$_3$, making holes the predominant charge carrier in these devices. In this way, we may interpret the following results as being primarily connected with hole injection and transport.

To test the effect of the treatments, baking or solvent treatment is done following deposition of the first 66 nm of the HTL to mirror the treatment location in the OLEDs (i.e.: 2/3 of the way to the EML). **Figure 5.6** gives the hole current density versus voltage characteristics for the hole-only devices with all HTL/HIL combinations. For CBP on MoO_3, both treatments lead to a substantial increase in hole current, while on PEDOT:PSS, baking alone leads to smaller increase than solvent treatment. For TCTA on MoO_3, only solvent treatment leads to an increase in hole current, while both solvent and baking treatments lead increased hole current on PEDOT:PSS. For NPB however, there are negligible differences in hole current density, and hence hole injection and transport properties, with the treatments. An increase in hole current density suggests that more holes (positive polarons) are being injected into the device and transported across the stack, possibly creating an unbalanced positive space charge and degrading the HTL material as a result. While this alone cannot explain all of the EL lifetime results (i.e.: why baking only leads to a similar lifetime on CBP to the vacuum case for MoO_3 but not on PEDOT:PSS), it does support the previous observation that the carbazole materials are more susceptible to poor performance from the treatments compared to NPB, particularly when MoO_3 is used as an HIL.
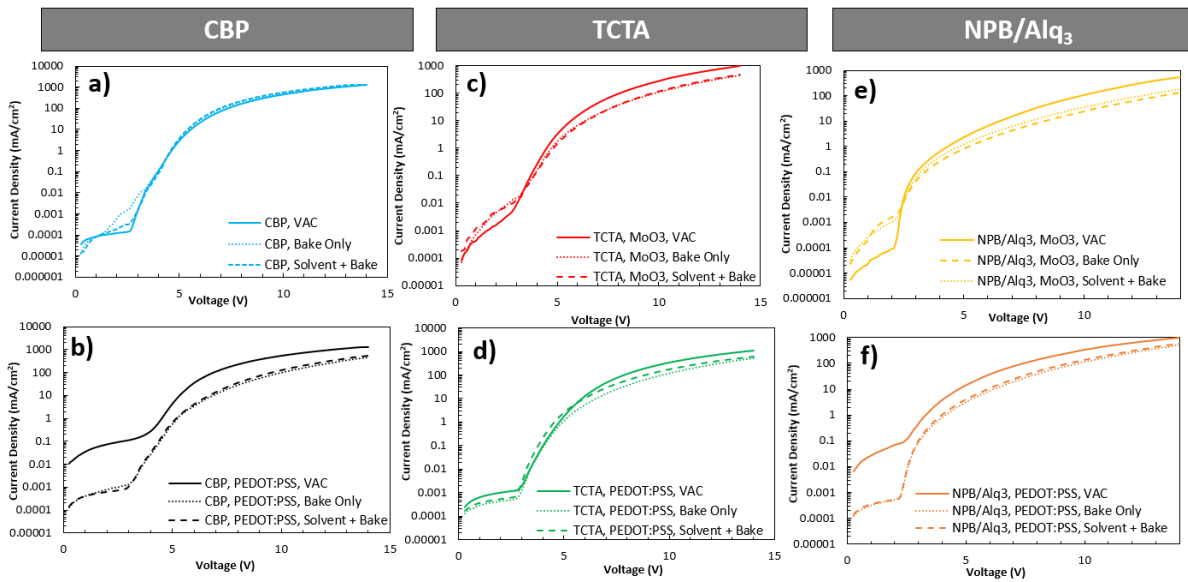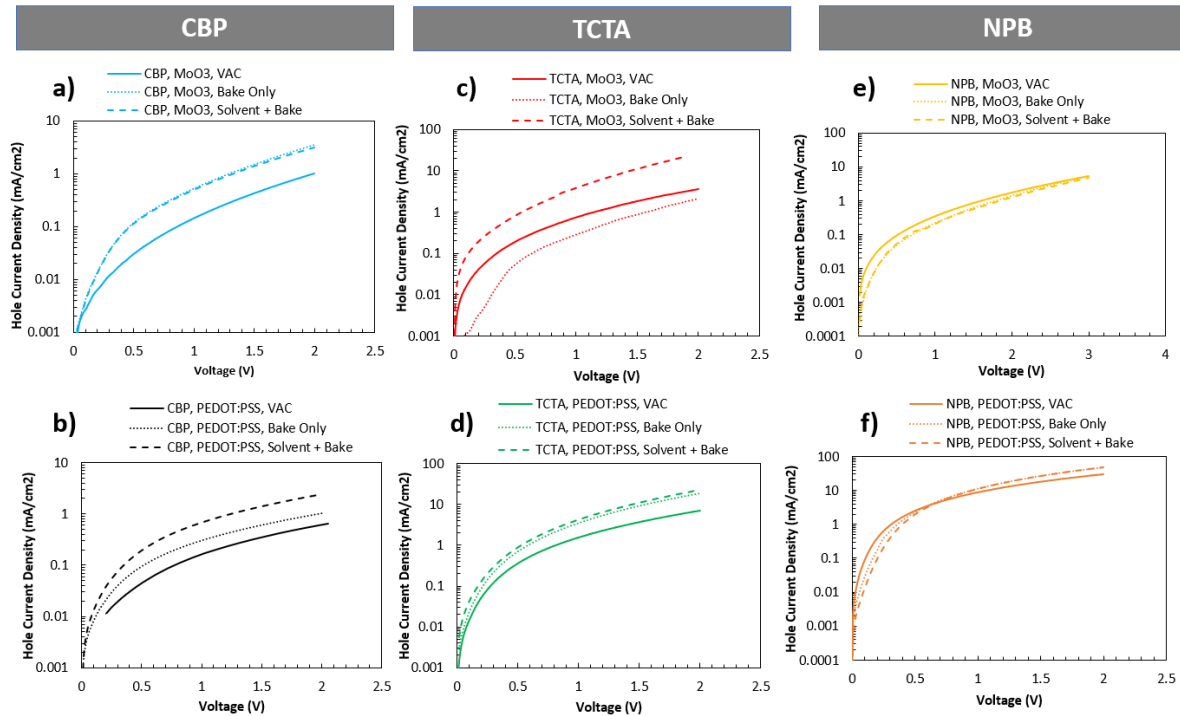

Figure 5.6: Hole current density versus voltage characteristics of hole-only devices with various treated and untreated HTLs on PEDOT:PSS and MoO_3 HILs.

5.6 Effect on Film Morphology

To investigate the possible effects of solvent and baking treatments on film morphology, the photoluminescence (PL) spectra, UV-visible absorbance spectra and transient PL response (TRPL) (also known as exciton lifetime) of 30 nm treated (solvent + bake and bake only) and untreated (vacuum) HTL films deposited on both PEDOT:PSS and MoO_3 HILs are examined.

5.6.1 PL Characteristics

Figure 5.7 gives the PL spectra of all HTL/HIL/treatment combinations. For CBP, significantly less PL is observed with both treatments on MoO_3 compared to PEDOT:PSS. On MoO_3, there is an 83% decrease in PL emission for the solvent treated case (relative to the vacuum control) and ~42% decrease with baking alone. On PEDOT:PSS, baking alone appears to increase PL emission by about ~30%, while solvent treatment results in only a small decrease. For TCTA on the other hand, the PL decrease is similar for the two treatments on a given HIL, ~94% on MoO_3 and ~89% on PEDOT:PSS. In contrast, NPB shows negligible decrease in PL emission on MoO_3 and a ~30% decrease with baking alone on PEDOT:PSS, while solvent treatment leads only to a decrease of ~20%. These results suggest that there are changes in film morphology (i.e.: formation of aggregates) with the treatments resulting in fewer excitons being able to recombine radiatively and produce PL emission. The consequences of this result with respect to device EQE and EL lifetime, however, vary considerably for each HTL/HIL combination; suggesting that reductions in PL emission alone cannot explain the observed differences in device behaviour.
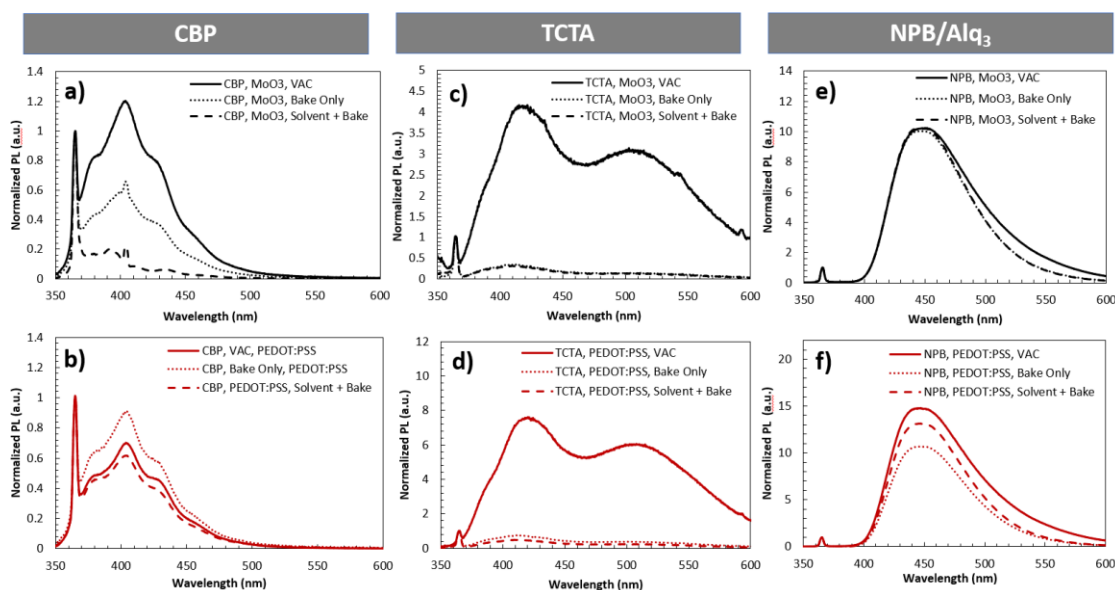
Figure 5.7: PL spectra of various treated and untreated films on MoO_3 and PEDOT:PSS HILs.

5.6.2 UV-Visible Absorption

The UV-visible absorption spectra of all HTL/HIL/treatment combinations are given in **Figure 5.8**. There are negligible differences in the absorbance with the treatments in all cases except for the CBP/MoO$_3$ case, which has a substantial increase in absorbance at longer wavelengths with solvent treatment compared to the vacuum and bake-only cases. An increase in absorbance at longer wavelengths is typically associated with increased aggregation in the film [12] and thus supports the earlier observation that CBP is more prone to aggregation with solvent treatment on MoO$_3$ compared to PEDOT:PSS. Since there are no changes to the absorbance of any of the other films, further investigation of film morphology is required (Section 5.6.3).
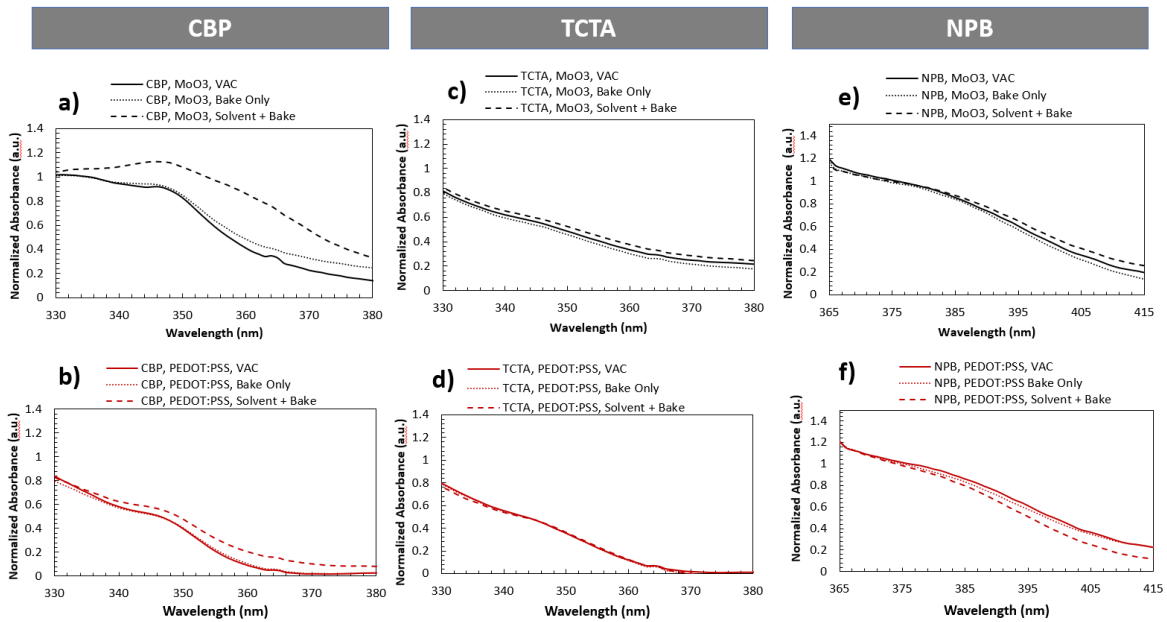
Figure 5.8: UV-vis absorbance of various treated and untreated films on MoO$_3$ and PEDOT:PSS HILs.

5.6.3 Transient PL Response/Exciton Lifetime (TRPL)

The TRPL response for all HTL/HIL film combination is given in **Figure 5.9**. For CBP, there is a substantial decrease in exciton lifetime for both treated films on MoO_3 compared to the vacuum controls, suggesting that the morphology of the treated and untreated films are substantially different. This combined with the greater decrease in PL emission as well as device EQE and EL lifetime observed with solvent treatment demonstrates that these solvent-induced morphological effects can lead to a deterioration in performance for OLEDs with CBP HTLs and MoO_3 HILs. However, with PEDOT:PSS, differences between exciton lifetimes for the three cases (solvent + bake, bake only, vacuum) are negligible, while baking alone appears to show an increase in PL emission. Overall, the changes are not as significant as with MoO_3. Despite these results, baking alone still results in a decrease in EL lifetime, though not as severe as that observed for solvent treatment. For TCTA, there is a slight decrease in exciton lifetime on MoO_3, but negligible changes are observed for PEDOT:PSS. Device EQE did not change very significantly for any treatments on either HIL, but EL lifetime was significantly worse with baking only and solvent treatment on MoO_3. This appears to be consistent with the observed decrease in PL emission and exciton lifetime of the TCTA films on MoO_3. On the other hand, for PEDOT:PSS, the 89% decrease in PL emission does not lead to lower EL lifetimes with solvent treatment, though it does for baking alone.

These results suggest that for TCTA on PEDOT:PSS, the morphological changes caused by solvent treatment (but not baking treatments) are less detrimental than for CBP; and corroborate the earlier observation that carbazole-based materials may be more sensitive to solvent and baking treatments when MoO_3 HILs are employed. Finally, NPB shows no differences in exciton lifetime with the treatments for both MoO_3 and PEDOT:PSS HILs. However, for PEDOT:PSS, decreases in PL emission are observed for both treatments, with bake only having the most considerable effect. This is consistent with the baking treatment having a more significant effect on the EL lifetime of NPB devices than solvent treatments (regardless of the HIL), like the TCTA/PEDOT:PSS case, despite the baking temperature being far below the Tg of NPB. It is possible that increased entropy resulting from solvent treatment slows down aggregation in the film resulting from the baking treatment, thereby preserving device EL lifetime. Altogether, these results demonstrate that solvent and baking treatments can have a considerable impact on film morphology. However, the extent of loss in PL emission and changes in exciton lifetime and absorbance with the treatments for each film do not always directly correlate with the extent of loss in device EQE and EL lifetime, suggesting that additional factors may be play a role.
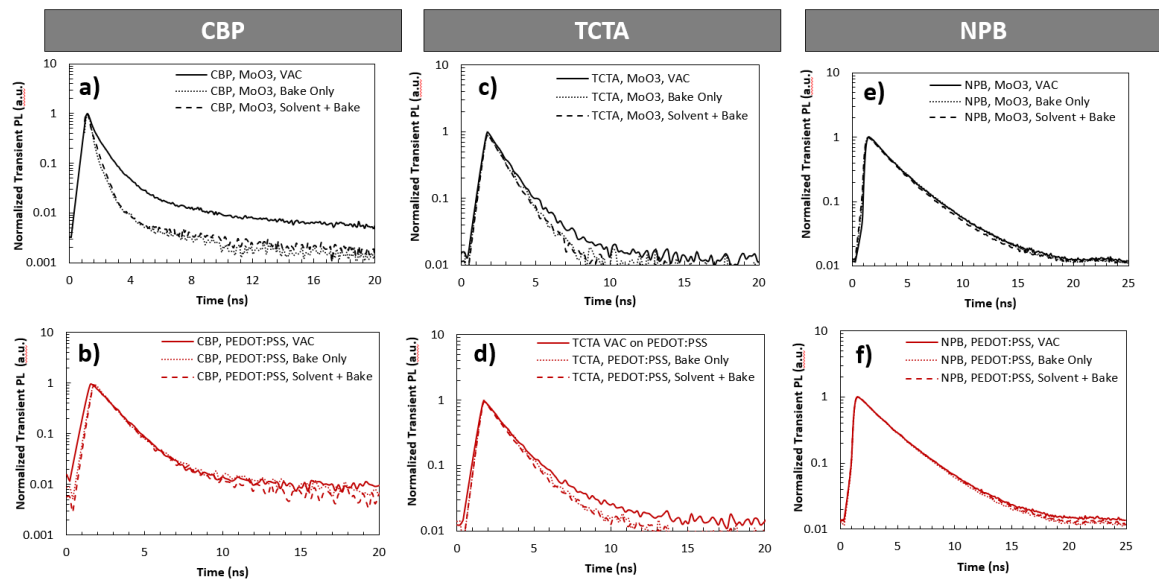
Figure 5.9: TRPL/exciton lifetime of various treated and untreated films on MoO_3 and PEDOT:PSS HILs.

5.7 Conclusion

In conclusion, results show that the effects of solvent and baking treatments on device efficiency and EL lifetime vary considerably by HTL/HIL combination. The carbazole-based phosphorescent HTL materials (CBP and TCTA) appeared to be most sensitive to solvent and baking treatments when an MoO_3 HIL was used. Device EQE and EL lifetime of fluorescent NBP/Alq_3 devices were more negatively impacted by baking alone compared to solvent treatment for both HILs. An examination of the morphological characteristics of treated and untreated HTLs for both HILs revealed that the extent of the morphological changes induced by the treatments is also highly material and HIL dependent. Further, morphological changes do not necessarily correlate with device EQE and EL lifetime, suggesting that additional factors likely play a role. Nevertheless, the choice of the HTL and HIL material both play a critical role in device EQE and EL lifetime. These findings demonstrate the importance of selecting materials that are less prone to solvent and baking-induced morphological effects and have implications for the development of novel hole transport materials for solution-processed OLEDs.

Chapter 6 - Mixing as an Approach to Mitigate Solvent-Induced Aggregation in CBP-Based Hole Transport Layers for Organic Light-Emitting Devices

The material in this chapter was submitted to the IEEE Journal of the Electron Devices Society in March 2019.

Chapter Summary

This chapter addresses the third sub-objective of the solvent and baking treatments component of this work (sub-objective 2c) – investigating a possible means to mitigate solvent and baking-induced morphological effects for HTL/HIL combinations sensitive to these treatments, as identified in the previous chapter (sub-objective 2a and 2b). To this end, we systematically investigate and compare the effects of solvent and high-temperature annealing treatments on vacuum-deposited, phosphorescent OLEDs with CBP-based HTLs and an MoO_3 HIL, which were shown to be most sensitive to solvent effects in the previous chapter. The bottom 20 nm of the CBP HTL is exposed to solvent vapours and high-temperature annealing near the CBP glass transition temperature. The remaining organic layers are subsequently deposited; all layers are deposited by thermal evaporation. For neat CBP films, solvent treatment leads to a reduction in device EQE and a severe decrease in EL lifetime relative to untreated vacuum controls. PL and TRPL data indicate that there is a significant decrease in CBP photoluminescence quantum yield (PLQY) and exciton lifetime with solvent treatment due to significant aggregate formation in these films. While baking at the CBP glass transition temperature alone (i.e.: in the absence of solvent) did appear to induce morphological changes in the CBP films, device EQE and EL stability remained unaffected, as shown previously. To mitigate the solvent-induced aggregation observed in the solvent-treated CBP films, 2,2',7,7'-Tetrakis(carbazol-9-yl)-9,9'-spiro-bifluorene (Spiro-CBP) was intermixed into the bottom 20 nm of the HTL deposited prior to treatment. A 1:1 ratio of Spiro-CBP to CBP was found to provide the optimal driving voltage. The EQE of the solvent treated and high-temperature annealed intermixed devices was remarkably similar to the vacuum control and the decrease in EL lifetime was much less significant compared to the neat CBP case. The observed solvent-induced aggregation in pure CBP films appears to be suppressed for the intermixed films, as demonstrated by the less significant decrease in PLQY and negligible change in exciton lifetime for the treated films compared to the vacuum controls. The results illustrate a simple means to mitigate solvent-induced effects for solution-processed devices with CBP HTLs.

6.1 Introduction

In the previous chapter, it was shown that solvent and high-temperature annealing or baking treatments induce morphological changes that contribute significantly to device degradation and short EL lifetimes in CBP-based phosphorescent OLEDs with MoO_3 HILs. Given that CBP is among the most ubiquitous and well-studied HTL materials in both vacuum and solution-processed devices [14], [15], [47], [98], [177], [184] and that MoO_3 is a very widely used HIL material since it has been shown to lead to improved device efficiency and EL lifetime [19], [135], [169], it is important to examine possible strategies for mitigating treatment-induced morphological effects. In this chapter, intermixing Spiro-CBP with CBP in the bottom 20 nm of the HTL deposited prior to the treatment is found to suppress solvent-induced morphological effects and improve the EQE and EL lifetime of solvent-treated devices relative to their neat CBP counterparts. The findings illustrate the critical role of solvents in the morphology of organic films and present a simple solution to suppressing solvent-induced aggregation, an important mechanism of degradation for OLEDs fabricated by solution-processing methods.

6.2 Experimental Methods

In this work, OLEDs with the structure ITO/MoO_3 (5 nm)/CBP (30 nm)/CBP:Ir(ppy)$_3$ (5%, 15 nm)/TPBi (40 nm)/LiF (1 nm)/Al (80 nm) were fabricated, where MoO_3, CBP, TPBi (2,2,2"-(1,3,5-benzinetriyl)-tris(1-phenyl-1-H-benzimidazole), Ir(ppy)$_3$ (tris(2-phenylpyridine)iridium(III)) and LiF are used as the hole injection, hole transport, electron transport, guest emitter and electron injection layers respectively. Indium tin oxide (ITO) and Al are used as the anode and cathode contacts respectively. Spiro-CBP was co-deposited with CBP for devices with intermixed HTLs. CBP, TPBi and Spiro-CBP were obtained from Shanghai Hang Feng Chemical Co., Ir(ppy)$_3$ was obtained from Luminescence Technology Corp.

Devices were fabricated on ITO patterned glass substrates (15 Ω/sq, Kintec); these were sonicated in deionized water/Micro-90 solution for 10 min and were subsequently annealed at 110°C for 10 min prior to use. All materials were deposited via thermal evaporation (base pressure $< 5 \times 10^{-6}$ Torr), using an Angstrom Engineering EvoVac system at a deposition rate of 0.1-2 Å/s.

To test the effect of solvent treatment and high-temperature annealing, substrates previously divided into two halves were used. For these experiments, the vacuum was broken following deposition of the bottom 20 nm of CBP. One half was then exposed to toluene (Sigma-Aldrich) vapours in a sealed container, with the substrate taped to the lid for 3 min. Both halves were then baked at 60°C for 5 min and subsequently re-loaded in the vacuum chamber to complete deposition of the remaining 10 nm of CBP and the other layers.

Current-voltage-luminance measurements were carried out using an Agilent 4155C Semiconductor Parameter Analyzer connected to a silicon photodiode. An Ocean Optics QE65000 spectrometer was used to measure the electroluminescence and photoluminescence spectra of the OLEDs, with photoluminescence induced by illumination with a 200 W Hg–Xe lamp controlled with an Oriel-77200 monochromator. All EL lifetime tests were carried out at a current density of 20 mA/cm^2 using a custom lifetime test setup. Transient photoluminescence response was measured with an Edinburgh Instruments FL920 spectrometer equipped with a 375 nm peak emission EPL375 picosecond pulsed laser diode.

Devices were kept in N$_2$ atmosphere throughout fabrication and characterization.

6.3 Effect of Treatments on Efficiency and Lifetime

We begin by investigating and comparing the effects of solvent exposure (3 minutes of exposure to toluene vapour and 5 minutes of baking at 60°C, denoted "Solvent + Bake") and baking only (5 minutes of baking at 60°C, denoted "Bake Only") on the bottom 20 nm of the HTL to untreated controls with pristine 30 nm CBP HTLs on OLED performance characteristics and EL lifetime. Limiting the treatment to the bottom 20 nm and keeping the top 10 nm untreated facilitates evaluation of the effects of the treatment on the HTL material independent of interface-induced effects at the HTL/EML interface. Toluene is chosen as the solvent in this study because of its ability to easily dissolve many common organic small molecules and its widespread use in the field [14], [15], [81]. 60°C was chosen as the baking temperature (CBP Tg = 62°C [177]). Drying temperatures used in solution processing of organic small molecules with low Tg such as CBP are typically selected to be just below the Tg of the material to effectively dry the films and eliminate residual solvents while not inducing crystallization from thermal stresses [15]. Therefore, for the solvent + bake case here, we expect the amount of any residual solvents in the film to be negligible, especially considering their very small thickness (20 nm) and the fact that the films are left under vacuum for 30 minutes before resuming the deposition of the subsequent layers. Following deposition of the bottom 20 nm of the CBP HTL, "bake only" and "solvent treated" samples are transferred to an N$_2$ glovebox, where the solvent and baking treatments take place. Control, i.e.: untreated devices, were also fabricated for comparison, as per the procedure outlined in Chapter 5. **Figure 6.1** gives the current density versus voltage (a), EQE versus current density (b), EL spectra (c) and EL lifetime characteristics (d) for OLEDs with solvent + bake, bake only and control HTLs. For the EL lifetime characteristics, devices are driven at a constant current density of 20 mA/cm^2; normalized luminance is plotted as a function of time on the primary y-axis, while the change in voltage with respect to the time-zero initial driving voltage (ΔV) is plotted on the secondary y-axis.

From **Figure 6.1 (a)**, the current density versus voltage characteristics for all three cases are remarkably similar, indicating that neither treatment causes substantial changes to carrier injection or transport. However, there is a significant drop in EQE for the solvent-exposed device compared to the bake-only and control cases, which have roughly similar EQE, as shown in **Figure 6.1 (b)**. The EL emission spectrum remains relatively unchanged with treatments (**Figure 6.1 (c)**). EL lifetime however is more substantially affected by solvent treatment than device EQE, as shown in **Figure 6.1 (d)**. The LT50 (time taken to reach half of the initial luminance of the device under constant current driving) for the solvent treated case is ~7x shorter than that of the bake-only and control cases This data suggests that the solvent treatment may cause some morphological changes and molecular re-organization in the CBP film, possibly causing the observed reduction in EL lifetime, whereas baking alone (despite being at a temperature near Tg) has a comparatively negligible effect.
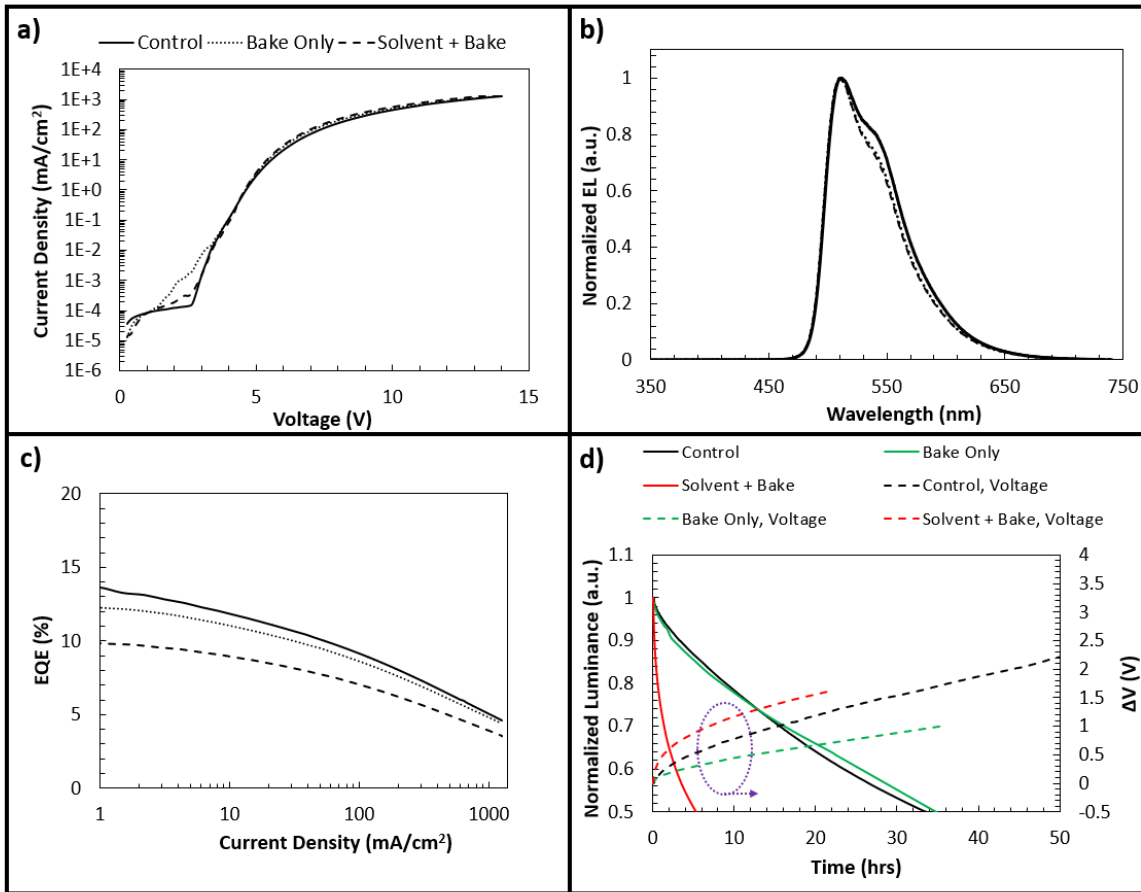
Figure 6.1: Current density versus voltage (a), EL spectrum (b), EQE versus current density (c), and EL lifetime characteristics (d) of vacuum, baked, and solvent-treated OLEDs.

6.4 Effect on Film Morphology

To investigate the possible effects of solvent treatment on film morphology, the photoluminescence (PL) spectra and transient PL response (TRPL) of 30 nm treated (solvent + bake and bake only) and untreated (control) CBP films deposited on ITO coated with 5 nm MoO_3 are examined. **Figure 6.2** gives the PL spectra **(a)** and TRPL response **(b)** of the three CBP films. PL and TRPL measurements were taken under 365 nm excitation, where CBP has significant absorption. For TRPL measurements, 400 nm emission, corresponding to the CBP emission peak, was collected. From **Figure 6.2 (a)**, there is ~50% immediate decrease in CBP PL intensity (390-430 nm [177]) for the bake only case. For the solvent-treated case, PL intensity decreases by ~84%. These substantial decreases in PL intensity under the same excitation power indicate a decrease in the PLQY of the material in case of the treated films, a notion that may be correlated with the formation of aggregates in the films [11]. This is further corroborated by the PL images taken under UV excitation presented in the inset of **Figure 6.2 (b)**, where crystalline formations (aggregates) sufficiently large to be seen by the unassisted eye can be detected in case of the "Solvent + Bake" films. The TRPL response traces (**Figure 6.2 (b)**) of the three films provide further evidence of aggregation, with both treatments resulting in a substantial decrease in exciton lifetime, pointing to increased quenching in the films, consistent with the decrease in their PLQY. The faster exciton quenching may be attributed to increased molecular aggregation as a result of the treatments, in line with the observed crystallization. For the bake-only case, TRPL data also suggest that film aggregation is present. The absence of detectable crystallinity in the PL images in this case however suggests that the aggregation is not to the same extent as for the solvent-treated film indicating that the morphological changes and molecular reorganization were less in this case. This may explain the relatively smaller impact of the bake-only scenario on device EQE and EL lifetime observed in **Figure 6.1 (c)** and **(d)**. Together, these results suggest that solvent treatment and baking near Tg can lead to substantial aggregation in the film, consistent with previous reports [98].
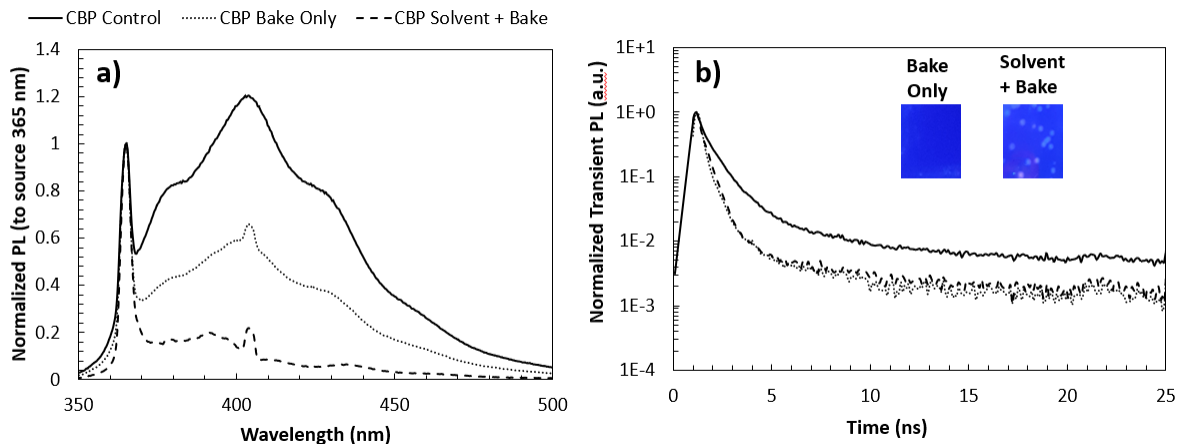
Figure 6.2: PL spectra (a) and TRPL response (b) of vacuum, baked and solvent treated-treated CBP films. (b) Inset: Photos of baked and solvent-treated CBP films under 365 nm UV light.

6.4 Material Intermixing as an Approach to Suppress Aggregation and Improve EL Lifetime

Given that exposure to solvent clearly induces molecular reorganization and aggregation in CBP films, a phenomenon that is likely playing a role in the lower EQE and EL lifetimes observed in these devices, suppressing or at least limiting this aggregation may help overcome this obstacle in solution-processed OLEDs. To this end, intermixing with a second material may effectively reduce this aggregation. In solution-processed devices, intermixing two host materials and a guest dopant in the emissive layer (EML) is a well-explored approach to suppress aggregation and achieve high-efficiency single-layer devices (i.e.: no HTL) for OLEDs with emission across the colour spectrum. Bipolar [99], [185]–[187] or mixed hosts [117], [188]–[191] utilizing a hole transporting material and an electron transporting material as co-hosts accompanying various emissive dopant materials have been shown to reduce turn-on voltages and greatly enhance device EQE for solution processed devices. Lemmer and coworkers [192] interestingly intermixed the EML host material with electrically isolating polystyrene to achieve favourable film-forming properties and similar efficiencies to vacuum-processed devices based on the CBP:Ir(ppy)$_3$ host/guest system. It is therefore worth investigating whether material intermixing can lead to improved EL lifetimes upon exposure to solvents.

For this purpose, we investigate and compare the effects of the previously described solvent and baking treatments on OLEDs with neat CBP HTLs and those in which the CBP is intermixed with another material. Spiro-CBP is selected as the intermixing material because of its similar molecular structure to CBP; thus, reducing the possibility of new chemical interactions. Additionally, Spiro-CBP has a HOMO close to that of CBP (HOMO = 5.8 eV [193] vs. 6.0 eV for CBP [144]); thus it should not significantly alter hole injection and transport properties or cause significant hole trapping in the HTL.

We begin by examining the luminance and driving voltage characteristics at 20 mA/cm^2 constant current driving (**Figure 6.3 (a)**) of OLEDs with the bottom 20 nm of their HTLs containing a CBP:Spiro-CBP mixture with 12.5%, 25%, 50%, 75% and 100% CBP, by volume. The device structure is: ITO/MoO$_3$ (5 nm) /CBP:Spiro-CBP (20 nm)/CBP (10 nm)/CBP:Ir(ppy)$_3$ (5%, 15 nm)/TPBi (40 nm)/LiF (1 nm)/Al (80 nm) with treatments done following the 20 nm CBP:SpiroCBP layer as done previously. It should be noted that devices with 100% Spiro-CBP HTLs tended to have very low efficiency and stability. Although the reasons for this are still unclear; one may conclude that any observed improvement resulting from intermixing Spiro-CBP with CBP cannot be attributed to simply replacing CBP with a better performing material.

From **Figure 6.3 (a)**, luminance is quite similar for all % CBP/treatment combinations. Similarly, all driving voltages were within 0.2 V of each other, consistent with the small difference in HOMO levels as expected. Interestingly, a close examination of **Figure 6.3 (a)** reveals that the device with 50% CBP content shows the lowest driving voltage for both treatments; increasing or decreasing CBP content increases the driving voltage. The small reduction in driving voltage for the 50% case suggests that hole injection and/or transport become more efficient with a 50% CBP:Spiro-CBP blend, a reasonable result given the slightly shallower HOMO of Spiro-CBP. In devices with higher Spiro-CBP content (< 50% CBP), the probability of holes resting on Spiro-CBP molecules increases. These holes become trapped on Spiro-CBP and must now overcome a 0.2 eV energy barrier to hop onto CBP molecules, making it more difficult to reach the EML; hence a higher driving voltage is required to release holes from these traps. For devices with CBP content > 50%, holes predominantly reside on CBP molecules. Since CBP has a deeper HOMO than Spiro-CBP, higher voltages are required for hole injection to CBP compared to Spiro-CBP, hence why the 100% CBP scenario has the highest driving voltage regardless of treatment. For the 50% CBP scenario, there are roughly an equal number of CBP and Spiro-CBP pathways through the HTL, thus hole trapping by Spiro-CBP is less likely and 50% of hole injection goes through Spiro-CBP instead of CBP. Together, these two mechanisms result in the lowest driving voltage, thus 50% CBP was deemed the optimal concentration.

As shown in **Figure 6.3 (b),** the current density versus voltage traces of treated and untreated devices with 50% CBP are remarkably similar; demonstrating that the treatments have a negligible effect on charge injection and transport. The EQE versus current density traces in **Figure 6.3 (c)** show a similar trend with no difference in EQE regardless of treatment, in contrast to the EQE trends for 100% CBP HTLs shown in **Figure 6.1 (c)**, where solvent treatment resulted in a somewhat lower EQE compared to the bake-only and control cases, likely attributable to aggregate formation induced by the solvent exposure. Most notably however, although the EL lifetime characteristics in **Figure 6.3 (d)** show that though both treatments lead to a decrease in LT50, the LT50 of the solvent treated case is only ~4x shorter than the control, compared with a 7-fold decrease for 100% CBP HTLs in **Figure 6.1 (d).** This can be seen from the luminescence versus time traces for the devices with the solvent treated CBP and CBP:Spiro-CBP HTLs in the inset of **Figure 6.3 (d)**, with the intermixed device demonstrating a 1.6x improvement in LT50**.** However, baking only leads to a ~2.5x decrease in LT50 for the 50% CBP HTL, whereas for the 100% CBP HTL, no decrease in LT50 was observed **Figure 6.1 (d)**.

Although the origins of this behaviour are unclear, the observations suggest that baking alone may be responsible for most of the degradation in LT50 for the 50% CBP HTL, with the solvent exposure contributing relatively less. Nevertheless, the EL lifetime of the solvent treated intermixed case relative to the control is significantly improved compared to the CBP-only devices, likely due to improved morphological stability induced by the material intermixing.
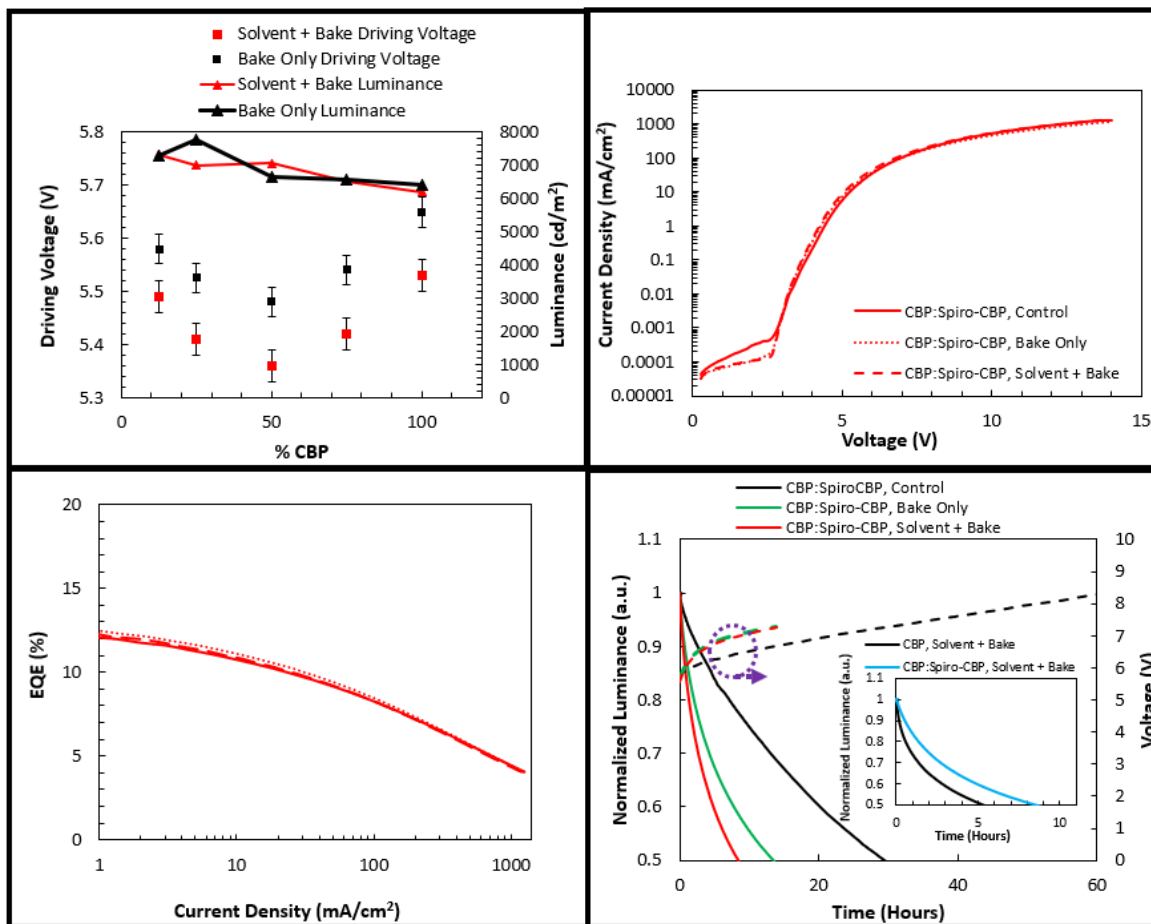
Figure 6.3: Driving voltage and initial luminance at 20 mA/cm^2 for various % CBP (a); current density versus voltage (b), EQE versus current density (c), and EL lifetime characteristics (d) of OLEDs with 50% and 100% CBP in the bottom 20 nm of the HTL and the three conditions; inset: comparison of solvent-treated 100% CBP vs. 50% CBP luminance versus time trends.

6.5 Origin of Improvement with Intermixing Spiro-CBP: Morphological Stability

To verify that the origin of the EL lifetime improvement observed in the solvent treated devices with intermixed HTLs is indeed due to improved morphological stability, the PL spectra (**Figure 6.4 (a)**) and TRPL response (**Figure 6.4 (b)**) of 30 nm treated (solvent + bake and bake only) and untreated (control) Spiro-CBP:CBP (50/50) films deposited on ITO coated with 5 nm MoO_3 are examined. As observed for CBP, there is a substantial decrease in PL emission intensity (~67%) with both treatments relative to the control. Consistent with the EL lifetime data, it appears that baking alone is responsible for most of the ensuing degradation, with solvent treatment having negligible effect on PL. This decrease in PL emission intensity with solvent treatment is not as significant as that observed for neat CBP (~74% relative to control, see **Figure 6.2 (a)**).   Additionally, as evident from the PL images in the inset of **Figure 6.4 (b)**, no detectable crystallization is observed in this case. This suggests that the solvent treatment-induced aggregation is indeed reduced via intermixing. Further, the control, baked and solvent-treated intermixed films have remarkably similar TRPL response (**Figure 6.4 (b)),** indicating that the treatments do not alter exciton lifetime in this case, suggesting that, in contrast to the case of the neat CBP films, molecular reorganization and aggregation must be less in case of the mixtures. Together, these results corroborate the observed EQE and EL lifetime trends for CBP only (**Figure 6.1 (d)**) and the intermixed films in **Figure 6.3 (d)** suggesting that the smaller deterioration in EQE and EL lifetime as a result of the solvent exposure may indeed be due to suppressing solvent-induced aggregation in the intermixed films. The fact that the solvent exposure has a smaller impact on the intermixed HTLs suggests that the solvent effects arise primarily from morphological changes and aggregation *during* the solvent treatment and not due to the presence of residual solvent in the films following the exposure step. Had significant amounts of residual solvents been present, they would affect other device layers that get deposited after the exposure step, thus one would expect to see no significant difference between the OLEDs with the intermixed HTLs and their counterparts with the neat HTLs.
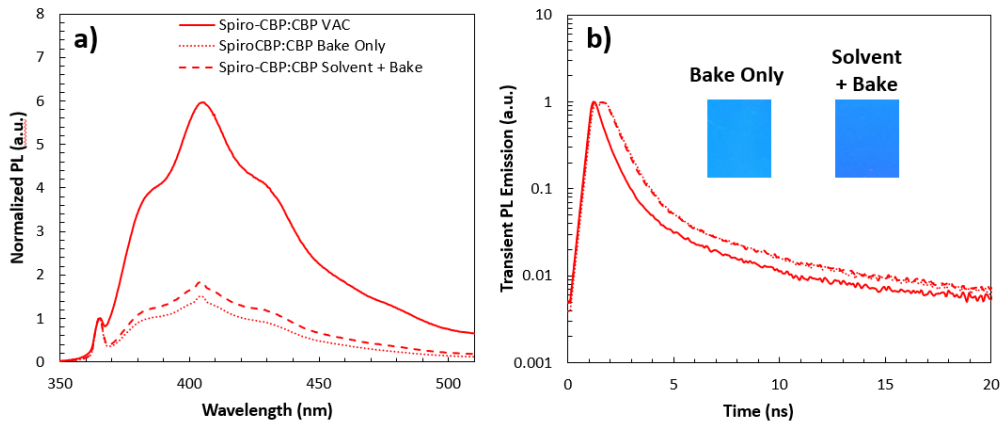
Figure 6.4: PL spectra (a) and TPRL response (b) of solvent treated, baked and vacuum intermixed films. Inset: Photos of baked and solvent-treated SpiroCBP:CBP films under 365 nm UV light.

6.6 Conclusion

In conclusion, results demonstrate that exposure to solvents induces aggregation in neat CBP films, which leads to short EL lifetimes and lower device EQE in OLEDs. PL and TRPL measurements give direct evidence of the effect of solvent exposure on film morphology and its corresponding reduction in the PLQY of solvent-treated films. Intermixing with Spiro-CBP in a 50/50 ratio suppresses solvent-induced aggregation, with the solvent-treated case having remarkably similar EQE and a substantially reduced decrease in EL lifetime relative to the untreated control. The results emphasize the key role of solvents and high-temperature annealing treatments frequently used in many solution processing techniques in the degradation of carbazole-based OLEDs and provide useful insight into how these adverse effects can be suppressed.

Chapter 7 – Conclusions and Future Work

7.1 Conclusions

The main objective of this research work was to understand the impact of solution-processable hole injection layers and solvent use with high-temperature annealing on the EL lifetime of vacuum-deposited, small-molecule OLEDs. The main findings of this research work can be summarized in terms of the specific research objectives as follows:

7.1.1 The Root Cause of the Lower EL Lifetime with PEDOT:PSS HILs

PEDOT:PSS HILs are susceptible to electron-induced degradation, a mechanism that can lead to relatively short EL lifetimes; and appear to be less susceptible to degradation by excitons and by holes. The use of hole transporting materials and device structures that minimize electron leakage to the HIL leads to significant improvements in device EL lifetime.

These conclusions are supported by the following findings:

1. The acidity of PEDOT:PSS is not singularly responsible for device degradation since all devices studied have an ITO/PEDOT:PSS interface and yet have very significant differences in their EL lifetimes. For example, when a PEDOT:PSS/MoO$_3$ hole injection layer is used in place of PEDOT:PSS alone, a ~20x improvement in the EL lifetime of OLEDs with CBP HTLs is observed.

2. As per hole-only device analysis, hole accumulation at the HIL/HTL interface does not play a major role in device degradation, thus holes are not responsible for the observed degradation;

3. Despite their presence near PEDOT:PSS, excitons are also not primarily responsible for this degradation, as per UV irradiation tests;

4. When electrons are introduced into the hole-only stack via electron-injecting LiF/Al contacts, significant degradation parallel to that occurring in full OLEDs is observed;

5. This degradation is found to be mitigated by:
    i) Introducing an electron-blocking layer between PEDOT:PSS and the HTL;
    ii) Employing HTL materials with poor electron mobility, i.e.: effective electron blocking characteristics.

7.1.2 The Impact of Solvents and Baking Treatments on the Electroluminescent Lifetime of Organic Light-Emitting Devices with Various Hole Transport/Hole Injection Layer Combinations

The effects of solvent and baking treatments on device efficiency and EL lifetime vary considerably by HTL/HIL combination, with CBP/MoO_3 being most prone to solvent-induced morphological effects. However, the extent of the morphological changes induced by the treatments is highly HTL and HIL dependent and morphological changes alone do not always correlate with device EQE and EL lifetime and suggests that material-specific factors should be likely be considered in future correlations of device characteristics to the morphology of corresponding organic films for solution-processed devices.

These conclusions are supported by the following findings:

1. The most significant changes in device efficiency and EL lifetime were observed for CBP and TCTA with MoO_3 HILs, suggesting that carbazole-based materials are more sensitive to solvent and baking treatments when an MoO_3 HIL is used instead of PEDOT:PSS;
    i) As per hole-only device analysis, CBP and TCTA have a more significant increase hole current density with solvent treatment on MoO_3 compared to PEDOT:PSS.
    ii) CBP has a significant decrease in both exciton lifetime and PL emission on MoO_3, as well as substantially more light absorption at longer wavelengths—characteristics often correlated with increased aggregation or crystallinity—whereas only the decrease in PL emission is observed on PEDOT:PSS.

2. For the PEDOT:PSS HIL, TCTA appears to be the most resistant to solvent-induced morphological changes, as reflected in the relatively smaller changes in device EQE and EL lifetime with the treatments;
    i) Baking alone appears to have a more significant effect on EL lifetime for the PEDOT:PSS/TCTA HIL/HL combination—solvent-treated TCTA on PEDOT:PSS has an equal EL lifetime to the vacuum control.
    ii) Yet both treatments appear to lead to similar decreases in PL emission for both HILs and minimal changes in exciton lifetime and UV-absorption are observed, suggesting morphological changes alone may not account for changes in device behaviour.

3. Fluorescent NPB/Alq_3 device EQE and EL lifetime appeared to be most sensitive to baking alone for both HILs and less sensitive to solvents compared to the carbazole HTLs;
    i) Changes in film morphology appear more significant for baking alone compared to solvents for both HILs, as observed via PL and TRPL analysis.

82

7.1.3 Intermixing to Mitigate Solvent-Induced Aggregation for the CBP/MoO₃ Combination

Solvent exposure of vacuum-deposited CBP HTLs can induce aggregation leading to short EL lifetimes and lower device EQE. PL and TRPL measurements give direct evidence of the effect of solvent treatment on film morphology and its corresponding reduction in the PLQY of solvent-treated CBP films. Intermixing with Spiro-CBP is shown to suppress solvent-induced aggregation and improve device EQE and EL lifetime.

These conclusions are supported by the following findings:

1. In neat CBP films, solvent treatment leads to a reduction in device EQE and a severe decrease in EL lifetime relative to untreated vacuum controls.
    i) PL and TRPL data indicate that there is a significant decrease in CBP PLQY and exciton lifetime with solvent treatment due to significant aggregate formation in these films.
2. Intermixing CBP and Spiro-CBP in a 1:1 ratio was found to improve device EQE and EL lifetime while minimizing solvent-induced aggregation.
    i) Among the mixing ratios tested, 1:1 was found to provide the optimal driving voltage;
    ii) A much less significant decrease in PLQY and negligible change in exciton lifetime with solvent treatment was observed for the intermixed films.

7.2 Future Work

This section outlines recommendations for future studies based on the conclusions and major findings derived from this work.

First, the EL lifetime and of OLEDs with solution-processed hole transport and possibly also emissive layers with PEDOT:PSS HILs should be compared to the vacuum-deposited devices in this work. It is recommended that TCTA be selected as the hole transport material and host for these devices because it has a high LUMO and very low electron mobility; thereby limiting the effects of electron-induced degradation. Furthermore, TCTA also has a high Tg of 151°C [76], making it less susceptible to crystallization during the annealing step compared to CBP [15], and thus is likely more suitable for solution processed devices.

Second, it is worth investigating alternative solution-processable HILs (e.g.: solution-processable MoO_3) and their possible impact on the device characteristics and EL lifetime of OLEDs with solution-processed versus vacuum deposited hole transport layers. This is because MoO_3 HILs have repeatedly been shown to improve EL lifetimes in phosphorescent vacuum-deposited devices. For the vacuum-deposited OLEDs, the solution-processable MoO_3 should also be compared with vacuum-deposited MoO_3. Such a study would facilitate an understanding of how closely the solution-processed MoO_3 can replicate the desirable effects achieved with vacuum-deposited MoO_3 HILs,

Third, the device characteristics and EL lifetime of solution-processed OLEDs with intermixed hole transport layers should be compared with those in this work. Spiro-CBP has a higher Tg (240°C [194]) than CBP and is equally soluble in many organic solvents. It would be interesting to see if intermixing with Spiro-CBP in OLEDs with solution-processed CBP hole transport layers and MoO_3 hole injection layers can help suppress solvent-induced aggregation as it does in this work for vacuum-deposited devices and MoO_3 hole injection layers and improve EL lifetime.

Finally, fully solution-processed devices (i.e.: all layers are solution-processed) should be investigated and fabricated by the blade-coating technique, since it does not demand the use of orthogonal solvents. This will ultimately provide a meaningful and practical comparison between vacuum deposited and solution-processed OLEDs. It is anticipated that implementing these recommendations will facilitate a more complete understanding of the limitations affecting the device performance and electroluminescent lifetime of solution-processed OLEDs.

Letters of Copyright Permission

Figure 2.1

This copyrighted material is owned by or exclusively licensed to John Wiley & Sons, Inc. or one of its group companies (each a"Wiley Company") or handled on behalf of a society with which a Wiley Company has exclusive publishing rights in relation to a particular work (collectively "WILEY"). By clicking "accept" in connection with completing this licensing transaction, you agree that the following terms and conditions apply to this transaction (along with the billing and payment terms and conditions established by the Copyright Clearance Center Inc., ("CCC's Billing and Payment terms and conditions"), at the time that you opened your RightsLink account (these are available at any time at http://myaccount.copyright.com).

Terms and Conditions

- The materials you have requested permission to reproduce or reuse (the "Wiley Materials") are protected by copyright.

- You are hereby granted a personal, non-exclusive, non-sub licensable (on a stand-alone basis), non-transferable, worldwide, limited license to reproduce the Wiley Materials for the purpose specified in the licensing process. This license, **and any CONTENT (PDF or image file) purchased as part of your order,** is for a one-time use only and limited to any maximum distribution number specified in the license. The first instance of republication or reuse granted by this license must be completed within two years of the date of the grant of this license (although copies prepared before the end date may be distributed thereafter). The Wiley Materials shall not be used in any other manner or for any other purpose, beyond what is granted in the license. Permission is granted subject to an appropriate acknowledgement given to the author, title of the material/book/journal and the publisher. You shall also duplicate the copyright notice that appears in the Wiley publication in your use of the Wiley Material. Permission is also granted on the understanding that nowhere in the text is a previously published source acknowledged for all or part of this Wiley Material. Any third party content is expressly excluded from this permission.

- With respect to the Wiley Materials, all rights are reserved. Except as expressly granted by the terms of the license, no part of the Wiley Materials may be copied, modified, adapted (except for minor reformatting required by the new Publication), translated, reproduced, transferred or distributed, in any form or by any means, and no derivative works may be made based on the Wiley Materials without the prior permission of the respective copyright owner.**For STM Signatory Publishers clearing permission under the terms of the STM Permissions Guidelines only, the terms of the license are extended to include subsequent editions and for editions in other languages, provided such editions are for the work as a whole in situ and does not involve the separate exploitation of the permitted figures or extracts,** You may not alter, remove or suppress in any manner any copyright, trademark or other notices displayed by the Wiley Materials. You may not license, rent, sell, loan, lease, pledge, offer as security, transfer or assign the Wiley Materials on a stand-alone basis, or any of the rights granted to you hereunder to any other person.

- The Wiley Materials and all of the intellectual property rights therein shall at all times remain the exclusive property of John Wiley & Sons Inc, the Wiley Companies, or their respective licensors, and your interest therein is only that of having possession of and the right to reproduce the Wiley Materials pursuant to Section 2 herein during the continuance of this Agreement. You agree that you own no right, title or interest in or to the Wiley Materials or any of the intellectual property rights therein. You shall have no rights hereunder other than the license as provided for above in Section 2. No right, license or interest to any trademark, trade name, service mark or other branding

86

("Marks") of WILEY or its licensors is granted hereunder, and you agree that you shall not assert any such right, license or interest with respect thereto

- NEITHER WILEY NOR ITS LICENSORS MAKES ANY WARRANTY OR REPRESENTATION OF ANY KIND TO YOU OR ANY THIRD PARTY, EXPRESS, IMPLIED OR STATUTORY, WITH RESPECT TO THE MATERIALS OR THE ACCURACY OF ANY INFORMATION CONTAINED IN THE MATERIALS, INCLUDING, WITHOUT LIMITATION, ANY IMPLIED WARRANTY OF MERCHANTABILITY, ACCURACY, SATISFACTORY QUALITY, FITNESS FOR A PARTICULAR PURPOSE, USABILITY, INTEGRATION OR NON-INFRINGEMENT AND ALL SUCH WARRANTIES ARE HEREBY EXCLUDED BY WILEY AND ITS LICENSORS AND WAIVED BY YOU.

- WILEY shall have the right to terminate this Agreement immediately upon breach of this Agreement by you.

- You shall indemnify, defend and hold harmless WILEY, its Licensors and their respective directors, officers, agents and employees, from and against any actual or threatened claims, demands, causes of action or proceedings arising from any breach of this Agreement by you.

- IN NO EVENT SHALL WILEY OR ITS LICENSORS BE LIABLE TO YOU OR ANY OTHER PARTY OR ANY OTHER PERSON OR ENTITY FOR ANY SPECIAL, CONSEQUENTIAL, INCIDENTAL, INDIRECT, EXEMPLARY OR PUNITIVE DAMAGES, HOWEVER CAUSED, ARISING OUT OF OR IN CONNECTION WITH THE DOWNLOADING, PROVISIONING, VIEWING OR USE OF THE MATERIALS REGARDLESS OF THE FORM OF ACTION, WHETHER FOR BREACH OF CONTRACT, BREACH OF WARRANTY, TORT, NEGLIGENCE, INFRINGEMENT OR OTHERWISE (INCLUDING, WITHOUT LIMITATION, DAMAGES BASED ON LOSS OF PROFITS, DATA, FILES, USE, BUSINESS OPPORTUNITY OR CLAIMS OF THIRD PARTIES), AND WHETHER OR NOT THE PARTY HAS BEEN ADVISED OF THE POSSIBILITY OF SUCH DAMAGES. THIS LIMITATION SHALL APPLY NOTWITHSTANDING ANY FAILURE OF ESSENTIAL PURPOSE OF ANY LIMITED REMEDY PROVIDED HEREIN.

- Should any provision of this Agreement be held by a court of competent jurisdiction to be illegal, invalid, or unenforceable, that provision shall be deemed amended to achieve as nearly as possible the same economic effect as the original provision, and the legality, validity and enforceability of the remaining provisions of this Agreement shall not be affected or impaired thereby.

- The failure of either party to enforce any term or condition of this Agreement shall not constitute a waiver of either party's right to enforce each and every term and condition of this Agreement. No breach under this agreement shall be deemed waived or excused by either party unless such waiver or consent is in writing signed by the party granting such waiver or consent. The waiver by or consent of a party to a breach of any provision of this Agreement shall not operate or be construed as a waiver of or consent to any other or subsequent breach by such other party.

- This Agreement may not be assigned (including by operation of law or otherwise) by you without WILEY's prior written consent.

- Any fee required for this permission shall be non-refundable after thirty (30) days from receipt by the CCC.

- These terms and conditions together with CCC's Billing and Payment terms and conditions (which are incorporated herein) form the entire agreement between you and WILEY concerning this licensing transaction and (in the absence of fraud) supersedes all prior agreements and representations of the parties, oral or written. This Agreement may not be amended except in writing signed by both parties. This Agreement shall be binding upon and inure to the benefit of the parties' successors, legal representatives, and authorized assigns.

- In the event of any conflict between your obligations established by these terms and conditions and those established by CCC's Billing and Payment terms and conditions, these terms and conditions shall prevail.

- WILEY expressly reserves all rights not specifically granted in the combination of (i) the license details provided by you and accepted in the course of this licensing transaction, (ii) these terms and conditions and (iii) CCC's Billing and Payment terms and conditions.

- This Agreement will be void if the Type of Use, Format, Circulation, or Requestor Type was misrepresented during the licensing process.

- This Agreement shall be governed by and construed in accordance with the laws of the State of New York, USA, without regards to such state's conflict of law rules. Any legal action, suit or proceeding arising out of or relating to these Terms and Conditions or the breach thereof shall be instituted in a court of competent jurisdiction in New York County in the State of New York in the United States of America and each party hereby consents and submits to the personal jurisdiction of such court, waives any objection to venue in such court and consents to service of process by registered or certified mail, return receipt requested, at the last known address of such party.

Use of Wiley Open Access articles for commercial, promotional, or marketing purposes requires further explicit permission from Wiley and will be subject to a fee.
Further details can be found on Wiley Online Library
http://olabout.wiley.com/WileyCDA/Section/id-410895.html

Other Terms and Conditions:

v1.10 Last updated September 2015

Figures 2.3 and 2.4

Title:	Root Causes of the Limited Electroluminescence Stability of Organic Light-Emitting Devices Made by Solution-Coating	
Author:	Yong Joo Cho, Hany Aziz	
Publication:	Applied Materials	
Publisher:	American Chemical Society	
Date:	May 1, 2018	

Copyright © 2018, American Chemical Society

PERMISSION/LICENSE IS GRANTED FOR YOUR ORDER AT NO CHARGE

This type of permission/license, instead of the standard Terms & Conditions, is sent to you because no fee is being charged for your order. Please note the following:

- Permission is granted for your request in both print and electronic formats, and translations.
- If figures and/or tables were requested, they may be adapted or used in part.
- Please print this page for your records and send a copy of it to your publisher/graduate school.
- Appropriate credit for the requested material should be given as follows: "Reprinted (adapted) with permission from (COMPLETE REFERENCE CITATION). Copyright (YEAR) American Chemical Society." Insert appropriate information in place of the capitalized words.
- One-time permission is granted only for the use specified in your request. No additional uses are granted (such as derivative works or other editions). For any other uses, please submit a new request.

If credit is given to another source for the material you requested, permission must be obtained from that source.

Content of Chapter 4

Title: Degradation of PEDOT:PSS hole injection layers by electrons in organic light emitting devices

Author: Elizabeth Salsberg,Hany Aziz

Publication: Organic Electronics

Publisher: Elsevier

Date: June 2019

© 2019 Elsevier B.V. All rights reserved.

Logged in as:
Elizabeth Salsberg

LOGOUT

Please note that, as the author of this Elsevier article, you retain the right to include it in a thesis or dissertation, provided it is not published commercially. Permission is not required, but please ensure that you reference the journal as the original source. For more information on this and on your other retained rights, please visit: https://www.elsevier.com/about/our-business/policies/copyright#Author-rights

BACK   CLOSE WINDOW

References

[1] M. Pope, H. P. Kallmann, and P. Magnante, "Electroluminescence in Organic Crystals," *J. Chem. Phys.*, vol. 38, pp. 2042–2043, 1963.

[2] W. Helfrich and W. G. Shneider, "Recombination Radiation in Antracene Crystals," *Phys. Rev. Lett.*, vol. 14, no. 7, pp. 229–232, 1965.

[3] P. S. Vincett, W. A. Barlow, R. A. Hann, and G. G. Roberts, "Electrical Conduction and Low Voltage Blue Electroluminescence in Vacuum-Deposited Organic Films," *Thin Solid Films*, vol. 94, no. 2, pp. 171–183, 1982.

[4] C. W. Tang and S. A. Van Slyke, "Organic electroluminescent diodes," *Appl. Phys. Lett.*, vol. 51, no. 12, pp. 913–915, 1987.

[5] D. J. Gaspar and E. Polikarpov, *OLED Fundamentals: Materials, Devices, and Processing of Organic Light-Emitting Diodes*. 2015.

[6] N. T. Kalyani, H. Swart, and S. J. Dhoble, "Future Prospects of Organic Light-Emitting Diodes," in *Principles and Applications of Organic Light Emitting Diodes (OLEDs)*, Cambridge: Woodhead Publishing, 2017, pp. 287–308.

[7] Y.-L. Chang, *Efficient Organic Light-Emitting Diodes (OLEDs)*. Boca Raton, Florida: Taylor & Francis, 2016.

[8] N. T. Kalyani, H. Swart, and S. J. Dhoble, "Solid-State Lighting," in *Principles and Applications of Organic Light Emitting Diodes (OLEDs)*, Cambridge: Woodhead Publishing, 2017, pp. 115–140.

[9] S. R. Forrest, "The path to ubiquitous and low-cost organic electronic appliances on plastic," *Nature*, vol. 428, pp. 911–918, 2004.

[10] Y. J. Cho, Y. Zhang, H. Yu, and H. Aziz, "The Root Causes of the Limited Stability of Solution-Coated Small-Molecule Organic Light-Emitting Devices: Faster Host Aggregation by Exciton-Polaron Interactions," *Adv. Funct. Mater.*, vol. 26, no. 47, pp. 8662–8669, 2016.

[11] Y. J. Cho and H. Aziz, "Root Causes of the Limited Electroluminescence Stability of Organic Light-Emitting Devices Made by Solution-Coating," *ACS Appl. Mater. Interfaces*, vol. 10, no. 21, pp. 18113–18122, 2018.

[12] Y. J. Cho, S. Taylor, and H. Aziz, "Increased Electromer Formation and Charge Trapping in Solution-Processed versus Vacuum-Deposited Small Molecule Host Materials of Organic Light-Emitting Devices," *ACS Appl. Mater. Interfaces*, vol. 9, no. 46, pp. 40564–40572, 2017.

[13] S. Stolz, Y. Zhang, U. Lemmer, G. Hernandez-Sosa, and H. Aziz, "Degradation Mechanisms in Organic Light-Emitting Diodes with Polyethylenimine as a Solution-Processed Electron Injection Layer," *ACS Appl. Mater. Interfaces*, vol. 9, no. 3, pp. 2776–2785, 2017.

[14] T. W. Lee *et al.*, "Characteristics of solution-processed small-molecule organic films and light-emitting diodes compared with their vacuum-deposited counterparts," *Adv. Funct. Mater.*, vol. 19, no. 10, pp. 1625–1630, 2009.

[15] L. Duan *et al.*, "Solution processable small molecules for organic light-emitting diodes," *J. Mater. Chem.*, vol. 20, no. 31, p. 6392, 2010.

[16] L. S. Huang, C. W. Tang, and M. G. Mason, "Enhanced electron injection in organic electroluminescence devices using an Al / LiF electrode," *Appl. Phys. Lett.*, vol. 70, pp. 152–154, 1997.

[17] H. Ma, H.-L. Yip, F. Huang, and A. K.-Y. Jen, "Interface Engineering for Organic Electronics," *Adv. Funct. Mater.*, vol. 20, no. 9, pp. 1371–1388, 2010.

[18] Y. Zhao *et al.*, "Transition metal oxides on organic semiconductors," *Org. Electron.*, vol. 15, no. 4, pp. 871–877, 2014.

[19] J. Meyer, S. Hamwi, M. Kröger, W. Kowalsky, T. Riedl, and A. Kahn, "Transition metal oxides for organic electronics: Energetics, device physics and applications," *Adv. Mater.*, vol. 24, no. 40, pp. 5408–5427, 2012.

[20] A. Bernsten *et al.*, "Stability of Polymer LEDs," *Opt. Mater. (Amst).*, vol. 9, pp. 125–133, 1998.

[21] M. M. De Kok *et al.*, "Modification of PEDOT:PSS as hole injection layer in polymer LEDs," *Phys. Status Solidi Appl. Res.*, vol. 201, no. 6, pp. 1342–1359, 2004.

[22] A. Elschner *et al.*, "PEDT/PSS for efficient hole-injection in hybrid organic light-emitting diodes," *Synth. Met.*, vol. 111, pp. 139–143, 2000.

[23] W. Brutting and C. Adachi, *Physics of Organic Semiconductors*, 2nd ed. Weinheim, Germany: Wiley-VCH Verlag GmbH, 2012.

[24] M. Klessinger and J. Michl, *Excited States and Photochemistry of Organic Molecules*. New York: Wiley-VCH Verlag GmbH, 1995.

[25] N. J. Turro, *Modern Molecular Photochemistry*. Menlo Park: Benjamin/Cummings, 1978.

[26] W. Helfrich and W. G. Shneider, "Transients of Volume-Controlled Current and of Recombination Radiation in Anthracene," *J. Chem. Phys.*, vol. 44, pp. 2902–2909, 1966.

[27] B. P. Strohriegl and J. V Grazulevicius, "Charge-Transporting Molecular Glasses," *Adv. Mater.*, no. 20, pp. 1439–1452, 2010.

[28] S. A. Van Slyke, C. H. Chen, and C. W. Tang, "Organic electroluminescent devices with improved stability," *Appl. Phys. Lett.*, vol. 69, pp. 2160–2162, 1996.

[29] J. Shi and C. W. Tang, "Doped organic electroluminescent devices with improved stability," *Appl. Phys. Lett.*, vol. 70, pp. 1665–1667, 1997.

[30] J. Chen and D. Ma, "Investigation of charge-carrier injection characteristics in NPB/Alq 3 heterojunction devices," vol. 325, pp. 225–230, 2006.

[31] H. Aziz and Z. D. Popovic, "Degradation Phenomena in Small-Molecule Organic Light-Emitting Devices," *Chem. Mater.*, vol. 16, no. 23, pp. 4522–4532, 2004.

[32] J. Shinar, *Organic Light-Emitting Devices: A Survey*. New York: AIP Press/Springer, 2002.

[33] M. A. Baldo *et al.*, "Highly efficient phosphorescent emission from organic electroluminescent devices," *Nature*, vol. 395, pp. 151–154, 1998.

[34] C. Adachi, M. A. Baldo, M. E. Thompson, and S. R. Forrest, "Nearly 100 % internal phosphorescence efficiency in an organic light-emitting device," *J. Appl. Phys.*, vol. 90, pp. 5048–5051, 2001.

[35] Y. Kawamura, K. Goushi, J. Brooks, J. J. Brown, H. Sasabe, and C. Adachi, "100 % phosphorescence quantum efficiency of complexes in organic semiconductor films," *Appl. Phys. Lett.*, vol. 86, pp. 071104-4-071104-7, 2005.

[36] M. A. Baldo, S. Lamansky, P. E. Burrows, M. E. Thompson, and S. R. Forrest, "Very high-efficiency green organic light-emitting devices based on electrophosphorescence," *Appl. Phys. Lett.*, vol. 75, no. 1, pp. 4–6, 1999.

[37] B. S. Reineke, T. C. Rosenow, B. Lüssem, and K. Leo, "Improved High-Brightness Efficiency of Phosphorescent Organic LEDs Comprising Emitter Molecules with Small Permanent Dipole Moments," *Adv. Mater.*, vol. 22, pp. 3189–3193, 2010.

[38] Z. B. Wang *et al.*, "Highly simplified phosphorescent organic light emitting diode with > 20% external quantum efficiency at > 10,000 cd/m2," *Appl. Phys. Lett.*, vol. 98, p. 073310-, 2011.

[39] Y. Zhang and H. Aziz, "Enhanced stability in inverted simplified phosphorescent organic light-emitting devices and its origins," *Org. Electron. physics, Mater. Appl.*, vol. 22, pp. 69–73, 2015.

[40] N. C. Giebink and S. R. Forrest, "Quantum efficiency roll-off at high brightness in fluorescent and phosphorescent organic light emitting diodes," *Phys. Rev. B*, vol. 77, no. 235215, pp. 1–9, 2008.

[41] C. Murawski, K. Leo, and M. C. Gather, "Efficiency Roll-Off in Organic Light-Emitting Diodes," *Adv. Mater.*, vol. 25, pp. 6801–6827, 2013.

[42] Z. D. Popovic *et al.*, "Improving the efficiency and stability of organic light-emitting devices using mixed emitting layers," in *Proc. SPIE 3476, Organic Light-Emitting Materials and Devices II*, 1998, no. 16 December 1998, pp. 68–73.

[43] Y. Kawamura, J. Brooks, J. J. Brown, H. Sasabe, and C. Adachi, "Intermolecular Interaction and a Concentration-Quenching Mechanism of Phosphorescent Ir (III) Complexes in a Solid Film," *Phys. Rev. Lett.*, vol. 96, p. 017404, 2006.

[44] W. Rieb, T. A. Beierlein, and H. Riel, "Optimizing OLED Structures for a-Si Display Applications via Combinatorial Methods and Enhanced Outcoupling," *Phys. Status Solidi*, vol. 201, no. 6, pp. 1360–1371, 2004.

[45] B. M. Pfeiffer, S. R. Forrest, K. Leo, and M. E. Thompson, "Electrophosphorescent p-i-n Organic Light-Emitting Devices for Very-High-Efficiency Flat-Panel Displays**," *Adv. Mater.*, vol. 14, no. 22, pp. 1633–1636, 2002.

[46] Y. Zhang and H. Aziz, "Insights into charge balance and its limitations in simplified phosphorescent organic light-emitting devices," *Org. Electron. physics, Mater. Appl.*, vol. 30, pp. 76–82, 2016.

[47] J. Jou, S. Kumar, A. Agrawal, and T. Li, "Approaches for fabricating high efficiency organic light emitting diodes," *J. Mater. Chem. C*, vol. 3, pp. 2974–3002, 2015.

[48] K. Leo, "Organic light-emitting diodes: Efficient and flexible solution," *Nat. Photonics*, vol. 5, no. December, pp. 1–3, 2011.

[49] L. Li, J. Liang, S. Chou, X. Zhu, X. Niu, and Q. Pei, "Nanocomposite Electrode with Efficient Light Extraction for Organic Light Emitting," *Sci. Rep.*, vol. 4, pp. 1–8, 2014.

[50] S. Möller and S. R. Forrest, "Improved light out-coupling in organic light emitting diodes employing ordered microlens arrays," *J. Appl. Phys.*, vol. 91, no. 5, pp. 3324–3327, 2002.

[51] K. Saxena, V. K. Jain, and D. S. Mehta, "A review on the light extraction techniques in organic electroluminescent devices," *Opt. Mater. (Amst).*, vol. 32, no. 1, pp. 221–233, 2009.

[52] F. Li, X. Li, J. Zhang, and B. Yang, "Enhanced light extraction from organic light-emitting devices by using microcontact printed silica colloidal crystals," *Org. Electron. physics, Mater. Appl.*, vol. 8, no. 5, pp. 635–639, 2007.

[53] S. F. Leung *et al.*, "Light management with nanostructures for optoelectronic devices," *J. Phys. Chem. Lett.*, vol. 5, no. 8, pp. 1479–1495, 2014.

[54] J. J. Shiang and A. R. Duggal, "Application of radiative transport theory to light extraction from organic light emitting diodes," *J. Appl. Phys.*, vol. 95, no. 5, pp. 2880–2888, 2004.

[55] J. J. Shiang, T. J. Faircloth, and A. R. Duggal, "Experimental demonstration of increased organic light emitting device output via volumetric light scattering," *J. Appl. Phys.*, vol. 95, no. 5, pp. 2889–2895, 2004.

[56] M. M.-H. Lu, "Microcavity Effects and Light Extraction Enhancement," in *OLED Fundamentals: Materials, Devices and Processing of Organic Light Emitting Diodes*, 1st ed., D. J. Gaspar and E. Polikarpov, Eds. Boca Raton, Florida: Taylor & Francis, 2015, pp. 299–337.

[57] S. Reineke *et al.*, "White organic light-emitting diodes with fluorescent tube efficiency," *Nature*, vol. 459, no. 7244, pp. 234–238, 2009.

[58] H.-W. Chang *et al.*, "Organic light-emitting devices integrated with internal scattering layers for enhancing optical out-coupling," *J. SID*, vol. 19, no. 2, pp. 196–201, 2011.

[59] W. C. H. Choy, W. K. Chan, and Y. Yuan, "Recent advances in transition metal complexes and light-management engineering in organic optoelectronic devices," *Adv. Mater.*, vol. 26, no. 31, pp. 5368–5399, 2014.

[60] T. W. Koh, J. M. Choi, S. Lee, and S. Yoo, "Optical outcoupling enhancement in organic light-emitting diodes: highly conductive polymer as a low-index layer on microstructured ITO electrodes," *Adv. Mater.*, vol. 22, no. 16, pp. 1849–1853, 2010.

[61] S. Reineke, M. Thomschke, B. Lüssem, and K. Leo, "White organic light-emitting diodes: Status and perspective," *Rev. Mod. Phys.*, vol. 85, no. 3, pp. 1245–1293, 2013.

[62] W. H. Koo *et al.*, "Light extraction from organic light-emitting diodes enhanced by spontaneously formed buckles," *Nat. Photonics*, vol. 4, no. 4, pp. 222–226, 2010.

[63] Z. B. Wang *et al.*, "Unlocking the full potential of organic light-emitting diodes on flexible plastic," *Nat. Photonics*, vol. 5, no. 12, pp. 753–757, 2011.

[64] W. Brütting, J. Frischeisen, T. D. Schmidt, B. J. Scholz, and C. Mayr, "Device efficiency of organic light-emitting diodes: Progress by improved light outcoupling," *Phys. Status Solidi Appl. Mater. Sci.*, vol. 210, no. 1, pp. 44–65, 2013.

[65] N. Kalyani, H. Swart, and S. J. Dhoble, "Organic Light-Emitting Diode Fabrication and Characterization Techniques," in *Principles and Applications of Organic Light Emitting Diodes (OLEDs)*, 1st ed., Elsevier, 2017, pp. 227–252.

[66] S. R. Forrest, "Ultrathin Organic Films Grown by Organic Molecular Beam Deposition and Related Techniques," *Chem. Rev.*, vol. 2665, no. 94, 1997.

[67] P. E. Burrows, G. Gu, V. Bulovi, Z. Shen, S. R. Forrest, and M. E. Thompson, "Achieving Full-Color Organic Light-Emitting Devices for Lightweight , Flat-Panel Displays," *IEEE Trans. Electron Devices*, vol. 44, no. 8, pp. 1188–1203, 1997.

[68] B. Geffroy, P. Roy, and C. Prat, "Organic light-emitting diode (OLED) technology : materials , devices and display technologies," *Polym. Int.*, vol. 55, pp. 572–582, 2006.

[69] J. H. Kwon, R. Pode, H. D. Kim, and H. K. Chung, "High Performance Organic Light Emitting Diode Displays," in *Applications of Organic and Printed Electronics*, E. Cantatore, Ed. Boston: Springer, 2013.

[70] Y. Kajiyama, K. Kajiyama, and H. Aziz, "Maskless RGB color patterning of vacuum-deposited small molecule OLED displays by diffusion of luminescent dopant molecules," *Opt. Express*, vol. 23, no. 13, pp. 16650–16661, 2015.

[71] Y. Kajiyama, K. Joseph, K. Kajiyama, S. Kudo, and H. Aziz, "Small feature sizes and high aperture ratio organic light-emitting diodes by using laser- patterned polyimide shadow masks," *Appl. Phys. Lett.*, vol. 104, 2014.

[72] F. C. Krebs, "Fabrication and processing of polymer solar cells : A review of printing and coating techniques," *Sol. Energy Mater. Sol. Cells*, vol. 93, pp. 394–412, 2009.

[73] K. Norrman, A. Ghanbari-Siahkali, and N. B. Larsen, "Studies of spin-coated polymer films," *Annu. Reports Prog. Chem. - Sect. C*, vol. 101, pp. 174–201, 2005.

[74] Y. Chang *et al.*, "Blade coating of Tris (8-hydroxyquinolinato) aluminum as the electron-transport layer for all-solution blue fl uorescent organic light-emitting diodes," *Org. Electron.*, vol. 29, pp. 99–106, 2016.

[75] B. A. Elschner, H. W. Heuer, F. Jonas, S. Kirchmeyer, R. Wehrmann, and K. Wussow, "Gallium Complexes in Three-Layer Organic Electroluminescent Devices," *Adv. Mater.*, vol. 13, no. 23, pp. 1811–1814, 2001.

[76] H. C. Yeh, H. F. Meng, H. W. Lin, T. C. Chao, M. R. Tseng, and H. W. Zan, "All-small-molecule efficient white organic light-emitting diodes by multi-layer blade coating," *Org. Electron. physics, Mater. Appl.*, vol. 13, no. 5, pp. 914–918, 2012.

[77] Y. Chang *et al.*, "Unmodified small-molecule organic light-emitting diodes by blade coating," *Org. Electron.*, vol. 13, no. 10, pp. 2149–2155, 2012.

[78] H. Chang *et al.*, "General application of blade coating to small-molecule hosts for organic light-emitting diode," *Synth. Met.*, vol. 196, pp. 99–109, 2014.

[79] C.-Y. Chen *et al.*, "Continuous blade coating for multi-layer large-area organic light-emitting diode and solar cell," *J. Appl. Phys.*, vol. 110, p. 094501, 2011.

[80] E. Menard *et al.*, "Micro- and Nanopatterning Techniques for Organic Electronic and Optoelectronic Systems," *Chem. Rev.*, vol. 107, pp. 1117–1160, 2007.

[81] R.-P. Xu, Y.-Q. Li, and J.-X. Tang, "Recent advances in flexible organic light-emitting diodes," *J. Mater. Chem. C*, vol. 4, pp. 9116–9142, 2016.

[82] D. A. Pardo, G. E. Jabbour, and N. Peyghambarian, "Application of Screen Printing in the Fabrication of Organic Light-Emitting Devices," *Adv. Mater.*, vol. 12, no. 17, pp. 1249–1252, 2000.

[83]   F. C. Krebs, J. Fyenbo, and M. Jørgensen, "Product integration of compact roll-to-roll processed polymer solar cell modules : methods and manufacture using flexographic printing , slot-die coating and rotary screen printing," *J. Mater. Chem.*, vol. 20, pp. 8994–9001, 2010.

[84]   G. Grau, J. Cen, H. Kang, R. Kitsomboonloha, and W. J. Scheideler, "Gravure-printed electronics: recent progress in tooling development , understanding of printing physics , and realization of printed devices Gravure-printed electronics : recent progress in tooling development , understanding of printing physics , and rea," 2016.

[85]   M. Montanino *et al.*, "Gravure printed PEDOT : PSS as anode for flexible ITO-free organic light emitting diodes," *Express Polym. Lett.*, vol. 11, no. 6, pp. 518–523, 2017.

[86]   B. M. Singh, H. M. Haverinen, P. Dhagat, and G. E. Jabbour, "Inkjet Printing — Process and Its Applications," *Adv. Mater.*, vol. 90014, pp. 673–685, 2010.

[87]   E. Tekin, P. J. Smith, and U. S. Schubert, "Inkjet printing as a deposition and patterning tool for polymers and inorganic particles," *Soft Matter*, vol. 4, pp. 703–713, 2008.

[88]   L. Zhou *et al.*, "Inkjet-Printed Small-Molecule Organic Light-Emitting Diodes : Halogen-Free Inks , Printing Optimization , and Large-Area Patterning," *ACS Appl. Mater. Interfaces*, vol. 9, pp. 40533–40540, 2017.

[89]   S. Jung, J. Kim, and H. Kim, "High performance inkjet printed phosphorescent organic light emitting diodes based on small molecules commonly used in vacuum processes," *Thin Solid Films*, vol. 520, no. 23, pp. 6954–6958, 2012.

[90]   B. C. N. Hoth, S. A. Choulis, P. Schilinsky, and C. J. Brabec, "High Photovoltaic Performance of Inkjet Printed Polymer : Fullerene Blends," *Adv. Mater.*, vol. 19, pp. 3973–3978, 2007.

[91]   S. Chung, S. O. Kim, S. Kwon, C. Lee, and Y. Hong, "All-Inkjet-Printed Organic Thin-Film Transistor Inverter on Flexible Plastic Substrate," *IEEE Electron Device Lett.*, vol. 32, no. 8, pp. 1134–1136, 2011.

[92]   Z. Zhan, J. An, Y. Wei, V. T. Tran, and H. Du, "Inkjet-printed optoelectronics," *Nanoscale*, vol. 9, pp. 965–993, 2017.

[93]   A. Teichler, J. Perelaer, and U. S. Schubert, "Inkjet printing of organic electronics - comparison of deposition techniques and state-of-the-art developments," *J. Mater. Chem. C*, vol. 1, pp. 1910–1925, 2013.

[94]   S. A. Carter, M. Angelopoulos, S. Karg, P. J. Brock, and J. C. Scott, "Polymeric anodes for improved polymer light-emitting diode performance," *Appl. Phys. Lett.*, vol. 70, p. 2067, 1996.

[95]   J. C. Carter *et al.*, "Operating stability of light-emitting polymer diodes based on poly(p-phenylene vinylene)," *Appl. Phys. Lett.*, vol. 71, p. 34, 1997.

[96]   A. Van Dijken, A. Perro, E. A. Meulenkamp, and K. Brunner, "The influence of a PEDOT:PSS layer on the efficiency of a polymer light-emitting diode," *Org. Electron. physics, Mater. Appl.*, vol. 4, no. 2–3, pp. 131–141, 2003.

[97]   R. Steim, F. R. Kogler, and C. J. Brabec, "Interface materials for organic solar cells," *J. Mater. Chem.*, vol. 20, no. 13, pp. 2499–2512, 2010.

[98]   K. S. Yook and J. Y. Lee, "Small molecule host materials for solution processed phosphorescent organic light-emitting diodes," *Adv. Mater.*, vol. 26, no. 25, pp. 4218–4233, 2014.

[99]   J. Chen *et al.*, "Solution-processable small molecules as efficient universal bipolar host for blue, green and red phosphorescent inverted OLEDs," *J. Mater. Chem.*, vol. 22, pp. 5164–5170, 2012.

[100] T. H. Han, M. R. Choi, C. W. Jeon, Y. H. Kim, S. K. Kwon, and T. W. Lee, "Ultrahigh-efficiency solution-processed simplified small-molecule organic light-emitting diodes using universal host materials," *Sci. Adv.*, vol. 2, no. 10, pp. 1–8, 2016.

[101] W. Cho *et al.*, "Solution-processable highly efficient deep-red and orange organic light-emitting diodes based on multi-functional Ir(iii) complexes," *J. Mater. Chem. C*, vol. 5, pp. 10029–10038, 2017.

[102] J.-H. Jou, S.-C. Fu, C.-C. An, J.-J. Shyue, C.-L. Chin, and Z.-K. He, "High efficiency yellow organic light-emitting diodes with a solution-process feasible iridium based emitter," *J. Mater. Chem. C*, vol. 5, pp. 5478–5486, 2017.

[103] Y. Chen *et al.*, "Highly efficient solution-processed phosphorescent organic light-emitting devices with double-stacked hole injection layers," *J. Appl. Phys.*, vol. 122, no. 6, pp. 1–8, 2017.

[104] M. Cai, T. Xiao, E. Hellerich, Y. Chen, R. Shinar, and J. Shinar, "High-efficiency solution-processed small molecule electrophosphorescent organic light-emitting diodes," *Adv. Mater.*, vol. 23, no. 31, pp. 3590–3596, 2011.

[105] S. Wang *et al.*, "Solution-Processed Phosphorescent Organic Light-Emitting Diodes with Ultralow Driving Voltage and Very High Power Efficiency," *Sci. Rep.*, vol. 5, no. June, pp. 1–9, 2015.

[106] J. Jou *et al.*, "High-efficiency blue organic light-emitting diodes using a 3 , 5-di (9 H -carbazol-9-yl) tetraphenylsilane host via a solution-process †," *J. Mater. Chem.*, vol. 20, pp. 8411–8416, 2010.

[107] B. C. Ho, W. Wong, G. Zhou, B. Yao, Z. Xie, and L. Wang, "Solution-Processible Multi-component Cyclometalated Iridium Phosphors for High-Efficiency Orange-Emitting OLEDs and Their Potential Use as White Light Sources," *Adv. Funct. Mater.*, vol. 17, pp. 2925–2936, 2007.

[108] G. Zhou, W. Wong, B. Yao, and L. Wang, "Multifunctional metallophosphors with anti-triplet – triplet annihilation properties for solution-processable electroluminescent devices," *J. Mater. Chem.*, vol. 18, pp. 1799–1809, 2008.

[109] J.-H. Jou, M.-C. Sun, H.-H. Chou, and C.-H. Li, "White organic light-emitting devices with a solution-processed and molecular host- employed emission layer," *Appl. Phys. Lett.*, vol. 87, p. 043508, 2006.

[110] B. C. Ho *et al.*, "Red-Light-Emitting Iridium Complexes with Hole-Transporting 9-Arylcarbazole Moieties for Electrophosphorescence Efficiency / Color Purity Trade-off Optimization," *Adv. Funct. Mater.*, vol. 18, pp. 319–331, 2008.

[111] J. Jou *et al.*, "High-efficiency blue organic light-emitting diodes using a 3 , 5-di (9 H -carbazol-9-yl) tetraphenylsilane host via a solution-process," *Joural Mater. Chem.*, vol. 20, pp. 8411–8416, 2010.

[112] N. Rehman, D. Hertel, K. Meerholz, H. Becker, and S. Heun, "Highly efficient solution-processed phosphorescent multilayer organic light- emitting diodes based on small-molecule hosts," *Appl. Phys. Lett.*, vol. 91, p. 103507, 2007.

[113] M. Nomura, Y. Shibasaki, M. Ueda, K. Tugita, M. Ichikawa, and Y. Taniguchi, "New amorphous electron-transporting materials based on Tris-benzimidazoles for all wet-process OLED devices," *Synth. Met.*, vol. 151, pp. 261–268, 2005.

[114] J. You, S. Tseng, H. Meng, F. Yen, I. Lin, and S. Horng, "All-solution-processed blue small molecular organic light-emitting diodes with multilayer device structure," *Org. Electron.*, vol. 10, no. 8, pp. 1610–1614, 2009.

[115] Z. Liu *et al.*, "Solution-processed small molecular electron transport layer for multilayer polymer light-emitting diodes," *Synth. Met.*, vol. 161, pp. 426–430, 2011.

[116] T. Earmme and S. A. Jenekhe, "High-performance multilayered phosphorescent OLEDs by solution-proessed commercial electron-transport materials," *J. Mater. Chem.*, vol. 22, pp. 4660–4668, 2012.

[117] Y. Chang, C. Yu, S. Yang, I. Hong, and S. Jiang, "Great improvement of operation-lifetime for all-solution OLEDs with mixed hosts by blade coating," *Org. Electron.*, vol. 42, pp. 75–86, 2017.

[118] N. Aizawa, Y. Pu, M. Watanabe, T. Chiba, K. Ideta, and N. Toyota, "Solution-processed multilayer small-molecule light-emitting devices with high-efficiency white-light emission," *Nat. Commun.*, vol. 5, pp. 1–7, 2014.

[119] L. S. C. Pingree, B. a MacLeod, and D. S. Ginger, "The changing face of PEDOT : PSS films: Substrate, bias, and processing effects on vertical charge transport," *J. Phys. Chem. C*, vol. 112, pp. 7922–7927, 2008.

[120] N. K. Patel, S. Cina, and J. H. Burroughes, "High-efficiency organic light-emitting diodes," *IEEE J. Sel. Top. Quantum Electron.*, vol. 8, no. 2, p. 346-361--, 2002.

[121] A. Elschner, S. Kirchmeyer, W. Lovenich, U. Merker, and K. Reuter, "PEDOT:PSS," in *PEDOT: Principles and Applications of an Intrinsically Conductive Polymer*, 1st ed., Boca Raton, Florida: CRC Press, 2010, pp. 113–166.

[122] S. Kirchmeyer and K. Reuter, "Scientific importance, properties and growing applications of poly(3,4-ethylenedioxythiophene)," *J. Mater. Chem.*, vol. 15, pp. 2077–2088, 2005.

[123] U. Lang, N. Naujoks, and J. Dual, "Mechanical characterization of PEDOT:PSS thin films," *Synth. Met.*, vol. 159, pp. 473–479, 2009.

[124] R. Paetzold, K. Heuser, D. Henseler, S. Roeger, G. Wittmann, and A. Winnacker, "Performance of flexible polymeric light- emitting diodes under bending conditions," *Appl. Phyiscs Lett.*, p. 3342, 2003.

[125] J. Huang, P. F. Miller, J. C. De Mello, A. J. De Mello, and D. D. C. Bradley, "Influence of thermal treatment on the conductivity and morphology of PEDOT / PSS films," *Synth. Met.*, vol. 139, pp. 569–572, 2003.

[126] P. Rannou and M. Nechtschein, "Ageing of Poly (3,4-ethylenedioxythiophene): Kinetics of conductivity decay and lifespan," *Synth. Met.*, vol. 101, p. 6779, 1999.

[127] X. Crispin *et al.*, "Stability of Poly (3 , 4-ethylene dioxythiophene)– Poly (styrene sulfonate): A Photoelectron Spectroscopy Study," *J. Polym. Sci. Part B Polym. Phys.*, vol. 41, pp. 2561–2583, 2003.

[128] S. Marciniak *et al.*, "Light induced damage in poly (3 , 4-ethylenedioxythiophene) and its derivatives studied by photoelectron spectroscopy," *Synth. Met.*, vol. 141, pp. 67–73, 2004.

[129] X. Crispin *et al.*, "Conductivity, morphology, interfacial chemistry, and stability of poly(3,4-ethylene dioxythiophene)-poly(styrene sulfonate): A photoelectron spectroscopy study," *J. Polym. Sci. Part B Polym. Phys.*, vol. 41, no. 21, pp. 2561–2583, 2003.

[130] A. W. D. Van Der Gon, J. Birgerson, M. Fahlman, and W. R. Salaneck, "Modification of PEDOT-PSS by low-energy electrons," *Org. Electron. Physics, Mater. Appl.*, vol. 3, no. 3–4, pp. 111–118, 2002.

[131] D. C. Martin *et al.*, "The Morphology of Poly (3 ,4-Ethylenedioxythiophene)," *Polym. Rev.*, vol. 50, no. 3, pp. 340–384, 2010.

[132] M. P. de Jong, L. J. van Ijzendoorn, and M. J. A. de Voigt, "Stability of the interface between indium-tin- poly (3,4 ethylenedioxythiophene)/styrenesulfonate) in polymer light- emitting diodes," vol. 2255, no. 2000, 2002.

[133] K. W. Wong, H. L. Yip, Y. Luo, K. Y. Wong, and W. M. Lau, "Blocking reactions between indium- tin oxide and poly (3,4-ethylene dioxythiophene): poly (styrene sulphonate) with a self-assembly monolayer," *Appl. Phys. Lett.*, vol. 80, no. 15, p. 2788, 2002.

[134] B. Roth *et al.*, "The critical choice of PEDOT:PSS additives for long term stability of roll-to-roll processed OPVs," *Adv. Energy Mater.*, vol. 5, no. 9, pp. 1–10, 2015.

[135] Q. Wang, G. Williams, and H. Aziz, "Photo-degradation of the indium tin oxide (ITO)/organic interface in organic optoelectronic devices and a new outlook on the role of ITO surface treatments and interfacial layers in improving device stability," *Org. Electron. physics, Mater. Appl.*, vol. 13, no. 10, pp. 2075–2082, 2012.

[136] Q. Fu, J. Chen, C. Shi, and D. Ma, "Room-Temperature Sol–Gel Derived Molybdenum Oxide Thin Films for Efficient and Stable Solution-Processed Organic Light-Emitting Diodes," *ACS Appl. Mater. Interfaces*, vol. 5, no. 13, pp. 6024–6029, 2013.

[137] S. Höfle *et al.*, "Molybdenum oxide anode buffer layers for solution processed, blue phosphorescent small molecule organic light emitting diodes," *Org. Electron. physics, Mater. Appl.*, vol. 14, no. 7, pp. 1820–1824, 2013.

[138] M. F. Xu *et al.*, "Aqueous solution-processed MoO3 as an effective interfacial layer in polymer/fullerene based organic solar cells," *Org. Electron. physics, Mater. Appl.*, vol. 14, no. 2, pp. 657–664, 2013.

[139] T. W. Lee, Y. Chung, O. Kwon, and J. J. Park, "Self-organized gradient hole injection to improve the performance of polymer electroluminescent devices," *Adv. Funct. Mater.*, vol. 17, no. 3, pp. 390–396, 2007.

[140] T. H. Han, Y. H. Kim, M. H. Kim, W. Song, and T. W. Lee, "Synergetic Influences of Mixed-Host Emitting Layer Structures and Hole Injection Layers on Efficiency and Lifetime of Simplified Phosphorescent Organic Light-Emitting Diodes," *ACS Appl. Mater. Interfaces*, vol. 8, no. 9, pp. 6152–6163, 2016.

[141] S. Ahn, S. H. Jeong, T. H. Han, and T. W. Lee, "Conducting Polymers as Anode Buffer Materials in Organic and Perovskite Optoelectronics," *Adv. Opt. Mater.*, vol. 5, no. 3, pp. 1–24, 2017.

[142] M. Lee *et al.*, "Efficient Green Coumarin Dopants for Organic Light-Emitting Devices," *Org. Lett.*, vol. 6, no. 8, pp. 1241–1244, 2004.

[143] N. Koch *et al.*, "Conjugated organic molecules on metal versus polymer electrodes: Demonstration of a key energy level alignment mechanism," *Appl. Phys. Lett.*, vol. 82, no. 1, pp. 70–72, 2003.

[144] J. Jou *et al.*, "Highly efficient orange-red phosphorescent organic light-emitting diode using 2,7-bis(carbazo-9-yl)-9,9-ditolylfluorene as the host," *Appl. Phys. Lett.*, vol. 96, no. 2010, p. 143306, 2011.

[145] X. Zhang *et al.*, "Exceeding 4% external quantum efficiency in ultraviolet organic light-emitting diode using PEDOT:PSS/MoO$_x$ double-stacked hole injection layer," *Appl. Phys. Lett.*, vol. 110, no. 4, p. 043301, 2017.

[146] J. S. Kim, R. H. Friend, I. Grizzi, and J. H. Burroughes, "Spin-cast thin semiconducting polymer interlayer for improving device efficiency of polymer light-emitting diodes," *Appl. Phys. Lett.*, vol. 87, no. 2, pp. 1–4, 2005.

[147] M. Shibata, Y. Sakai, and D. Yokoyama, "Advantages and disadvantages of vacuum-deposited and spin-coated amorphous organic semiconductor films for organic light-emitting diodes," *J. Mater. Chem. C*, vol. 3, pp. 11178–11191, 2015.

[148] R. J. Mcmahon, M. D. Ediger, T. Wu, L. Yu, and S. Satija, "Organic Glasses with Exceptional Thermodynamic and Kinetic Stability," *Science (80-.).*, vol. 315, pp. 353–357, 2007.

[149] D. Yokoyama, A. Sakaguchi, M. Suzuki, and C. Adachi, "Horizontal molecular orientation in vacuum-deposited organic amorphous films of hole and electron transport materials," *Appl. Phys. Lett.*, vol. 93, p. 173302, 2008.

[150] D. Yokoyama, "Molecular orientation in small-molecule oganic light-emitting diodes," *J. Mater. Chem.*, vol. 21, pp. 19187–19202, 2011.

[151] X. Xing *et al.*, "Essential Differences of Organic Films at the Molecular Level via Vacuum Deposition and Solution Processes for Organic Light- Emitting Diodes," *J. Phys. Chem. C*, vol. 117, pp. 25405–25408, 2013.

[152] Y. Esaki, T. Komino, T. Matsushima, and C. Adachi, "Enhanced Electrical Properties and Air Stability of Amorphous Organic Thin Films by Engineering Film Density," *J. Phys. Chem. Lett.*, vol. 8, pp. 5891–5897, 2017.

[153] S. Scholz, D. Kondakov, B. Lüssem, and K. Leo, "Degradation mechanisms and reactions in organic light-emitting devices," *Chem. Rev.*, vol. 115, no. 16, pp. 8449–8503, 2015.

[154] R. Zallen, *The Physics of Amorphous Solids*. New York: Wiley, 1983.

[155] S. Tokito, H. Tanaka, K. Noda, A. Okada, and Y. Taga, "Thermal stability in oligomeric triphenylamine/tris(8-quinolinolato)aluminum electroluminescent devices," *Appl. Phys. Lett.*, vol. 70, p. 1929, 1997.

[156] Y. Shirota, "Organic materials for electronic and optoelectronic devices," *J. Mater. Chem.*, vol. 10, pp. 1–25, 2000.

[157] K. R. J. Thomas, J. T. Lin, Y. Tao, and C. Ko, "Light-Emitting Carbazole Derivatives: Potential Electroluminescent Materials," *J. Am. Chem. Soc.*, vol. 123, pp. 9404–9411, 2001.

[158] L. Zhu, C. W. Brian, S. F. Swallen, P. T. Straus, M. D. Ediger, and L. Yu, "Surface Self-Diffusion of an Organic Glass," *Phys. Rev. Lett.*, vol. 106, p. 256103, 2011.

[159] S. Gong *et al.*, "Simple CBP isomers with high triplet energies for highly efficient blue electrophosphorescence," *J. Mater. Chem.*, vol. 22, pp. 2894–2899, 2012.

[160] J. J. Park *et al.*, "Small molecule interlayer for solution processed phosphorescent organic light emitting device," *Org. Electron. physics, Mater. Appl.*, vol. 10, no. 1, pp. 189–193, 2009.

[161] Q. Wang, B. Sun, and H. Aziz, "Exciton – Polaron-Induced Aggregation of Wide-Bandgap Materials and its Implication on the Electroluminescence Stability of Phosphorescent Organic Light-Emitting Devices," *Adv. Funct. Mater.*, vol. 24, pp. 2975–2985, 2014.

[162] Q. Wang and H. Aziz, "Exciton-Polaron-Induced Aggregation of Organic Electroluminescent Materials: A Major Degradation Mechanism in Wide-Bandgap Phosphorescent and Fluorescent Organic Light-Emitting Devices," *Adv. Opt. Mater.*, vol. 3, no. 7, pp. 967–975, 2015.

[163] X. Sallenave *et al.*, "Sensitivity of Redox and Optical Properties of Electroactive Carbazole Derivatives to the Molecular Architecture and Methoxy Substitutions," *J. Phys. Chem. C*, vol. 122, pp. 10138–10152, 2018.

[164] S. Kumar *et al.*, "Solution-processable naphthalene and phenyl substituted carbazole core based hole transporting materials for efficient organic light-emitting diodes," *J. Mater. Chem. C*, vol. 5, pp. 9854–9864, 2017.

[165] W. H. Kim, A. J. Mäkinen, N. Nikolov, R. Shashidhar, H. Kim, and Z. H. Kafafi, "Molecular organic light-emitting diodes using highly conducting polymers as anodes," *Appl. Phys. Lett.*, vol. 80, no. 20, pp. 3844–3846, 2002.

[166] Y. Zhou *et al.*, "Improved stability of OLEDs with mild oxygen plasma treated PEDOT:PSS," *J. Lumin.*, vol. 122–123, no. 1–2, pp. 602–604, 2007.

[167] M. Girtan and M. Rusu, "Role of ITO and PEDOT:PSS in stability/degradation of polymer:fullerene bulk heterojunctions solar cells," *Sol. Energy Mater. Sol. Cells*, vol. 94, no. 3, pp. 446–450, 2010.

[168] Z. Hongmei, X. Jianjian, Z. Wenjin, and H. Wei, "Effect of PEDOT:PSS vs. MoO3 as the hole injection layer on performance of C545T-based green electroluminescent light-emitting diodes," *Displays*, vol. 35, no. 4, pp. 171–175, 2014.

[169] F. Wang, X. Qiao, T. Xiong, and D. Ma, "The role of molybdenum oxide as anode interfacial modification in the improvement of efficiency and stability in organic light-emitting diodes," *Org. Electron. physics, Mater. Appl.*, vol. 9, no. 6, pp. 985–993, 2008.

[170] S. Tokito, K. Noda, and Y. Taga, "Metal oxides as a hole-injecting layer for an organic electroluminescent device," *J. Phys. D. Appl. Phys.*, vol. 29, pp. 2750–2753, 1996.

[171] T.-H. Han, W. Song, and T.-W. Lee, "Elucidating the Crucial Role of Hole Injection Layer in Degradation of Organic Light-Emitting Diodes," *ACS Appl. Mater. Interfaces*, vol. 7, no. 5, pp. 3117–3125, 2015.

[172] K. Jeuris, L. Groenendaal, and H. Verheyen, "Light stability of 3, 4-ethylenedioxythiophene-based derivatives," *Synth. Met.*, vol. 132, p. 289, 2003.

[173] N. C. Giebink *et al.*, "Intrinsic luminance loss in phosphorescent small-molecule organic light emitting devices due to bimolecular annihilation reactions," *J. Appl. Phys.*, vol. 103, no. 4, pp. 0–9, 2008.

[174] Y. Zhao, J. Chen, W. Chen, and D. Ma, "Poly(3,4-ethylenedioxythiophene):Poly(styrenesulfonate)/MoO 3 composite layer for efficient and stable hole injection in organic semiconductors," *J. Appl. Phys.*, vol. 111, no. 4, pp. 1–6, 2012.

[175] Y. Zhang, M. M. A. Abdelmalek, Q. Wang, and H. Aziz, "Degradation mechanism in simplified phosphorescent organic light-emitting devices utilizing one material for hole transport and emitter host," *Appl. Phys. Lett.*, vol. 103, no. 6, 2013.

[176] Y. Zhang, M. Sims, S. Li, and H. Aziz, "Triplet-induced degradation : An important consideration in the design of solution-processed hole injection materials for organic light-emitting devices," *Org. Electron.*, vol. 48, pp. 217–222, 2017.

[177] S. Gong *et al.*, "Simple CBP isomers with high triplet energies for highly efficient blue electrophosphorescence," *J. Mater. Chem.*, vol. 22, pp. 2894–2899, 2012.

[178] Q. Wang, G. Williams, T. Tsui, and H. Aziz, "Photochemical deterioration of the organic/metal contacts in organic optoelectronic devices," *J. Appl. Phys.*, vol. 112, no. 6, pp. 0–7, 2012.

[179] G. Li, D. Zhu, T. Peng, Y. Liu, Y. Wang, and M. R. Bryce, "Very high efficiency orange-red light-emitting devices with low roll-off at high luminance based on an ideal host-guest system consisting of two novel phosphorescent iridium complexes with bipolar transport," *Adv. Funct. Mater.*, vol. 24, no. 47, pp. 7420–7426, 2014.

[180] T. Minakata, M. Tanamura, Y. Mitamura, M. Imashiro, and A. Horiguchi, "Challenges for ultra-thin and highly flexible OLEDs fabricated by roll to roll process," *2016 Compd. Semicond. Week [Includes 28th Int. Conf. Indium Phosphide Relat. Mater. 43rd Int. Symp. Compd. Semicond.*, vol. 2, no. 2012, pp. 1–2, 2016.

[181] J.-H. Jou *et al.*, "High efficiency yellow organic light-emitting diodes with a solution-processed molecular host-based emissive layer," *J. Mater. Chem. C*, vol. 1, no. 8, p. 1680, 2013.

[182] W. R. Mateker *et al.*, "Molecular Packing and Arrangement Govern the Photo-Oxidative Stability of Organic Photovoltaic Materials," 2015.

[183] Y. Qiu, L. W. Antony, J. J. De Pablo, and M. D. Ediger, "Photostability Can Be Significantly Modulated by Molecular Packing in Glasses," *J. Am. Chem. Soc.*, vol. 138, pp. 11282–11289, 2016.

[184] H. Kim, Y. Byun, R. R. Das, B.-K. Choi, and P.-S. Ahn, "Small molecule based and solution processed highly efficient red electrophosphorescent organic light emitting devices," *Appl. Phys. Lett.*, vol. 91, no. 9, p. 093512, 2007.

[185] W. Lin, W. Huang, M. Huang, and C. Fan, "A bipolar host containing carbazole/dibenzothiophene for efficient solution-processed blue and white phosphorescent OLEDs," *J. Mater. Chem. C*, vol. 1, pp. 6835–6841, 2013.

[186] Y.-T. Lee, Y.-T. Chang, M.-T. Lee, P.-H. Chiang, C.-T. Chen, and C.-T. Chen, "Solution-processed bipolar small molecular host materials for single-layer blue phosphorescent organic light-emitting diodes," *J. Mater. Chem. C*, vol. 2, pp. 382–391, 2014.

[187] C. Chen, Y. Liu, Z. Chen, H. Wang, M. Wei, and C. Bao, "High efficiency warm white phosphorescent organic light emitting devices based on blue light emission from a bipolar mixed-host," *Org. Electron.*, vol. 45, pp. 273–278, 2017.

[188] D. Dong *et al.*, "Hole-transporting small molecules as a mixed host for efficient solution processed green phosphorescent organic light emitting diodes," *Org. Electron. physics, Mater. Appl.*, vol. 38, pp. 29–34, 2016.

[189] Q. Fu, J. Chen, and C. Shi, "Solution-Processed Small Molecules As Mixed Host for Highly Efficient Blue and White Phosphorescent Organic Light-Emitting Diodes," *ACS Appl. Mater. Interfaces*, vol. 4, pp. 6579–6586, 2012.

[190] Y. Jin, J. Soo, W. Sik, R. Pode, and J. Hyuk, "Soluble processed low-voltage and high efficiency blue phosphorescent organic light-emitting devices using small molecule host systems," *Org. Electron.*, vol. 13, pp. 586–592, 2012.

[191] L. Hou *et al.*, "Efficient solution-processed small-molecule single emitting layer electrophosphorescent white light-emitting diodes," *Org. Electron.*, vol. 11, no. 8, pp. 1344–1350, 2010.

[192] S. Höfle *et al.*, "Suppressing molecular aggregation in solution processed small molecule organic light emitting diodes," *Org. Electron. physics, Mater. Appl.*, vol. 15, no. 1, pp. 337–341, 2014.

[193] T. Spehr, R. Pudzich, T. Fuhrmann, and J. Salbeck, "Highly efficient light emitters based on the spiro concept," *Org. Electron.*, vol. 4, pp. 61–69, 2003.

[194] T. P. I. Saragi, T. Spehr, A. Siebert, T. Fuhrmann-lieker, and J. Salbeck, "Spiro Compounds for Organic Optoelectronics," *Chem. Rev.*, vol. 107, pp. 1011–1065, 2007.